



universität  
wien

# DIPLOMARBEIT

Titel der Diplomarbeit

Studies of atomic diffusion in NiPt  
by X-ray photon correlation spectroscopy

angestrebter akademischer Grad

Magister der Naturwissenschaften (Mag. rer.nat.)

Verfasserin / Verfasser:	Markus B. Stana
Matrikel-Nummer:	0606591
Studienrichtung (lt. Studienblatt):	Physik
Betreuerin / Betreuer:	ao. Univ.-Prof. Dr. Bogdan Sepiol

Wien, am 24.06.2011



# Abstract

Understanding diffusion mechanisms is important, as it helps us to gain a better knowledge of the processes taking place in the surrounding matter. Grasping these processes can lead to an improvement of technical applications. From a commercial point of view it helps to reduce the rejections when manufacturing doped semiconductors and to find cheaper ways to fabricate heavy duty steels. Either way, diffusion is simply fascinating from a scientific point of view.

X-ray photon correlation spectroscopy is a method which allows us to observe diffusion at an atomic scale. Although the theoretical background, with its basics stated by Van Hove over half a century ago, would have allowed for experiments to be conducted for quite a while now, the technical requirements did not. The first successful experiment on a binary alloy was conducted just about four years ago [LEITNER et al., 2009]. As X-ray sources with an ever higher intensity are developed, however, more and more systems will become available for examination.

In this thesis a nickel-platinum system was investigated. After a short introduction of theoretical foundations I will try to lay the cornerstones for a successful experiment. As the samples used in the experiment are desired to be single crystals, I will give a specification of the manufacturing processes. I will also deal with the possibility of investigating a polycrystalline sample. For reasons of comparability a program was written to simulate diffusion processes in a very simple frame, which will be introduced. Also the experiment per se with its setup and technical requirements will be discussed. The last part will provide data evaluation.

# Zusammenfassung

Die thematische Auseinandersetzung mit Diffusionsmechanismen ist von allgemeiner Wichtigkeit, da sie uns hilft, ein besseres Verständnis der Prozesse in der uns umgebenden Materie zu gewinnen. Ein Erfassen dieser Prozesse führt zu einer Verbesserung technischer Anwendungen. Wirtschaftlich gesehen hilft es beispielsweise den Ausschuss bei der Produktion von dotierten Halbleitern und die Herstellungskosten für Hochleistungsstahl zu verringern. Aus wissenschaftlicher Sicht gesehen ist Diffusion jedoch schlichtweg faszinierend.

*X-ray photon correlation spectroscopy* (zu deutsch Röntgen-Photonen-Korrelations-Spektroskopie) ist eine Methode, die es uns erlaubt Diffusion auf atomarer Skala zu untersuchen. Obwohl der theoretische Hintergrund, dessen Grundlagen von Van Hove vor über einem halben Jahrhundert aufgestellt wurden, Experimente schon länger zugelassen hätte, waren solche aufgrund unzureichender technischer Voraussetzungen nicht möglich. Das erste erfolgreiche Experiment mit einer zweiatomigen Legierung wurde erst vor vier Jahren durchgeführt [LEITNER et al., 2009]. Die kontinuierliche Weiterentwicklung von Röntgenquellen mit einer zunehmend höheren Intensität wird jedoch mehr und mehr Systeme zugänglich machen.

In dieser Arbeit wurde ein Nickel-Platin System untersucht. Nach einer kurzen Einführung in die Theorie werde ich die Eckpfeiler eines erfolgreichen Experiments behandeln. Nachdem es erstrebenswert ist, einkristalline Proben für das Experiment zu verwenden, werde ich eine kurze Beschreibung der Herstellungsprozesse geben. Außerdem werde ich mich mit der Möglichkeit der Untersuchung von polykristallinen Proben auseinandersetzen. Um eine Vergleichsbasis zu schaffen, wurde ein Programm zur Simulation von Diffusionsprozessen auf einer sehr einfachen physikalischen Basis geschrieben, welches ich vorstellen werde. Auch das Experiment an sich, mit seinem Aufbau und den technischen Voraussetzungen wird beschrieben. Der abschließende Teil wird der Auswertung der Daten gewidmet.

# Acknowledgements

First and foremost I want to thank Michael Leitner for all his input and support. He had an answer to all my questions and never seemed to get tired of them. There can be no greater advantage than sharing an office with a person like him when writing a thesis.

Next I want to thank Bogdan Sepiol for introducing me to the world of experimental physics. Not only did he provide me with the opportunity to work at a synchrotron more than once. He also patiently taught me techniques for preparing samples and shared his comprehensive knowledge.

A major part of my thanks also goes to my girlfriend Eva-Maria, who not only helped with the layout of my thesis and some graphics but supported me in the daily engagement with the topic and my studies in general.

For proofreading I thank my sister Sarah, Wolfgang Pilz, Manuel Ross and all the above mentioned.

I also want to thank all those who made it possible for me to study physics. Especially my parents, who not only supported me financially but also heard me out when I was in doubt and found the right words to get me going again. My thank goes to the state of Austria, which made it possible to get an affordable university education and financial support. I sincerely hope it stays that way for further generations.

# Contents

<b>Abstract</b>	<b>iii</b>
<b>Zusammenfassung</b>	<b>iv</b>
<b>Acknowledgements</b>	<b>v</b>
<b>1 Theory</b>	<b>1</b>
1.1 Reciprocal Space . . . . .	1
1.1.1 Scattering Theory . . . . .	2
1.2 Types of lattices . . . . .	5
1.2.1 Alloys . . . . .	7
1.2.2 Real crystals . . . . .	7
1.3 Diffusion . . . . .	8
1.3.1 Energetic states . . . . .	8
1.3.2 Calculating jump probabilities . . . . .	9
1.3.3 Macroscopic types of diffusion . . . . .	11
1.3.4 Chemical diffusion . . . . .	14
1.3.5 Diffusion mechanisms . . . . .	14
1.4 Arrhenius theory . . . . .	15
1.5 The Correlation Functions . . . . .	16
1.5.1 Finding the amplitude correlation function . . . . .	18
1.5.2 Connecting amplitude- and intensity correlation function	21

<b>2</b>	<b>Preparing the sample</b>	<b>24</b>
2.1	Finding the ideal sample thickness . . . . .	25
2.2	Manufacturing the samples . . . . .	25
2.2.1	Recrystallizing . . . . .	26
<b>3</b>	<b>The simulation program</b>	<b>34</b>
3.1	Basic outline . . . . .	34
3.2	Closer description of methods used . . . . .	36
3.2.1	Building the lattice . . . . .	36
3.2.2	Calculating jump probabilities . . . . .	36
3.2.3	Calculating the shells . . . . .	37
3.2.4	Calculating the correlation function . . . . .	38
<b>4</b>	<b>The experiment</b>	<b>40</b>
4.1	Synchrotrons . . . . .	40
4.2	Coherence of the beam . . . . .	41
4.3	Experimental setup . . . . .	42
4.3.1	Experimental conditions . . . . .	43
<b>5</b>	<b>Data evaluation</b>	<b>44</b>
5.1	Estimating atomic interaction with short range order intensity	46
5.2	Finding the activation energy . . . . .	48
5.3	$2\Theta$ dependency . . . . .	51
5.3.1	Finding the diffusion mechanisms . . . . .	53
5.3.2	Monte Carlo simulation . . . . .	58
5.4	Finding the diffusion constant . . . . .	64
5.4.1	Interdiffusion via self diffusion . . . . .	64
5.4.2	Small angle approximation . . . . .	65
5.4.3	Einstein relation . . . . .	65
5.4.4	Interdiffusion in thin layers . . . . .	66

<b>6</b>	<b>Conclusion</b>	<b>68</b>
<b>A</b>	<b>Elaborate calculations</b>	<b>69</b>
A.1	Solving equation 1.4 . . . . .	69
A.2	Calculating the angle dependent scattered radiation . . . . .	71
A.3	Calculating $\Gamma_{\text{inc}}$ . . . . .	71
A.3.1	Calculating for fcc . . . . .	72
A.4	Source code . . . . .	77
A.4.1	Building the lattice . . . . .	77
A.4.2	Calculating nearest neighbors . . . . .	78
	<b>Literature</b>	<b>82</b>



# Chapter 1

## Theory

The discussion whether the material that surrounds us is divisible in ever smaller pieces or not took centuries, starting in ancient Greece. Finally E. Rutherford (1911) conducted his famous experiment and it was proven that our surroundings are made up of atoms, from Greek *atomos* which means indivisible.

But how are these atoms distributed in space? Max Von Laue, and, about the same time around 1912, Sir W.H. Bragg and his son W.L. Bragg solved this issue by using X-rays to investigate the structure of matter. So when looking at the time scale it seems, that after finally deciding what space is made of it was a piece of cake to find out what the spatial distribution looks like. Or was it? X-rays give the spatial distribution of atoms at a certain point in time. However, at temperatures above 0 K the distribution is not static and the atoms move. Although it is possible to describe such movement at large scales it is not easy to do so at microscopic scales. This thesis tries make a contribution to a solution to this problem.

### 1.1 Reciprocal Space

How can one determine the structure of matter? Looking at it only takes you that far as microscopic methods have a limit. Waves are diffracted at structures of the size of their wavelength. Therefore it is not possible to optically investigate structures below 300 nm. So when it comes down to very small length scales, one has to use a different method. The approach of choice is to use a scatter diagram.

### 1.1.1 Scattering Theory

Light is an electromagnetic wave, so it can be described by the Maxwell equations. Using the Lorenz gauge condition, these can be written as:

$$\square \begin{pmatrix} \Phi \\ \vec{A} \end{pmatrix} = \frac{4\pi}{c} \begin{pmatrix} c\rho \\ \vec{j} \end{pmatrix} \quad (1.1)$$

where  $\square = \frac{1}{c^2} \frac{\partial^2}{\partial t^2} - \Delta$ .

We try to find a solution for  $\Phi$  ( $\vec{A}$  can be treated in the same way). The solution for the electric potential is the sum of the general solution of the related homogeneous equation and a particular solution. For the homogeneous part we have  $\square\Phi_h = 0$ , which is the wave equation with the solution of a plane wave (1.2).

$$\Phi_h(\vec{r}, t) = \Psi_0(\vec{r}, t) e^{i(\vec{k}\vec{r} - \omega t)} \quad (1.2)$$

Finding the particular solution is a little bit more tricky. We now have to find the Green function which solves  $\square G = \delta^3(r)\delta(t)$ . By rewriting both sides of the original equation using the Fourier transforms one gets:

$$\begin{aligned} \square\Phi_p(\vec{r}, t) &= \frac{1}{\sqrt{2\pi}} \int d\omega \square(\tilde{\Phi}(\vec{r}, \omega) e^{i\omega t}) \\ 4\pi\rho_p(\vec{r}, t) &= \frac{1}{\sqrt{2\pi}} \int d\omega 4\pi\tilde{\rho}(\vec{r}, \omega) e^{i\omega t} \end{aligned}$$

This gives equation (1.3), which, for  $\tilde{\rho} = 0$ , is known as the Helmholtz equation.

$$\left(\frac{-\omega^2}{c^2} - \Delta\right)\tilde{\Phi}_p(\vec{r}, \omega) = 4\pi\tilde{\rho}(\vec{r}, \omega) \quad (1.3)$$

We proceed by performing yet another Fourier transform.

$$\frac{1}{\sqrt{2\pi}^3} \int d^3k \left(\frac{\omega^2}{c^2} + \Delta\right) \mathcal{F}(\tilde{\Phi}_p)(\vec{k}, \omega) e^{i\vec{k}\vec{r}} = \frac{-4\pi}{\sqrt{2\pi}^3} \int d^3k \mathcal{F}(\tilde{\rho})(\vec{k}, \omega) e^{i\vec{k}\vec{r}}$$

By equalizing the integrands we get:

$$\left(\frac{\omega^2}{c^2} - |\vec{k}|^2\right) \mathcal{F}(\tilde{\Phi}_p)(\vec{k}, \omega) = -4\pi \mathcal{F}(\tilde{\rho})(\vec{k}, \omega).$$

Coming back to the Green function we have:

$$\left(|\vec{k}|^2 - \frac{\omega^2}{c^2}\right) \mathcal{F}(\tilde{G}) = \mathcal{F}(\delta)^3(k) \tilde{\delta}(\omega) = \frac{1}{\sqrt{2\pi}} \frac{1}{\sqrt{2\pi}} \frac{1}{\sqrt{2\pi}} \frac{1}{\sqrt{2\pi}},$$

so what we get is:

$$\mathcal{F}(\tilde{G})(\vec{k}, \omega) = \frac{1}{4\pi^2} \frac{1}{(|\vec{k}|^2 - \frac{\omega^2}{c^2})}.$$

Now we have to roll backward:

$$G(\vec{r}, t) = \frac{1}{\sqrt{2\pi}^3} \int d\omega \int d^3k \frac{1}{4\pi^2} \frac{1}{(|\vec{k}|^2 - \frac{\omega^2}{c^2})} e^{i\vec{k}\vec{r}} e^{i\omega t} \quad (1.4)$$

This equation can be solved by using complex analysis (see appendix and [NOLTING, 2007] p354 ff ). We consider a wave originating from  $\vec{r}'$  at time  $t'$  and received at time  $t_r$  at  $\vec{r}_r$ . With  $\vec{r}_r - \vec{r}' \geq 0$  we get the particular solution:

$$G(\vec{r}_r - \vec{r}', t_r - t') = \frac{1}{4\pi c |\vec{r}_r - \vec{r}'|} \delta(|\vec{r}_r - \vec{r}'| - c(t_r - t')) \quad (1.5)$$

This solution is called retarded solution.

We now get the special solution by convoluting the Green function with the charge distribution:

$$\begin{aligned} \Phi_r(\vec{r}_r, t_r) &= G * \rho \\ &= \int d^3r' \frac{1}{4\pi |\vec{r}_r - \vec{r}'|} \delta\left(\frac{|\vec{r}_r - \vec{r}'|}{c} - (t_r - t')\right) \\ &\quad \cdot \rho(\vec{r}_r - (\vec{r}_r - \vec{r}'), t_r - (t_r - t')) \\ &= \int d^3r' \frac{\rho(\vec{r}', t - \frac{|\vec{r} - \vec{r}'|}{c})}{4\pi |\vec{r} - \vec{r}'|} \end{aligned} \quad (1.6)$$

To simplify things we assume that electrons oscillate periodically around their positions in the lattice (which is especially true if they are excited by a periodic wave):

$$\rho(\vec{r}, t) = \text{Re}(\rho(\vec{r})e^{-i\omega t})$$

Equation (1.6) therefore becomes

$$\begin{aligned} \Phi_r(\vec{r}, t) &= \int d^3r' \frac{\rho(\vec{r}') e^{i\omega(t - \frac{|\vec{r} - \vec{r}'|}{c})}}{4\pi |\vec{r} - \vec{r}'|} \\ &= \frac{e^{-i\omega t}}{4\pi} \int d^3r' \frac{\rho(\vec{r}') e^{i\omega(\frac{|\vec{r} - \vec{r}'|}{c})}}{|\vec{r} - \vec{r}'|} \end{aligned}$$

We are only interested in the field far from the source, which means  $\vec{r} \gg \vec{r}'$ . Therefore we can expand the denominator in the integral:

$$\begin{aligned} |\vec{r} - \vec{r}'| &= \sqrt{(\vec{r} - \vec{r}')^2} = \sqrt{\vec{r}^2 - 2\vec{r}\vec{r}' + \vec{r}'^2} \\ &\approx |\vec{r}| \sqrt{1 - \frac{\vec{r}\vec{r}'}{\vec{r}^2}} \approx |\vec{r}| \left(1 - \frac{\hat{r}\vec{r}'}{r}\right) = |\vec{r}| - \hat{r}\vec{r}' \end{aligned}$$

In the far field approximation, using the relation  $kc = \omega$ , we get:

$$\begin{aligned}\Phi_r(\vec{r}, t) &= \frac{e^{-i\omega t}}{4\pi} \int d^3r' \frac{\rho(\vec{r}') e^{i\omega(\frac{|\vec{r}|}{c} - \hat{r} \cdot \vec{r}')}}{|\vec{r}| - \hat{r} \cdot \vec{r}'} \\ &\approx \frac{e^{i\omega(\frac{|\vec{r}|}{c} - t)}}{4\pi} \int d^3r' \frac{\rho(\vec{r}') e^{-i\omega(\frac{\hat{r} \cdot \vec{r}'}{c})}}{|\vec{r}|} \\ &= \frac{e^{ik(|\vec{r}| - ct)}}{4\pi|\vec{r}|} \int d^3r' \rho(\vec{r}') e^{-i\vec{k} \cdot \vec{r}'}\end{aligned}$$

It can be easily seen that the electric potential in the far field is proportional to the Fourier transform of the density distribution. This especially holds for the case where the atoms are excited by a nearly monochromatic wave.

If there is more than one type of atom in the lattice, we can write the charge distribution as a sum of different charge distributions for each kind of atom ( $i$ ) convoluted with the associated concentration:

$$\rho(\vec{r}) = \sum_i (\rho_i * c_i)(\vec{r})$$

Using the Fourier transform we can write this as:

$$\begin{aligned}\mathcal{F}(\rho)(\vec{k}) &= \sum_i \mathcal{F}(\rho_i(\vec{k})) \cdot \mathcal{F}(c_i(\vec{k})) \\ &= \sum_i \int d^3r \rho_i(\vec{r}) e^{i\vec{k} \cdot \vec{r}} \cdot \int d^3r \sum_{j=1}^{N_i} \delta(\vec{r} - \vec{r}_i) e^{i\vec{k} \cdot \vec{r}}\end{aligned}$$

The electrons of the inner shells play the important part in the density distribution. So by neglecting outer shells we can say that for wavelengths in the order of atomic distances, density variations at the scale of 0.1 times the atomic ratio are negligible. Therefore for  $|\vec{k}| \ll 1$  we have  $e^{i\vec{k} \cdot \vec{r}} \approx 1$ .

$$\begin{aligned}\mathcal{F}(\rho)(\vec{k}) &= \sum_i \int d^3r \rho_i(\vec{r}) \cdot \int d^3r \sum_{j=1}^{N_i} \delta(\vec{r} - \vec{r}_i) e^{i\vec{k} \cdot \vec{r}} \\ &= \sum_i Z_i \sum_{j=1}^{N_i} e^{i\vec{k} \cdot \vec{r}_i} \\ \rho(\vec{r}) &= \sum_i \mathcal{F}^{-1}(Z_i \sum_{j=1}^{N_i} e^{i\vec{k} \cdot \vec{r}_i})\end{aligned} \tag{1.7}$$

The electric potential can therefore be written as:

$$\Phi_r(\vec{r}, t) \approx \frac{e^{ik(|\vec{r}|-ct)}}{4\pi|\vec{r}|} \left( \sum_i \mathcal{F}^{-1} \left( Z_i \sum_{j=1}^{N_i} e^{i\vec{q}\vec{r}_i} \right) \right) \delta(\vec{k}) \quad (1.8)$$

$$= \frac{1}{4\pi|\vec{r}|} \left( \sum_i \mathcal{F}^{-1} \left( Z_i \sum_{j=1}^{N_i} e^{i\vec{q}\vec{r}_i} \right) \right) \quad (1.9)$$

In an experiment the space-resolved intensity can be measured. It is given by  $I \propto AA^*$ .  $A$  is the amplitude of the electromagnetic field and because of the superposition principle of electromagnetic waves the sum over all amplitudes. The electric field is related to the electric potential by  $E = -\nabla\Phi$ . For the electric field this means that we have a plane wave from the homogeneous solution and a sum of spherical waves from the special solutions with an amplitude proportional to a constant which is determined by the spatial distribution of the types of atoms as shown in equation (1.7). So  $I \propto \sum_i A_i A_i^*$ .  $Z_i$  is the number of electrons in the shell of an atom of type  $i$  and  $A_i$  the corresponding amplitude of the field of one atom. For X-rays the first Born approximation is sufficient. This means that, talking in the particle picture, a single photon only interacts with one atom while passing through the sample. This is valid due to the very small elastic scattering cross section compared to absorption for X-rays. Therefore we can neglect the wave fronts of the spherical waves leading to new spherical waves.

The solution to the problem of how to investigate structures in matter, which can not be resolved by optical light, is provided by the fact that the far field of electromagnetic waves depends on the position and scattering length of the scatterers in the lattice.

## 1.2 Types of lattices

We have seen how information about the real space lattice can be gained by means of scattering experiments. So what do these experiments tell us about the arrangement of atoms? The most basic component of a lattice is the unit cell. It is the parallelepiped spanned by the basis vectors of the crystal lattice. I distinguish between the elementary cell, which is the unit cell with the lowest possible volume, and a general unit cell, which can include more than one atom of the same type. The whole crystal is formed by one unit cell after another in every direction in space. As this thesis deals with metals, there will only be a short introduction into the three most common lattice types. Fortunately these are also the ones with the highest geometry.

**The simple cubic lattice (*sc*)** is the most simple and most symmetrical of all lattice types. For the common unit cell one can think of a cube with an atom in each of its eight corners. The geometrical unit cell in this type is equal to the elementary cell. The lattice vectors have all equal length  $a$  and are perpendicular. So the shortest distance between two atoms (nearest neighbor distance) is  $a$  (see black lines in figure 1.1). This type has one atom in the unit cell, namely one eighth of an atom at each of the four corners. It has six nearest neighbors at distances  $a$  and twelve next-nearest neighbors at distances  $\sqrt{2}a$ .

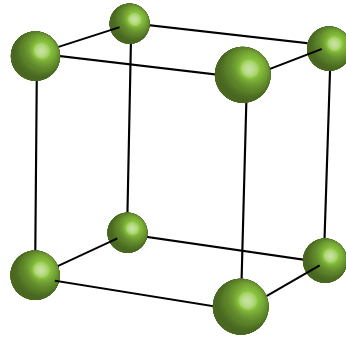


**Figure 1.1:** Simple cubic lattice (*sc*)

**The body centered lattice (*bcc*)** This cell type is basically a simple cubic lattice with one additional atom in the middle. If  $a$  again is the distance between two atoms at the edge, the nearest neighbor distance is now  $a \cdot \frac{\sqrt{3}}{2}$ . It has two atoms in the unit cell (one eighth of one in every corner as with the *sc* plus the one in the middle). The number of next-nearest neighbors is 6 and their distance is  $a$ . See figure 1.2.

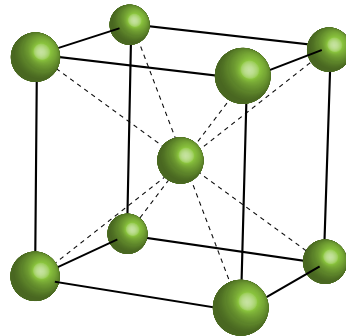


**Figure 1.2:** Body centered cubic lattice (*bcc*)

**The face centered lattice (*fcc*)** This type, instead of having an additional atom in the center of the volume, has one additional atom in the center of every surface as can be seen in figure 1.3. It has four atoms in the unit cell (again four times a quarter from the edges plus six times a half from the surfaces) and a nearest neighbor number of twelve. The number of next-nearest neighbors is 6, the distance between nearest neighbors  $\frac{\sqrt{2}}{2}a$  and the distance between next-nearest neighbors is  $a$ .

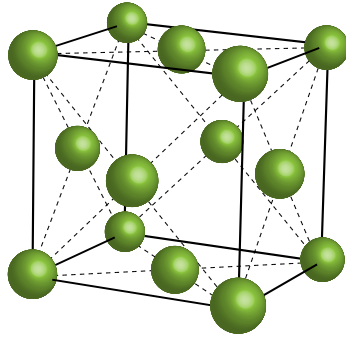


**Figure 1.3:** Face centered cubic lattice (*fcc*)

### 1.2.1 Alloys

Most crystals are not built by only one sort of atoms. Naturally elements, apart from noble gases, tend to mingle. In crystals this leads to solid solutions or intermetallic alloys. The way various types of atoms are arranged in the lattice differs, and depends on the concentration. Different arrangements have different properties and are characterized as phases.

### 1.2.2 Real crystals

We get a perfect single crystal replicating the same sequence of atoms into every direction in space. A real crystal, however, looks somewhat different. As crystals do not exist since the beginning of time, they had to be formed at some point. In this crystallization process outer influences, like temperature gradients, stress, or forces like gravity, play a role. This leads to misplacements in the crystallite structure and to the growth of grain boundaries. In fact even in the laboratory it is very difficult to get a single crystal of macroscopic size. Also at temperatures above 0 K vacancies appear.

However, when a real crystal is formed it does not mean that it has reached its final form. The vacancies can move, the grains can grow or shrink and boundaries can change. In most materials diffusion plays an important role in these processes.

## 1.3 Diffusion

The name “solid state” suggests that atoms, contrary to gases or liquids, behave rather statistically. But do they really behave like bricks in a wall? The thermal motion of particles in a liquid was first described by R. Brown [BROWN, 1828] and a theory for this motion was established by Fick [FICK, 1855] and others. Later it was discovered that this concept also aids our understanding of certain mechanisms in solids, like phase transitions. So the answer to the question is no. Atoms do not behave like bricks, but move around. To get an understanding of the matter surrounding us, it is therefore rewarding to gain a deeper insight into diffusion processes.

### 1.3.1 Energetic states

If an atom jumps from one position in the lattice to another, the lattice as a collective system changes its energetic state. The resulting energetic steps have to be overcome by the kinetic energy of the atoms, which follows the Boltzmann distribution at a certain temperature. Thereby diffusion is governed by energetic barriers and the temperature.

A thermodynamic system is characterized by its thermodynamic state function. This can be the inner energy, the Gibbs free energy, the Helmholtz free energy and so on. An important consideration for our problem is the fact that all these state functions follow the minimization principle. If we take the Gibbs free energy ( $G$ ) to characterize the states of our lattice, this means that we will have a driving force for the diffusion ( $dG < 0$ ) until the equilibrium state is reached ( $dG = 0$  and  $G = G_{min}$ ). Usually many components add up to the energy of a system, for example the mixing enthalpy  $TS$  and the tension energy resulting from displacements and grain boundaries. Contrary to liquids and gases, where convection rules this process, in solids diffusion is the important mechanism. We are, however, interested in diffusion in an equilibrium state of the system. This means that the atomic jumps are not due to a driving force. If  $G = G_{min}$  the system should be completely ordered and every atom should be handcuffed to its position by an energetic barrier it has to overcome. This is only true at a temperature of 0 K. At higher temperatures the kinetic energy is sufficient for the atoms to go to a non optimal position, thus leading to diffusion. On the one hand the probability  $p$  for an atom to jump is determinate by the temperature. This temperature gives rise to the kinetic energy the atom needs to overcome a certain energetic barrier. Therefore, on the other hand, it is also determined by the energetic barrier it has to overcome. This behavior is given by the Boltzmann factor:

$$p = e^{\frac{-E_{\text{barrier}}}{k_B T}}.$$



In the following I will only consider pair potentials between nearest and next-nearest neighbors to describe the energetic states of the system. This means that geometrical effects are neglected. Therefore especially simulations for alloys with atoms of approximately the same size, so for example for atoms in the same periodic column, are rewarding.

### 1.3.2 Calculating jump probabilities

The energetic state of a system is defined by its Hamiltonian. We have kinetic energy for all temperatures above 0 K, but also forms of potential energy can play a role as described above. For the sake of simplicity I will only consider pair potentials for the potential energy term. This will, of course, lead to a Hamiltonian that does not represent the real system, but gives a good approximation. Each atom in the lattice has a number of nearest and next-nearest neighbors, which interact with each other via a potential ( $P_{\text{NN}}$  for nearest and  $P_{3\text{N}}$  for next-nearest neighbors). These potentials are positive if the force between the atoms is repelling and negative if it is attractive. So summing over all the potentials gives the potential energy ( $V_i$ ) for an atom at a certain position  $i$  (1.10). For a system with only pair interaction, summing over all potential energies gives the Hamiltonian of the system.  $Z_{\text{NN}}$  is the number of nearest and  $Z_{3\text{N}}$  the number of next-nearest neighbors.

$$H(t) = E_{\text{kin}} + \sum_i V_i(t) = \sum_i \left( \sum_{j=1}^{Z_{\text{NN}}} P_{\text{NN}}^{ij} + \sum_{j=1}^{Z_{3\text{N}}} P_{3\text{N}}^{ij} \right) \quad (1.10)$$

Note that the Hamiltonian for pair potentials in a binary alloy can also be defined like equation (1.11) (see [LEITNER and VOGL, 2011]).

$$H(\sigma) = E_{\text{kin}} + \sum_{\vec{x} \neq \vec{y}} V(\vec{x} - \vec{y}) \sigma(\vec{x}) \sigma(\vec{y}), \quad (1.11)$$

where  $\sigma(\vec{x})$  gives the occupancy state at site  $\vec{x}$  (for a detailed treatment see 1.5).

As discussed above the important factor governing diffusion is the difference in energetic states before and after a jump. We therefore neglect the kinetic term in the Hamiltonian from now on. If only two occupants of the lattice exchange their position, the resulting energy difference is the sum of two times the pair potentials ( $P_{ij} = P_{ji}$ ) for both candidates with their associates. Let us consider a vacancy on the position  $i_1$  and an atom at  $i_2$ . Now  $P_{\text{NN}}^{i_1 j}$  is the pair potential of the vacancy and of one of its  $Z_{\text{NN}}$  nearest neighbor atoms ( $P_{3\text{N}}^{i_1 j}$  with one of the  $Z_{3\text{n}}$  next-nearest neighbors) and  $P_{\text{NN}}^{i_2 j}$  respectively  $P_{3\text{N}}^{i_2 j}$  the potential for a particular atom with its nearest respectively next-nearest neighbor. The energy difference can then be given

as the sum of the involved pair potentials (those that can change) before and after the jump:

$$\begin{aligned}
H(t) &= \sum_{j=1}^{Z_{NN}} (P_{NN}^{i_1j} + P_{NN}^{i_2j}) + \sum_{j=1}^{Z_{NN}} (P_{NN}^{j i_1} + P_{NN}^{j i_2}) \\
&\quad + \sum_{j=1}^{Z_{3N}} (P_{3N}^{i_1j} + P_{3N}^{i_2j}) + \sum_{j=1}^{Z_{3N}} (P_{3N}^{j i_1} + P_{3N}^{j i_2}) \\
&= 2 \cdot \sum_{j=1}^{Z_{NN}} (P_{NN}^{i_1j}(t) + P_{NN}^{i_2j}(t)) + 2 \cdot \sum_{j=1}^{Z_{3N}} (P_{3N}^{i_1j}(t) + P_{3N}^{i_2j}(t))
\end{aligned}$$

$$\begin{aligned}
\Delta H &= H(t + \Delta t) - H(t) \\
&= 2 \cdot \sum_{j=1}^{Z_{NN}} (P_{NN}^{i_1j}(\Delta t) + P_{NN}^{i_2j}(\Delta t) - P_{NN}^{i_1j}(t) - P_{NN}^{i_2j}(t)) \\
&\quad + 2 \cdot \sum_{j=1}^{Z_{3N}} (P_{3N}^{i_1j}(\Delta t) + P_{3N}^{i_2j}(\Delta t) - P_{3N}^{i_1j}(t) - P_{3N}^{i_2j}(t))
\end{aligned}$$

The probability for an atom to overcome a barrier with a certain energy is given by the Boltzmann factor:  $p_i \propto \exp\left(\frac{-E_i}{k_B T}\right)$ . In the past many concepts have been found to describe the energetic barrier, taking into account the geometry of the crystal for calculating saddle point energies making the problem arbitrarily difficult. I will use the easiest model for describing the energetic barriers, the Metropolis algorithm, which does not take the energy landscape into account.

### Metropolis model

Let the energetic state for an atom at lattice site  $i$  be  $E_i$ . The ratio of two probabilities for atoms at two different energy states according to the Boltzmann factor to sit at these sites can then be written as:

$$\frac{p_i}{p_j} = e^{\frac{E_j - E_i}{k_B T}}. \quad (1.12)$$

I now introduce the rate with which an atom jumps from position  $i$  to position  $j$  as  $\nu_{i \rightarrow j}$  and vice versa  $\nu_{j \rightarrow i}$ . In equilibrium we have no net flux between the states, so:  $p_i \nu_{i \rightarrow j} = p_j \nu_{j \rightarrow i}$ . Putting this into equation (1.12) we get

$$\frac{p_i}{p_j} = \frac{\nu_{j \rightarrow i}}{\nu_{i \rightarrow j}} = e^{\frac{E_j - E_i}{k_B T}}. \quad (1.13)$$

Now we consider a constraint:  $\forall E_i \geq E_j : \nu_{i \rightarrow j} = 1$ . This means if the potential energy at position  $j$  is smaller than the one at position  $i$ , it is favorable for the atom to jump from  $j$  to  $i$  (downhill jump) and it will always do so. For the jump frequency from the lower energetic state to the higher (uphill jump), this leads to:

$$\nu_{j \rightarrow i} = e^{\frac{E_j - E_i}{k_B T}} (\forall E_i < E_j). \quad (1.14)$$

Now if we only consider one single time step, the jump frequency gives the probability  $\omega$  for the atom to jump ( $\omega_{ji} = \nu_{j \rightarrow i} \cdot dt$ ). For further treatment we imagine that atoms attempt to jump to another lattice site with a frequency  $\nu_0$ , however not all jump attempts are successful. In the discussed case this leads to:

$$\forall E_i \geq E_j : \nu_{i \rightarrow j} = \nu_0 \text{ and } \forall E_i \leq E_j : \nu_{i \rightarrow j} = \nu_0 \cdot e^{\frac{E_j - E_i}{k_B T}}$$

### 1.3.3 Macroscopic types of diffusion

Depending on the system in question (whether it is a pure metal or an alloy with a certain concentration of different components) we can distinguish between different kinds of diffusion, each having a specific diffusion constant  $D$ . Here I will shortly introduce the most important ones, giving a summary of [MEHRER, 2007].

If all atoms in the lattice are identical, it is not possible to distinguish between them, hence it is not possible to measure diffusion. We can, however, introduce atoms with the same chemical behavior which are distinguishable, namely isotopes. Isotopes can be measured by Mössbauer spectroscopy (usually  $^{57}\text{Fe}$  but also possible for some other elements) or, if they are radioactive, they can be tagged by their radiation. Neutrons are in general sensitive to the number of nucleons in the nucleus and can therefore also be used to distinguish between isotopes.

Measurement of diffusion with small quantities of distinguishable isotopes (down to ppm) is called a tracer diffusion experiment.

### Self diffusion

Let us start by considering a pure metal. One can use tracer diffusion to investigate the behavior of the atoms. The concentration of detectable isotopes should not be too high. Although the different isotopes of one element have the same electron configuration and therefore the same interaction potentials, they have different mass which can have an influence.

Also for a homogeneous alloy with a concentration  $A_x$  and  $B_{1-x}$  two tracer self diffusion coefficients can be defined. In this case it is even more important not to introduce too many detectable isotopes because this would change the mixing ratio. In general the tracer self diffusion coefficients of the two elements are not the same and differ from the self diffusion coefficients of the pure elements.

### Impurity diffusion

A small quantity of a substance  $C$  in a pure metal  $A$  but also in a homogeneous alloy ( $A + B$ ) is called an impurity. These impurity atoms can diffuse on the lattice and can again be measured by tracer diffusion experiments. The corresponding diffusion coefficient is called impurity diffusion coefficient or also foreign diffusion coefficient.

### Interdiffusion

Let us consider two alloys with a different concentration of components. The easiest case would be to have one pure metal of the one kind, and a second of another. If the two components are brought into contact, diffusion can take place due to the concentration gradient until the minimization principle of free energy is met. One can perform a diffusion experiment by measuring the quantity of one component having diffused into the other at certain times. Usually this is done by evaluating the concentrations layer by layer parallel to the interface.

How can this be described more quantitatively? Let us consider a volume with a certain concentration gradient. Let the concentration in direction  $x$  be  $c(x)$ . Now if we move into the direction parallel to the gradient, after a distance of  $\Delta x$  we get a concentration: Although

$$c(x + \Delta x) = c(x) + \frac{\partial c}{\partial x} \Delta x$$

Let us consider that the particles have a certain frequency for changing their position  $\nu_0$ . If there is a force field  $F$  parallel to the concentration gradient, the particles are more likely to move in a preferred direction, dependent on the force. So let there be a jump frequency  $\nu_{12} = \nu_0 p$  into the forward direction and  $\nu_{21} = \nu_0 p^{-1}$  backwards.  $p$  is determined by the transition state theory and given as

$$p = e^{\frac{F \Delta x}{2k_B T}}$$

The number of particles sitting in a one-dimensional volume  $\Delta x$  is given by  $n_1$  in  $x$  and  $n_2$  in  $x + \Delta x$ . The net flux is  $n_1$  times the frequency the atoms jump from  $x$  to  $x + \Delta x$  minus vice versa.

$$j = n_1 \nu_{12} - n_2 \nu_{21}$$

Putting in above values we get:

$$j = c(x) \cdot \Delta x \cdot \nu_0 \cdot p - c(x + \Delta x) \cdot \Delta x \cdot \nu_0 \cdot p^{-1}$$

Expanding for  $p$  and for  $c(x + \Delta x)$  leads to:

$$j = c(x) \cdot \Delta x \cdot \nu_0 \left(1 + \frac{F \Delta x}{2k_B T}\right) - \left(c(x) + c'(x) \Delta x\right) \cdot \Delta x \cdot \nu_0 \left(1 - \frac{F \Delta x}{2k_B T}\right)$$

So we get:

$$\begin{aligned} j &= \nu_0 \Delta x \left( c(x) \left(1 + \frac{F \Delta x}{2k_B T} - 1 + \frac{F \Delta x}{2k_B T}\right) - c'(x) \Delta x \cdot \left(1 - \frac{F \Delta x}{k_B T}\right) \right) \\ &= \nu_0 \Delta x \left( c(x) \frac{F \Delta x}{k_B T} - c'(x) \left( \Delta x - \underbrace{\Delta x \frac{F \Delta x}{k_B T}}_{\rightarrow 0} \right) \right) \end{aligned}$$

Now we introduce a constant  $\tilde{D} = \nu_0 \Delta x^2$ . This is, in this case, the interdiffusion constant. Putting all this together into the equation for the flux we get equation (1.15) which is the first of Fick's laws.

$$j = -\tilde{D} \frac{\partial c(x)}{\partial x} + \tilde{D} \frac{F}{k_B T} c(x) \quad (1.15)$$

Using the continuity equation  $\frac{\partial c(x,t)}{\partial t} = -\frac{\partial j(x,t)}{\partial x}$  we can convert equation (1.15) to equation (1.16) which is the second of Fick's laws.

$$\frac{\partial c}{\partial t} = \tilde{D} \frac{\partial^2 c}{\partial x^2} - \frac{\tilde{D} F}{k_B T} \frac{\partial c}{\partial x} \quad (1.16)$$

Fick's laws are not only valid for interdiffusion. The empirical connection between the self-diffusion and the interdiffusion constants was given by Darken [DARKEN, 1948]:

$$\tilde{D} = C_B \hat{V}_B D_A^I + C_A \hat{V}_A D_B^I \quad (1.17)$$

Here  $C_i$  is the concentration of the element in the alloy,  $D_i^I$  is the self-diffusion coefficient in the alloy with the given concentration and  $\hat{V}_i$  gives the partial molar volumes.

### 1.3.4 Chemical diffusion

Chemical diffusion is sometimes used as a synonym for interdiffusion. I will treat the term a little more specifically. While interdiffusion corresponds to a concentration gradient at a macroscopic scale, I will use chemical diffusion for a similar process on a microscopic scale. Due to statistical mechanics, variations in the local concentration can be possible. Averaging over big enough areas in the sample will get rid of this variations and one will get a homogeneous concentration. On the microscopic scale however these fluctuations can lead to diffusion.

### 1.3.5 Diffusion mechanisms

The important mechanism for this thesis is the vacancy mechanism. Vacancy defects are fairly common in real lattices. Let us consider a simple cubic lattice. If we pick out a particular unit cell, we have one atom in every corner. If one atom is missing we have a hole in the lattice. This is called a vacancy. They can form due to an imperfect mixing ratio of two types of atoms in an alloy, at phase boundaries, but also because of the thermodynamic activity. An atom from another site in the lattice (usually a next neighbor atom) can now jump into that vacancy under certain conditions (see section 1.3.2).

The longer its jumping vector the more unlikely a jump gets. Therefore the dominating mechanism is nearest neighbor jumps.

### Correlation of jumps

As stated above, the probability of an atomic jump is given by the kinetic energy of the atoms and by the energetic barrier they have to overcome. This means that the history of how the system evolved is not of interest. So we have strict Markov behavior. But is this really the case?

If we consider a lattice with very few vacancies and a vacancy mechanism of diffusion we get the following picture: if a vacancy is in a next neighbor site of an atom, the atom is due to jump with a certain possibility. On the other hand, if there is no vacancy nearby, the atom is to remain where it is for as many jumps as it takes a vacancy to come by. This however means that after an atom has already switched its position with a vacancy it is likely to switch back. Therefore an atom which has already jumped is more likely to jump again than any arbitrary atom (including all the atoms with no vacancy nearby).

This of course, from the atoms point of view, would mean that the history is important and we therefore would have a non Markov behavior. Now let's

consider a system with very few vacancies. If a vacancy is in the neighborhood of an atom the atom jumps frequently until the vacancy leaves. The major part of the lattice however remains static during that time. Therefore one can distinguish two timescales. The first is the vacancy changing neighborhood. On the second timescale a chain of atomic jumps take place when a vacancy encounters an atom. This chain of jumps can lead to the atom ending up where it started after the encounter, but it can also lead to effective nearest or further neighbor displacements. The relation between the effective jump rate  $\tau_{\text{eff}}^{-1}$  and the atomic jump rate  $\tau^{-1}$  with the number of jumps within an encounter  $Z_{\text{eff}}$  can be given as [HEITJANS and KÄRGER, 1998]:

$$\frac{1}{\tau_{\text{eff}}} = \frac{1}{\tau \cdot Z_{\text{eff}}}$$

We can now treat each complete encounter as one effective jump which leads again to Markov behavior. This is the case as long as one encounter includes only one vacancy. Usually the number of vacancies in a lattice is very low compared to the number of atoms ( $10^{-7}$ ). So the encounter model is valid. For greater numbers of vacancies, e.g. at higher temperatures this is, however, not the case. As in the encounter model a next-nearest neighbor jump is seen as two nearest neighbor jumps, its probability ( $p_{3N}$ ) can be seen as the sum over the product of possibilities of two particular nearest neighbor jumps:

$$p_{3N} = \sum p_{NN_1} \cdot p_{NN_2}$$

This explains why with increasing length of the jump vector the jump gets less probable as stated above.

Another type of diffusion mechanism that should be mentioned is the interstitial mechanism. Small atoms, e.g. hydrogen or carbon, can diffuse on a sub-lattice in between the atoms of the main components on the main lattice. In this case we usually have a very low number of interstitial atoms. We can now consider the free spaces on the interstitial lattice as a great number of vacancies. This leads to Markov behavior for small numbers of interstitial atoms as it is very unlikely for them to interact with each other. Of course with a growing number of interstitial atoms this does not hold any more.

Other diffusion mechanisms are possible but further details would go beyond the scope of this introduction.

## 1.4 Arrhenius theory

We can see from equation (1.14) that the jump probability does depend on the temperature. So does the diffusion coefficient  $D$ , as it is directly proportional

to the jump frequency  $\nu$ . This behavior was first treated by Arrhenius. I will give a short summary. The reaction rate constant is proportional to the Boltzmann factor with a constant  $A$  and the activation energy  $E_a$ :

$$k = A \cdot e^{\frac{-E_a}{RT}} \quad (1.18)$$

$R$  is the Reynolds number, as the theory originates from chemistry and was therefore used for units of mole. We can easily convert to atoms by using the Boltzmann constant  $k_B$  instead. With a simple two parameter fit one gets the activation energy.

## 1.5 The Correlation Functions

Let us consider a lattice where diffusion takes place. The atoms move around and we can interpret each lattice configuration at a certain point in time as one particular state  $\sigma$ . As we consider a Bravais lattice, the atoms sit at certain positions, given by their position vector  $\vec{a}$ . We have three different guys on our lattice. Atoms of types  $A$  and  $B$  and vacancies ( $V$ ). I introduce a function  $\vec{\sigma}$  to describe the state of the lattice at a certain point in time  $t$ . The entries of  $\vec{\sigma}$  give the information which atom sits at a site  $\vec{a}$ .

$$(\vec{\sigma})_i(\vec{a}, t) = \begin{cases} 0 & \text{if not } i \text{ at } \vec{a} \\ 1 & \text{if } i \text{ at } \vec{a} \end{cases} \quad (1.19)$$

For example, if we have an  $A$  atom at  $\vec{a}$  we have  $(\vec{\sigma})_A(\vec{a}, t) = 1$ ,  $(\vec{\sigma})_B(\vec{a}, t) = 0$  and  $(\vec{\sigma})_V(\vec{a}, t) = 0$ , therefore:

$$\vec{\sigma}(\vec{a}, t) = \begin{pmatrix} 1 \\ 0 \\ 0 \end{pmatrix}$$

We can obtain information about the movement in the lattice by comparing these states for certain times. The relative vector between two sites is denoted as  $\Delta\vec{a} = \vec{a}_2 - \vec{a}_1$ . Now let us consider an  $A$  atom that jumps from  $\vec{a}_1$  to  $\vec{a}_2$  in the time  $\Delta t$ . As we consider the vacancy mechanism, this can only happen if  $(\vec{\sigma})_V(\vec{a}_2, t) = 1$ :

$$\left| \begin{array}{l} \text{before jump} \\ \vec{\sigma}(\vec{a}_1, t) = \begin{pmatrix} 1 \\ 0 \\ 0 \end{pmatrix} \\ \vec{\sigma}(\vec{a}_2, t) = \begin{pmatrix} 0 \\ 0 \\ 1 \end{pmatrix} \end{array} \right| \left| \begin{array}{l} \text{after jump} \\ \vec{\sigma}(\vec{a}_1, t + \Delta t) = \begin{pmatrix} 0 \\ 0 \\ 1 \end{pmatrix} \\ \vec{\sigma}(\vec{a}_2, t + \Delta t) = \begin{pmatrix} 1 \\ 0 \\ 0 \end{pmatrix} \end{array} \right|$$



Noting that  $(\vec{\sigma})_i(\vec{a}_2, t) = (\vec{\sigma})_i(\vec{a}_1 + \Delta\vec{a}, t)$ , we can use this to define the correlation functions as:

$$G_{ij}(\Delta\vec{a}, \Delta t) = \langle (\vec{\sigma})_i(\vec{a}, t) (\vec{\sigma})_j(\vec{a} + \Delta\vec{a}, t + \Delta t) \rangle \quad (1.20)$$

with  $i, j = A, B$  or  $V$ .

The important information for scattering experiments lies in the distribution of scatterers in space. With X-ray experiments the scatterers are electrons. The number of electrons for different types of atoms is given by  $Z_i$ . With this the electron correlation function can be defined as:

$$\begin{aligned} G_e(\Delta\vec{a}, \Delta t) = & Z_A^2 \cdot G_{AA} + Z_A Z_B \cdot G_{AB} \\ & + Z_A Z_B \cdot G_{BA} + Z_B^2 \cdot G_{BB} \end{aligned} \quad (1.21)$$

Note that all terms including  $G_{iV}$  or  $G_{Vi}$  are zero for  $Z_V = 0$ . We can then define the intermediate scattering function as the Fourier transform of the electron correlation function:

$$I(\vec{q}, t) := \mathcal{F}(G_e(\Delta\vec{a}, \Delta t)) \quad (1.22)$$

In order to find  $G_e$  we need to find the time evolution of the probability to find the lattice in a certain state. We consider an ensemble of systems and  $\langle . \rangle$  denotes the averaging over the ensemble. Let us take the average of  $\sigma_i$  over the ensemble and call it  $p_i$ . As we consider the vacancy mechanism, atoms can only jump if a vacancy is nearby, leading to jump frequencies of  $\nu_{iV} = \nu_{Vi}$  with  $i = A, B$ . Therefore the time evolution of the probabilities is given as:

$$\begin{aligned} \frac{\partial}{\partial t} \begin{pmatrix} p_A \\ p_B \\ p_V \end{pmatrix} (\vec{a}, t) = & \left\langle \sum_{\Delta\vec{a}} \begin{pmatrix} \sigma_A(\vec{a} + \Delta\vec{a}, t) \cdot \sigma_V(\vec{a}, t) \nu_{AV} - \sigma_A(\vec{a}, t) \cdot \sigma_V(\vec{a} + \Delta\vec{a}, t) \nu_{AV} \\ \sigma_B(\vec{a} + \Delta\vec{a}, t) \cdot \sigma_V(\vec{a}, t) \nu_{BV} - \sigma_B(\vec{a}, t) \cdot \sigma_V(\vec{a} + \Delta\vec{a}, t) \nu_{BV} \\ \sigma_V(\vec{a} + \Delta\vec{a}, t) \cdot (\sigma_A(\vec{a}, t) \nu_{AV} + \sigma_B(\vec{a}, t) \nu_{BV}) \\ - \sigma_V(\vec{a}, t) \cdot (\sigma_A(\vec{a} + \Delta\vec{a}, t) \nu_{AV} + \sigma_B(\vec{a} + \Delta\vec{a}, t) \nu_{BV}) \end{pmatrix} \right\rangle \end{aligned} \quad (1.23)$$

Unfortunately equation (1.23) can not be solved analytically. We have to adopt some simplifications. If we assume  $\sigma_V$  to be a constant and the number of vacancies to be very low, so that we can write  $\sigma_B = 1 - \sigma_A$ , we can simplify 1.23 leading to a conceptual formulation consistent with the derivation in the following section.

Because of the low number of vacancies, the contrast is only determined by the difference between  $Z_A$  and  $Z_B$ . By subtracting  $Z_B$  we can rewrite equation (1.21) as:

$$\begin{aligned} G_e(\Delta\vec{a}, \Delta t) &= (Z_A - Z_B)(Z_A - Z_B) \cdot G_{AA} + \text{const} \\ \frac{G_e(\Delta\vec{a}, \Delta t)}{(Z_A - Z_B)^2} - \text{const}^* &= G_{AA} \end{aligned} \quad (1.24)$$

The correlation function is further connected to the coherent scattering function via another one in the time regime [HEMPELMANN, 2000].

$$S(\vec{q}, \omega) := \tilde{I}(\vec{q}, \omega) = \mathcal{F}(\tilde{G}_e(\Delta\vec{a}, \omega))$$

I also define:

$$\mathcal{J}(\vec{q}, t) = \mathcal{F}(G_{AA}(\Delta\vec{a}, t)) \quad (1.25)$$

It can easily be shown that  $I(\vec{q}, t)$  and  $\mathcal{J}(\vec{q}, t)$  differ only by a constant factor, so they describe the same physical behavior. In the following I will only use  $\mathcal{J}$  as the intermediate scattering function and I will use  $G(\Delta\vec{a}, t) = G_{AA}(\Delta\vec{a}, t)$ . The next step is to determine what the intermediate scattering function looks like.

### 1.5.1 Finding the amplitude correlation function

The first person to treat the relation between the pair distribution function  $g(\vec{r})$  and time to describe the distribution of particles in space and time was [VAN HOVE, 1954].

Here I will give a different approach. In order to simplify things I will treat the case of a Bravais lattice from the beginning. I will also disregard interaction between the particles, meaning that the jump probability for an atom ( $\omega$ ) does not depend on its neighbors. We will only treat one type of atom, for example A-atoms. Let us denote the probability density for an A-atom to be at  $\vec{a}$  at time  $t$  by  $P(\vec{a}, t)$ . The evolution of this function over time is then given by the number of atoms which do not leave their lattice site (with a probability of  $1 - \omega$ ) plus the sum over all atoms jumping from  $\vec{a} - \Delta\vec{a}$  to  $\vec{a}$ .

$$P(\vec{a}, t + \Delta t) \approx P(\vec{a}, t) \left( 1 - \sum_{\Delta\vec{a}} \omega(\Delta\vec{a}) \right) + \sum_{\Delta\vec{a}} P(\vec{a} - \Delta\vec{a}, t) \omega(\Delta\vec{a}) \quad (1.26)$$

The probability for an atom to leave its lattice site in time  $\Delta t$  is given by its normalized jump frequency  $\hat{\nu}$  multiplied with the time interval.

$$\omega(\Delta\vec{a}) = \hat{\nu}(\Delta\vec{a}) \Delta t$$

Rearranging this equation and using the explicit form of the jump probability we get:

$$\frac{P(\vec{a}, t + \Delta t) - P(\vec{a}, t)}{\Delta t} \approx \sum_{\Delta \vec{a}} (-\hat{\nu}(\Delta \vec{a})) P(\vec{a}, t) + \sum_{\Delta \vec{a}} \hat{\nu}(\Delta \vec{a}) P(\vec{a} - \Delta \vec{a}, t)$$

The limit  $t \rightarrow 0$  gives a differential equation:

$$\frac{dP(\vec{a}, t)}{dt} = \sum_{\Delta \vec{a}} \hat{\nu}(\Delta \vec{a}) (-P(\vec{a}, t) + P(\vec{a} - \Delta \vec{a}, t))$$

We can solve this by using a Fourier transform in the space regime:

$$\begin{aligned} \frac{d\mathcal{F}(P)(\vec{q}, t)}{dt} &= \sum_{\Delta \vec{a}} \hat{\nu}(\Delta \vec{a}) (-\mathcal{F}(P(\vec{a}, t)) + \mathcal{F}(P(\vec{a} - \Delta \vec{a}, t))) \\ &= \sum_{\Delta \vec{a}} \hat{\nu}(\Delta \vec{a}) (-1 \cdot \int d\vec{a} P(\vec{a}, t) e^{-i \cdot \vec{a} \cdot \vec{q}} + \int d\vec{a} P(\vec{a} - \Delta \vec{a}, t) e^{-i \cdot \vec{a} \cdot \vec{q}}) \\ &= \sum_{\Delta \vec{a}} \hat{\nu}(\Delta \vec{a}) (-1 \cdot \int d\vec{a} P(\vec{a}, t) e^{-i \cdot \vec{a} \cdot \vec{q}} + \int d\vec{a}' P(\vec{a}', t) e^{-i \cdot (\vec{a}' + \Delta \vec{a}) \cdot \vec{q}}) \\ &= \sum_{\Delta \vec{a}} \hat{\nu}(\Delta \vec{a}) \mathcal{F}(P)(\vec{q}, t) (-1 + e^{-i \vec{q} \cdot \Delta \vec{a}}) \end{aligned} \quad (1.27)$$

For every vector  $\Delta \vec{a}$  there exists a fellow with the same absolute value, pointing into the opposite direction and therefore the same  $\omega$ . So we can write:

$$\sum_{\Delta \vec{a}} e^{i \Delta \vec{a} \cdot \vec{q}} = \sum_{\Delta \vec{a}_i}^{N/2} (e^{i \Delta \vec{a}_i \cdot \vec{q}} + e^{-i \Delta \vec{a}_i \cdot \vec{q}}) = \sum_{\Delta \vec{a}_i}^{N/2} 2 \cdot \cos(\Delta \vec{a}_i \cdot \vec{q}) = \sum_{\Delta \vec{a}}^N \cos(\Delta \vec{a} \cdot \vec{q})$$

We can solve this differential equation and get:

$$\mathcal{F}(P)(\vec{q}, t) = e^{\sum_{\Delta \vec{a}} \hat{\nu}(\Delta \vec{a}) (\cos(\vec{q} \cdot \Delta \vec{a}) - 1) t + \text{const.}} \quad (1.28)$$

As a boundary condition we choose to know the position of a certain atom at a certain point in time. We choose the atom to sit at  $\vec{a} = \vec{0}$  at the time  $t_0 = 0$ . The probability for the same sort of atom to be at a certain site is given by the atomic concentration  $c_i$  and therefore constant. The boundary condition can be written as:

$$P(\vec{a}, t_0) = \delta(\vec{a})(1 - c_i) + c_i \quad (1.29)$$

As the Fourier transform of a constant is a delta function, it only adds to the zero reflex and not to the speckle pattern. Using the boundary condition 1.29 on equation (1.28) we get:

$$\mathcal{F}(P)(\vec{q}, t) = e^{\sum_{\Delta \vec{a}} \hat{\nu}(\Delta \vec{a}) (\cos(\vec{q} \cdot \Delta \vec{a}) - 1) t} \quad (1.30)$$

If we choose the atom to sit at  $\vec{0}$  at  $t_0$  to be the one with the greater scattering length (therefore the one with bigger  $Z$ ), we can see that  $P(\vec{a}, t)$  is equal to the pair correlation function. So we can write:

$$\mathcal{J}(\vec{q}, t) = \mathcal{F}(G(\vec{q}, t)) = \mathcal{F}(P)(\vec{q}, t) = e^{\sum_{\Delta\vec{a}} \hat{\nu}(\Delta\vec{a})(\cos(\vec{q} \cdot \Delta\vec{a} - 1))t} \quad (1.31)$$

The incoherent line width  $\Gamma_{\text{inc}}$  can be defined as:

$$\Gamma_{\text{inc}} = \sum_{\Delta\vec{a}} \hat{\nu}(\Delta\vec{a})(1 - \cos(\vec{q} \cdot \Delta\vec{a})) \quad (1.32)$$

Leading to:

$$\mathcal{J}(\vec{q}, t) = e^{-\Gamma_{\text{inc}} \cdot t} \quad (1.33)$$

As shown in chapter 1.1.1 the amplitude of the electromagnetic wave is connected to the density distribution via a Fourier transform. Therefore the amplitude of a wave originating from a certain atom at site  $\vec{a}$  is proportional to the Fourier transform of the state function.

$$A(\vec{q}, t) \propto \mathcal{F}(\sigma)(\vec{q}, t) \quad (1.34)$$

With equation (1.20) for  $AA$  and a Fourier transformation in the space regime we get <sup>1</sup>:

$$\begin{aligned} \mathcal{J}(\vec{q}, \Delta t) &= \mathcal{F}_{\Delta\vec{a}}(G(\Delta\vec{a}, \Delta t)) \\ &= \mathcal{F}_{\Delta\vec{a}}(\langle \sigma(\vec{a}, t) \sigma(\vec{a} + \Delta\vec{a}, t + \Delta t) \rangle) \\ &= \mathcal{F}_{\Delta\vec{a}}\left(\left\langle \frac{1}{V} \int d\vec{a} \sigma(\vec{a}, t) \sigma(\vec{a} + \Delta\vec{a}, t + \Delta t) \right\rangle\right) \\ &= \mathcal{F}_{\Delta\vec{a}}\left(\frac{1}{V} \left\langle \int d\vec{a}' \sigma(\vec{a}' - \Delta\vec{a}, t) \sigma(\vec{a}', t + \Delta t) \right\rangle\right) \\ &= \mathcal{F}_{\Delta\vec{a}}\left(\frac{1}{V} \langle (\sigma(-\vec{a}', t) *_{\vec{a}'} \sigma(\vec{a}', t + \Delta t))(\Delta\vec{a}) \rangle\right) \\ &= \frac{1}{V} \langle \mathcal{F}(\sigma)(-\vec{q}, t) \cdot \mathcal{F}(\sigma)(\vec{q}, t + \Delta t) \rangle \\ &= \frac{1}{V} \langle \mathcal{F}(\sigma)(\vec{q}, t)^* \cdot \mathcal{F}(\sigma)(\vec{q}, t + \Delta t) \rangle \end{aligned} \quad (1.35)$$

Using 1.34 this leads to:

$$\mathcal{J}(\vec{q}, \Delta t) = \frac{\langle A(\vec{q}_0, t) A(\vec{q}_0 + \vec{q}, t + \Delta t)^* \rangle}{C} \quad (1.36)$$

---

<sup>1</sup> \* denotes the convolution

### 1.5.2 Connecting amplitude- and intensity correlation function

We get a normalized amplitude correlation function by dividing by the average intensity. It is defined as (1.37). We can also define the normalized intensity correlation function as (1.38).

$$\mathcal{J}^{(1)}(\Delta t) = \frac{\langle A(t) \cdot A(t + \Delta t)^* \rangle}{\langle A(t) \cdot A(t)^* \rangle} \quad (1.37)$$

$$\mathcal{J}^{(2)}(\Delta t) = \frac{\langle I(t) \cdot I(t + \Delta t) \rangle}{\langle I(t) \rangle} \quad (1.38)$$

We will now show how those two are connected.

The intensity over all atoms at a certain time is given by:

$$I(t) = \sum_{i,j} A_i(t) A_j(t)^* \quad \text{and} \quad I(t + \Delta t) = \sum_{k,l} A_k(t + \Delta t) A_l(t + \Delta t)^*$$

So the unnormalized intensity correlation function  $\hat{\mathcal{J}}^{(2)}$  can be written as:

$$\hat{\mathcal{J}}^{(2)} = \sum_{i,j,k,l} \langle A_i(t) A_j(t)^* A_k(t + \Delta t) A_l(t + \Delta t)^* \rangle \quad (1.39)$$

In the following I will consider domains of atoms emitting spherical waves. The amplitudes of these waves within the domain are correlated, but if we compare the total amplitude with one of another domain, we see that these amplitudes are distributed randomly, as long as we have enough sources. This means, to be concrete, that the sample in question must be emitting radiation from an area big enough to contain a sufficient number of domains. So the probability for one domain to have a certain amplitude is independent from the other domains.

Let  $p_A^i(t)$  be the probability density for domain  $i$  to have a certain amplitude  $A_i$  and  $p_A^j(t)$  the probability for domain  $j$  for any other  $A_j$ . The probability for the two particular domains to have the particular amplitudes  $A_i$  and  $A_j$  is then  $p_A^{i,j}(t)$  which is the product of the single probabilities  $p_A^{i,j}(t) = p_A^i(t) \cdot p_A^j(t)$ . Therefore the expectation value of a product of amplitudes for different domains (  $\langle \sum_{i,j} p_A^i(t) A_i \cdot p_A^j(t) A_j \rangle$  ) can be written as the product of expectation values.

We will now carry out a case-by-case analysis. First we assume one of the domains to differ from all three others. Let w.l.o.g.  $i \neq j$  and  $i \neq k$  and  $i \neq l$ . As  $\langle A_i(t) \rangle = 0$ , we conclude that all cases implying this possibility are equal to zero. Next we have to distinguish the cases where two domains

are equal. If one pair is equal the other has to be equal as well. Otherwise one domain would differ from all others and we would be back at our first conclusion. The possible cases are:

$$i = j \text{ and } k = l, i \neq k$$

$$i = k \text{ and } j = l, i \neq j$$

$$i = l \text{ and } j = k, i \neq j$$

Next we examine the case where three domains are equal. If the fourth domain is different, we are back at our first conclusion. This leaves only the case where all domains are equal:

$$i = j = k = l$$

As a result we can rewrite equation (1.39) as:

$$\begin{aligned} \hat{\mathcal{J}}^{(2)} = & \sum_i \langle A_i(t) A_i(t)^* \rangle \sum_k \langle A_k(t + \Delta t) A_k(t + \Delta t)^* \rangle \\ & + \sum_i \langle A_i(t) A_i(t + \Delta t) \rangle \sum_j \langle A_j(t)^* A_j(t + \Delta t)^* \rangle \\ & + \sum_i \langle A_i(t) A_i(t + \Delta t)^* \rangle \sum_j \langle A_j(t)^* A_j(t + \Delta t) \rangle \\ & + \sum_i \langle A_i(t) A_i(t + \Delta t)^* A_i(t)^* A_i(t + \Delta t) \rangle \end{aligned}$$

Rearranging this equation and renaming some indices leads to:

$$\begin{aligned} \hat{\mathcal{J}}^{(2)} = & \sum_{i \neq j} (\langle A_i(t) A_i(t)^* \rangle \cdot \langle A_j(t + \Delta t) A_j(t + \Delta t)^* \rangle \\ & + \langle A_i(t) A_i(t + \Delta t) \rangle \cdot \langle A_j(t)^* A_j(t + \Delta t)^* \rangle \\ & + \langle A_i(t) A_i(t + \Delta t)^* \rangle \cdot \langle A_j(t)^* A_j(t + \Delta t) \rangle) \\ & + \sum_i \langle A_i(t) A_i(t + \Delta t)^* A_i(t)^* A_i(t + \Delta t) \rangle \end{aligned}$$

It can be seen that the terms with pairs are proportional to  $N^2$  while the expression with four equal domains is proportional to  $N$ . Therefore, for a large number of domains, the last term can be neglected.

So let us investigate the remaining terms. In the first term we have  $\langle A_i(t) A_i(t)^* \rangle = \langle |A_i(t)|^2 \rangle$ . The same is valid, of course, for the part with  $\Delta t$ . We can rewrite this term as:

$$\sum_{i \neq j} \langle |A_i(t)|^2 \rangle \cdot \langle |A_j(t + \Delta t)|^2 \rangle = \langle I(t) \rangle \cdot \langle I(t + \Delta t) \rangle$$

Now we regard the next term. Noting that the phase factor  $\phi$  is not correlated with the modulus, we can write:

$$\begin{aligned}\langle A_i(t)A_i(t + \Delta t) \rangle &= \langle |A_i(t)|e^{i\phi} \cdot |A_i(t + \Delta t)|e^{i(\phi + \Delta\phi)} \rangle \\ &= \langle e^{i2\phi} \rangle \langle |A_i(t)| \cdot |A_i(t + \Delta t)|e^{i\Delta\phi} \rangle\end{aligned}$$

The phase factor is randomly distributed, so  $\langle e^{i2\phi} \rangle = 0$ . Therefore this term is zero.

Taking all this into account we get a more clearly arranged relation:

$$\hat{\mathcal{J}}^{(2)} = \langle I(t) \rangle \cdot \langle I(t + \Delta t) \rangle + \sum_{i \neq j} \langle A_i(t)A_i(t + \Delta t)^* \rangle \cdot \langle A_j(t)^*A_j(t + \Delta t) \rangle$$

We can rewrite equation (1.37) as:

$$\mathcal{J}^{(1)}(\Delta t) = \frac{\sum i \langle A_i(t) \cdot A_i(t + \Delta t)^* \rangle}{\langle A(t) \cdot A(t)^* \rangle}$$

Therefore we get:

$$\begin{aligned}\hat{\mathcal{J}}^{(2)} &= \langle I(t) \rangle \cdot \langle I(t + \Delta t) \rangle + \mathcal{J}^{(1)} \langle I(t) \rangle \cdot \mathcal{J}^{(1)*} \langle I(t) \rangle \\ \mathcal{J}^{(2)} &= \frac{\mathcal{G}^{(2)}}{\langle I(t) \rangle^2} = \frac{\langle I(t) \rangle^2 + |\mathcal{J}^{(1)}|^2 \langle I(t) \rangle^2}{\langle I(t) \rangle^2} \\ \mathcal{J}^{(2)} &= 1 + |\mathcal{J}^{(1)}|^2\end{aligned}\tag{1.40}$$

Now, if we define:

$$\Gamma_{\text{inc}} = \frac{1}{\tau}$$

we can write the amplitude correlation function as:

$$\mathcal{J}^{(1)} = e^{-\frac{t}{\tau}}\tag{1.41}$$

Using equation (1.40) and 1.41 we get  $\mathcal{J}^{(2)} = 1 + (e^{-\frac{t}{\tau}})^2$ . The baseline can slightly differ from one, due to effects discussed later on, so we write the intensity correlation function as:

$$\mathcal{J}^{(2)} = c + e^{-\frac{2 \cdot t}{\tau}}\tag{1.42}$$

## Chapter 2

# Preparing the sample

As stated before, XPCS is a very comprehensive method and can be used, at least in the future, on a variety of systems. The systems of interest in this thesis are nickel based. In order to get a relatively high electronic contrast (see (1.24)), we used alloys of nickel ( $Z = 28$ ) and platinum ( $Z = 78$ ), but also a nickel - palladium ( $Z = 46$ ) alloy. Three types of alloys were made:  $\text{Ni}_{97}\text{Pt}_3$ ,  $\text{Ni}_{60}\text{Pt}_{40}$  and  $\text{Ni}_{72}\text{Pd}_{28}$ .

To perform a successful scattering experiment, the samples must have the right thickness. If they are too thick, too much of the intensity is absorbed and one does not get a signal on the detector. On the other hand, if they are too thin the beam passes right through without enough interaction. The experiments are performed in transmission geometry with the sample perpendicular to the beam. The transmission of intensity is determined by the thickness of the sample  $d$  and the attenuation coefficient  $\mu$ . Calculation of the scattered radiation exiting the sample for a certain angle of incidence ( $2\Theta$ ) can be found in appendix A.2 and results in:

$$I(2\Theta) = I_0 \cdot \frac{e^{-\mu \frac{d}{\cos(2\Theta)}} - e^{-\mu d}}{\mu \left(1 - \frac{1}{\cos(2\Theta)}\right)} \quad (2.1)$$

The attenuation coefficient  $\mu$  depends on the cross section, the density of the matter and the energy of the radiation. For further reading see [HENKE et al., 1993]. We can now obtain the optimal sample thickness from equation (2.1) by minimization:

$$\frac{\partial I(2\Theta)}{\partial d} = 0,$$

leading to:

$$d(2\Theta) = \frac{\ln(\cos(2\Theta))}{\mu \left(1 - \frac{1}{\cos(2\Theta)}\right)} \quad (2.2)$$



The optimal sample thickness can be calculated for solids using the tool provided by *The Center for X-ray Optics of Berkeley*<sup>1</sup>.

## 2.1 Finding the ideal sample thickness

An important parameter for finding the attenuation coefficient is the density of the material. It was calculated, according to Vegards rule [VEGARD, 1921], by looking up the lattice constant<sup>2</sup> and calculating the average weighted by the percentages<sup>3</sup>. As all the three alloys have fcc structure, the density is

	Ni	Pd	Pt
Lattice constant (Å)	3.52	3.89	3.92
Atomic weight (u)	58.71	106.40	195.09
Density at 20°C (g/cm <sup>3</sup> )	8.91	11.99	21.45

**Table 2.1:** Parameters of pure components

then calculated by putting four atoms into the cube. The calculated densities are given in table 2.2. Note that if one would only average over the densities proportional to the portion of the elements, one would get an error of up to 8%.

	Ni <sub>72</sub> Pd <sub>28</sub>	Ni <sub>97</sub> Pt <sub>3</sub>	Ni <sub>60</sub> Pt <sub>40</sub>
Weight per atom (g)	1.20E-22	1.04E-22	1.88E-22
Weight per unit cell (g)	4.79E-22	4.17E-22	7.52E-22
Volume (Å <sup>3</sup> )	47.58	44.06	49.84
Density calc. (g/Å <sup>3</sup> )	1.01E-23	9.47E-24	1.51E-23
Density calc. (g/cm <sup>3</sup> )	10.06	9.47	15.10

**Table 2.2:** Calculated densities for alloys

Using the package provided by the university of Berkeley, the attenuation lengths were calculated as given in table 2.3.

## 2.2 Manufacturing the samples

The alloys were produced by melting the metals in a crucible. The resulting ingots had the form of a spheroid with the length of about four centimeters

<sup>1</sup>[http://henke.lbl.gov/optical\\_constants/](http://henke.lbl.gov/optical_constants/)

<sup>2</sup><http://cst-www.nrl.navy.mil/bind/pd.html>

<sup>3</sup>the densities were taken from WIKIPEDIA and are given in table 2.1

	Ni <sub>72</sub> Pd <sub>28</sub>	Ni <sub>97</sub> Pt <sub>3</sub>	Ni <sub>60</sub> Pt <sub>40</sub>
Ideal thickness $2\Theta = 0^\circ$ ( $\mu\text{m}$ )	9.1	17.2	4.4
Ideal thickness $2\Theta = 20^\circ$ ( $\mu\text{m}$ )	8.5	16.1	4.1

**Table 2.3:** Calculated ideal sample thicknesses at 8 keV

and the diameter of about five millimeters. They were then cut into discs of about one millimeter thickness using a diamond saw. For cold rolling the samples, I used plates of stainless steel.

### 2.2.1 Recrystallizing

The first series of samples was cold rolled and heated repeatedly several times. First the sample was cold rolled to half of its thickness, then it was heat treated at 1000°C. This was repeated until the attenuation length was reached. The images taken with SAXS<sup>4</sup> looked promising, showing an increase in the regime of diffuse scattering and a focusing of intensity along the Debye-Scherrer-rings in spots. Unfortunately we had used a steel mesh as a specimen holder in the heating process, leading to iron and chrome contamination. As the light source at the synchrotron has an energy of 8 keV and the X-ray edge of iron lies at 7.1 keV the samples could not be measured due to the high iron fluorescence. Therefore, at beam-time HS-4228 at the ESRF we had to measure samples that were only cold rolled and not heat treated. Figure 2.1 shows the cold rolled Ni<sub>97</sub>Pt<sub>3</sub> sample in comparison to the heat treated one.

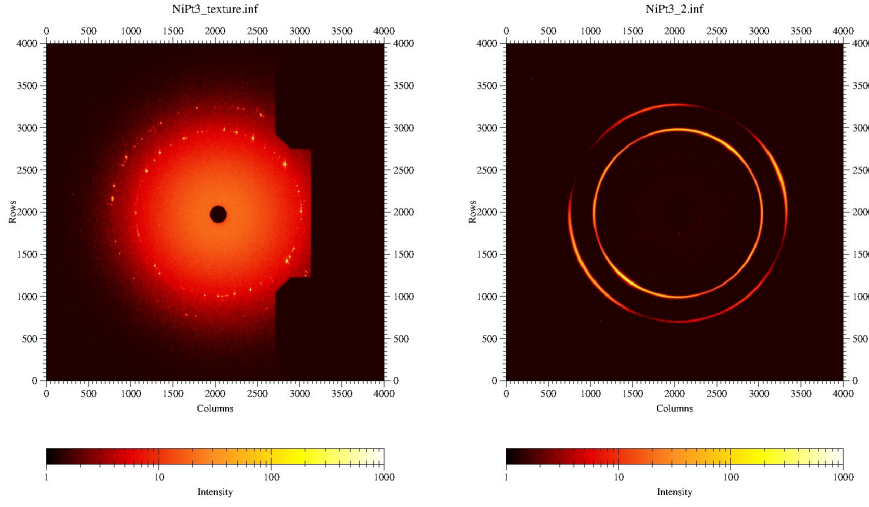
The next generation of samples was cold rolled to the ideal thickness in one step. This was done by repeated cold rolling in one direction, in order to give the sample a preferential orientation. The achieved sample thickness varied slightly due to technical limitations. Table 2.4 gives an overview of the samples and their actual thicknesses.

	Ni <sub>72</sub> Pd <sub>28</sub>	Ni <sub>97</sub> Pt <sub>3</sub>	Ni <sub>60</sub> Pt <sub>40</sub>
Actual sample thickness ( $\mu\text{m}$ )	11	17	6

**Table 2.4:** Achieved sample thickness

The samples were then cleaned in an acetone ultra-sonic bath. In order to achieve recrystallization, the samples were annealed.

<sup>4</sup><http://nanozentrum.univie.ac.at/home/bruker-nanostar/>



(a) First heat treated  $\text{Ni}_{97}\text{Pt}_3$  film sample      (b) Not heat treated cold rolled  $\text{Ni}_{97}\text{Pt}_3$  film

**Figure 2.1:** Wide angle images taken at SAXS with the Image Plate

Heating	Time (h)	Temperature ( $^{\circ}\text{C}$ )
1	20.17	615
2	68.42	615
3	44.92	730

**Table 2.5:** Heating history of  $\text{Ni}_{97}\text{Pt}_3$  thin film

The ideal temperature for the heat treatment is 0.6 times the melting temperature<sup>5</sup>. For both NiPt samples the melting temperature lies at  $1450^{\circ}\text{C}$  so the ideal heating temperature would be at  $760^{\circ}\text{C}$ . For  $\text{Ni}_{72}\text{Pd}_{28}$  where the melting temperature lies at  $1360^{\circ}\text{C}$ , the ideal heating temperature is  $705^{\circ}\text{C}$ . The tables 2.5 to 2.7 give an overview of the heat treatment for the film samples.

After the heat treatment, the film samples were analyzed with SAXS in ultrashort configuration to get the widest angles possible. The images (see figure 2.2) show recrystallization patterns along the first Debye-Scherrer-ring. However Laue diffractometry showed the recrystallized grains to be smaller than the Laue beam (diameter of about 1 mm).

<sup>5</sup>according to Dr. Pichl

Heating	Time (h)	Temperature (°C)
1	17.25	615
2	68.42	615
3	44.92	730

**Table 2.6:** Heating history of  $\text{Ni}_{60}\text{Pt}_{40}$  thin film

Heating	Time (h)	Temperature (°C)
1	20.17	615
2	46.58	615
3	46.33	630
4	138.33	700

**Table 2.7:** Heating history of  $\text{Ni}_{72}\text{Pd}_{28}$  thin film

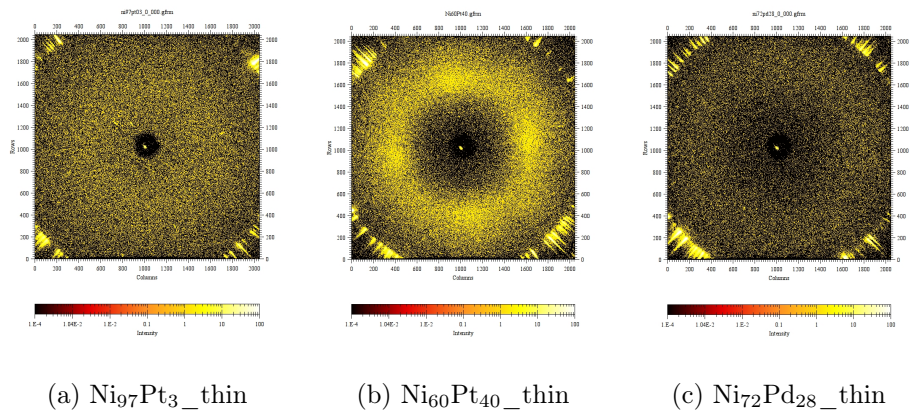


**Figure 2.2:** Wide angle images taken at SAXS

According to [SLAKHORST, 1975] Ni alloy recrystallization can lead to cube grains. For thin film samples this could mean that the single crystal grain cannot become bigger than the thickness of the sample. This is opposed by the idea of the surface having an effect on the recrystallization, leading to all grains orienting parallel to the surface. To determine empirically if the thickness of the sample can constrain the growth, a third generation of samples was created. In order to produce bulk samples with large single crystal grains, discs of a few millimeter thickness were cut. These were then cleaned and heat treated.

The heat cycles for the thick samples are given in table 2.8 to 2.10. In all three cases heatings 2 to 6 were done without interruption (no cooling in between).

Heating	Time (h)	Temperature (°C)
1	48.67	750
2	111.17	1000
3	03.00	900
4	03.00	800
5	03.50	700
6	41.17	600

**Table 2.8:** Heating for the bulk sample of  $\text{Ni}_{97}\text{Pt}_3$

Heating	Time (h)	Temperature (°C)
1	48.67	750
2	111.17	1000
3	03.00	900
4	03.00	800
5	03.50	700
6	41.17	600

**Table 2.9:** Heating for the bulk sample of  $\text{Ni}_{60}\text{Pt}_{40}$

Heating	Time (h)	Temperature (°C)
1	138.34	700
2	111.17	1000
3	03.00	900
4	03.00	800
5	03.50	700
6	41.17	600

**Table 2.10:** Heating for the bulk sample of  $\text{Ni}_{72}\text{Pd}_{28}$

After the sixth heating session the recrystallization result was visible with the naked eye. Pictures were taken with the light microscope to visualize this (figures 2.3, 2.4 and 2.5). The big domain in the lower left corner of picture 2.3 was cut out. It was then ground to the ideal sample thickness. Using Laue diffractometry we tried to find the orientation of the single crystal sample. However, as figure 2.6 shows, this was not possible as the domain consisted of multiple grains with different orientations.

In order to find out if the rolled samples were contaminated during manufacturing we used the Zeiss ESEM<sup>6</sup> of the University of Vienna to

---

<sup>6</sup><http://nanozentrum.univie.ac.at/home/zeiss-supra-55-vp/>

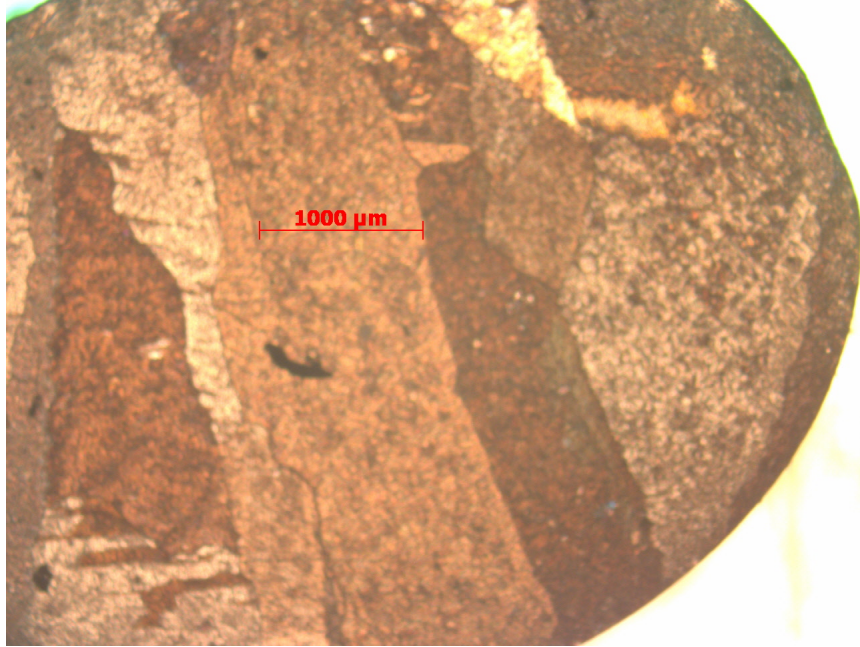


**Figure 2.3:** Light microscope photograph of Ni<sub>97</sub>Pt<sub>3</sub> thick sample

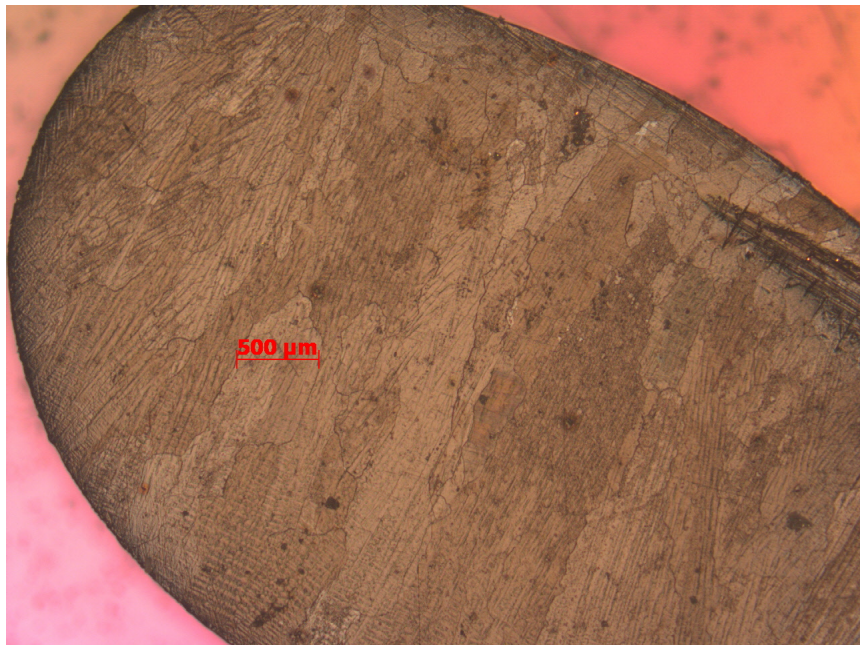


**Figure 2.4:** Light microscope photograph of Ni<sub>60</sub>Pt<sub>40</sub> thick sample



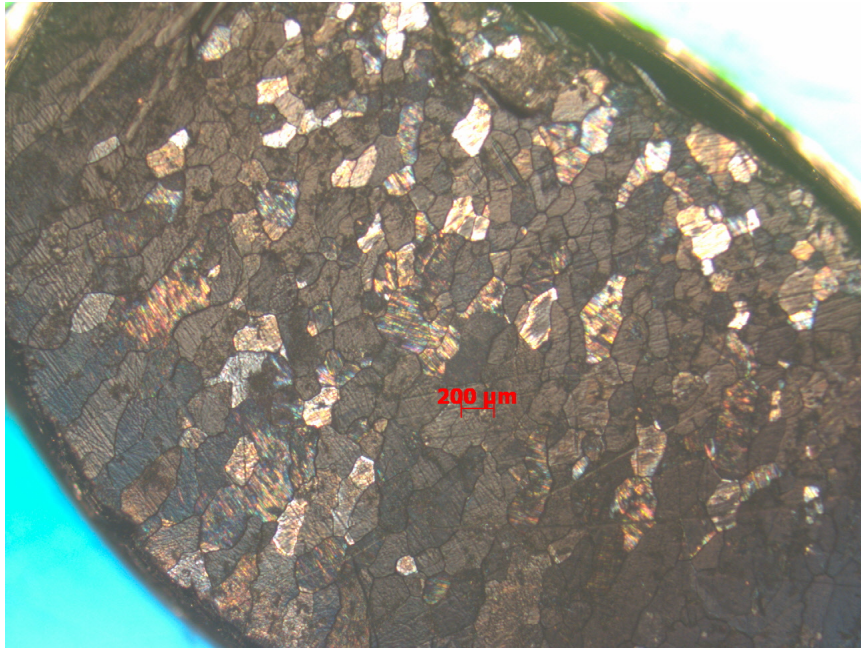


**Figure 2.5:** Light microscope photograph of Ni<sub>72</sub>Pd<sub>28</sub> thick sample

determine the chemical composition. This was done only qualitatively without standardization. The beam energy was 20 keV and the measurement was carried out in UHV. This energy allowed characterization via the emitted characteristic energies. In the case of Ni this was mainly the  $K_{\alpha}$ -line at an energy of 7.47 keV, for Pd the  $L_{\alpha}$ -line at 2.84 keV and for Pt the  $K_{\alpha}$  at 9.44 keV. The measured spectra are given in figures 2.7, 2.8 and 2.9.

One can see from the spectra, that apart from oxygen and carbon, which were expected to be found, there are also very vague traces of Pd, Au and Al, but no Fe.

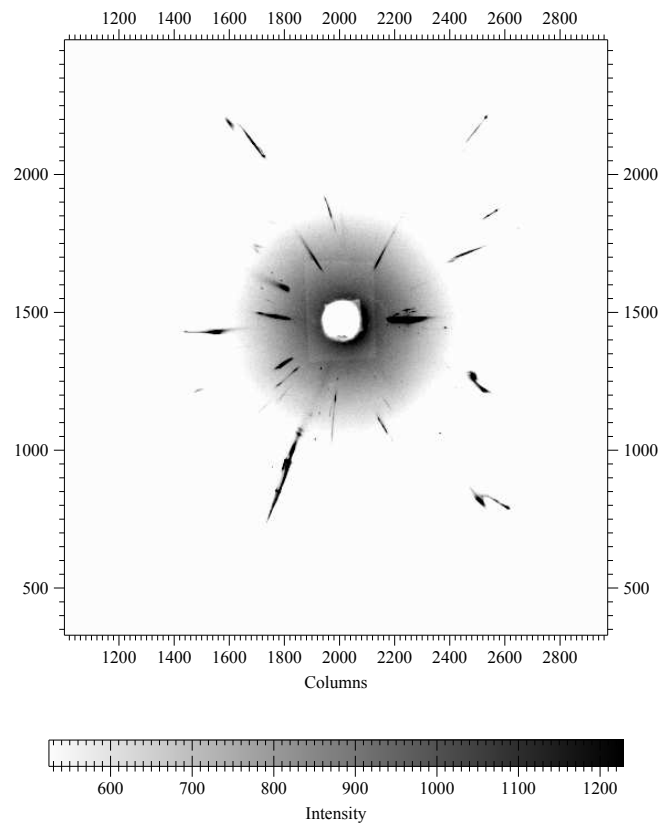


**Figure 2.6:** Laue diagramm of polished  $\text{Ni}_{97}\text{Pt}_3$  domain sample of which we hoped it was a single grain



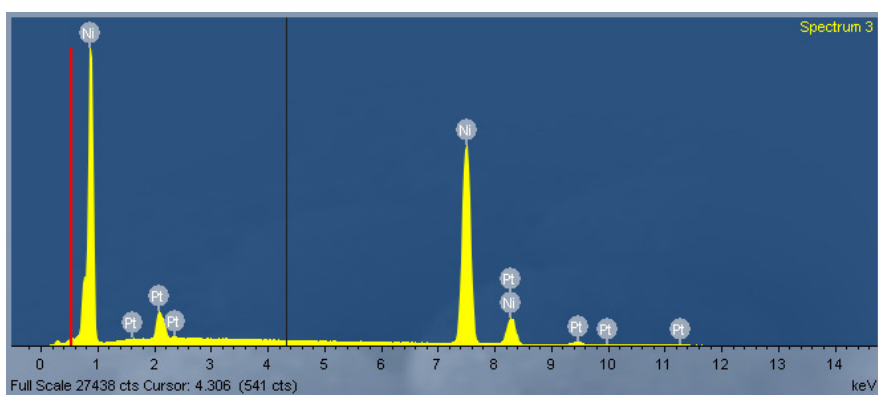


**Figure 2.7:** Chemical spectrum of the  $\text{Ni}_{97}\text{Pt}_3$  sample

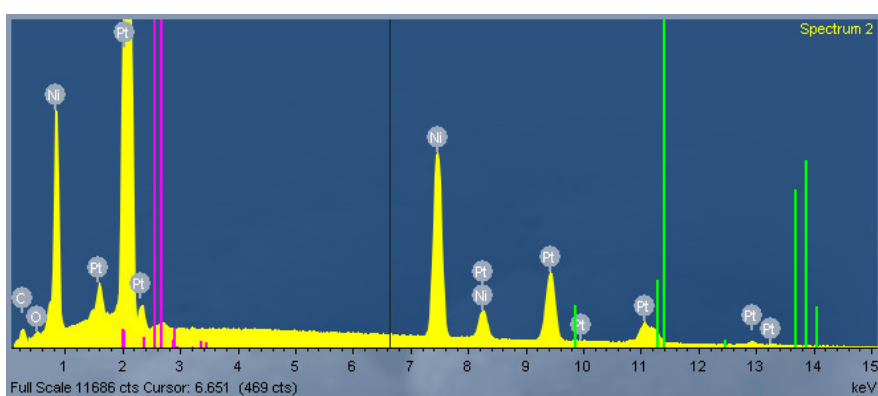


**Figure 2.8:** Chemical spectrum of the  $\text{Ni}_{60}\text{Pt}_{40}$  sample

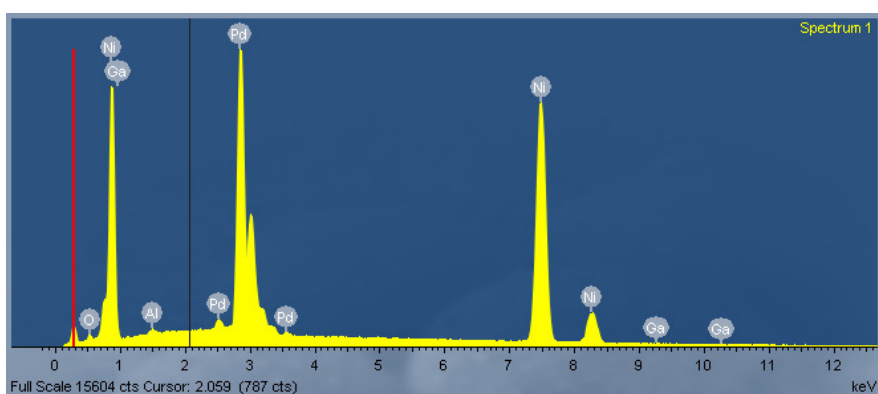


**Figure 2.9:** Chemical spectrum of the  $\text{Ni}_{72}\text{Pd}_{28}$  sample

## Chapter 3

# The simulation program

The program aims to simulate an XPCS experiment. Atoms diffuse due to a Monte Carlo simulation. The states of the system at different points in time are taken to calculate an amplitude correlation function. This is contrary to the experiment, where the intensity correlation function is used, but it leads to better statistics. The program has a polycrystal mode, allowing to average over several points in reciprocal space, sorted into shells. This allows to simulate the behavior of a multi grain sample.

### 3.1 Basic outline

The basic outline of the program is as follows:

1. Reading parameters from the input file.
2. Building a lattice (sc, bcc or fcc possible) with the two types of atoms randomly distributed on it.
3. Calculating the voxel - shells for the  $q$ -space in case of a polycrystal, otherwise allocating the voxels around the  $q$ -vector of interest.
4. Sorting and storing the coordinates for the voxels in question.
5. If more than one vacancy is used, the vacancy coordinates are stored in a separate array.

The next steps are repeated in a loop until the desired number of Monte Carlo steps is reached:

6. A random vacancy is chosen.

7. The positions of the nearest and of the next nearest neighbors of the chosen vacancy are calculated.
8. A random neighbor of the vacancy is chosen.
9. The energy barriers (see equation (1.10)) between the system at a current state and the case that the vacancy would exchange position with its neighbor in question is calculated.
10. The jump probability is calculated according to (1.14) ( $\omega_{jump}$ ).
11. A random number between 0 and 1 is calculated ( $\omega_{rand}$ ).
12. If  $\omega_{jump} > \omega_{rand}$  the vacancy exchanges position with the atom in question.
13. If thermalization is activated, this is repeated for the number of thermalization steps.

After thermalization the following steps are performed additionally after each Monte Carlo step.

14. The Fourier transform of the lattice is performed using FFTW<sup>1</sup>, providing a  $N \times N \times N$  map of the reciprocal space.
15. The voxels of the map of reciprocal space are sorted according to the shells calculated earlier and the corresponding amplitudes are calculated.
16. If the number of loop cycles after thermalization is bigger than the correlation period  $t_c$ , the amplitude correlation function is calculated.
17. Optionally a cut through the map of reciprocal space can be printed.
18. Optionally the real space can be printed.

After the given number of loop cycles is reached, the loop ends.

19. The intensity correlation function is calculated from the amplitude correlation function according to equation (1.40). As this equation is only valid for the expectation values, the statistics for the amplitude correlation function have to be very good.
20. Each shell of voxels in the reciprocal space corresponds to a  $q$ -value. The physical analogy and the corresponding  $2\Theta$  value to this  $q$ -value are calculated.
21. The intensity correlation data corresponding to each shell for a  $q$ -value is fitted according to equation (1.42) with  $c = 1$ .

---

<sup>1</sup><http://www.fftw.org/>

22. The fitted parameters are then put into a file with corresponding  $q$ -values.

## 3.2 Closer description of methods used

I will now go into detail for some of the modules listed above.

### 3.2.1 Building the lattice

The grid is built of  $N \times N \times N$  sites, forming a simple cubic lattice. Not every site is occupied by an atom though. The occupation is chosen according to the type of lattice (sc, bcc or fcc), leading to the according superlattice. In the simple cubic case only one eighth of the possible sites are occupied, leading to twice the edge length. The algorithm for the implementation of such a lattice construction can be found in the appendix (A.4.1). The lattice sites that are not occupied are marked with a value  $I$ . Those sites that are part of the lattice are all filled with atoms of type  $A$  at the beginning. To introduce the second component of the alloy, we dice a position in the lattice. In specific we dice three values between 1 and  $N$ .

If the position has the value  $A$  it is changed to the value  $F$ . This is done until the desired concentration is reached. Thereafter we again dice positions in the lattice. Again for  $A$  values we introduce vacancies with the value  $V$  according to the number of vacancies. This gives a completely arbitrary state of the lattice as the initial value. We have a total of  $M$  lattice sites occupied by atoms or vacancies (with values  $A$ ,  $F$  or  $V$ ).

### 3.2.2 Calculating jump probabilities

Each loop cycle of the program corresponds to a time step  $t_{\text{step}}$ .  $M \cdot t_{\text{step}}$  gives a Monte Carlo step. A Monte Carlo step is the average time it takes every atom in the lattice to attempt a jump. After every Monte Carlo step the Fourier transform is made. If one wants the alloy in equilibrium (this means that the short range order intensity will remain static) one can choose to temper for a number of Monte Carlo steps before beginning with the Fourier transform.

So each Monte Carlo step is divided into  $M$  time steps. In each of these time steps one vacancy is picked at random. For this vacancy the potential energy ( $E_V$ ) is calculated as described above. Then one of the next neighbors of the vacancy is picked at random and its potential energy is also calculated ( $E_{NN}$ ). Therefore the attempt frequency  $\nu_0$  corresponds to a trial per time

step. Now if  $E_V \leq E_{NN}$  we have the downhill case and the atom jumps from its position into the vacancy. If on the other hand the energy at the position of the vacancy is bigger, we have to use equation (1.14) to calculate the jump probability. We do so by dicing a number between zero and one ( $\omega_{\text{rand}}$ ). Now if  $\omega_{\text{rand}} \geq \omega_{ji}$  the atom jumps, but if  $\omega_{\text{rand}} < \omega_{ji}$  the atom stays where it is.

### 3.2.3 Calculating the shells

Each amplitude of a wave vector has a corresponding voxel in the  $q$ -space. Each of these voxels changes in time and therefore has a corresponding amplitude correlation function. As the program aims to simulate the output of an experiment using a polycrystal, it averages over a number of voxels, corresponding to the different orientations of the grains. To be precise, one would only average over voxels having the same norm of a vector position in  $q$ -space with the origin at the zero point reflex. As this would lead to a very poor statistics, the  $q$ -space is divided into a number of shells with their center at the zero reflex. The biggest shell must be small enough not to include the second Bragg reflex. The number of shells the voxels are divided in can be chosen in the Input file. In the real space lattice only particular positions are occupied, leading to an image in reciprocal space which includes more than one Brillouin zone (2 for fcc, 4 for bcc or 8 for sc). In order to avoid averaging over a Braggpeak, which would lead to very bad statistics, a maximal radius of the outer shell is given. For the fcc case this is  $\sqrt{3 \cdot (N/2)^2}$  (see sketch figure 3.1).

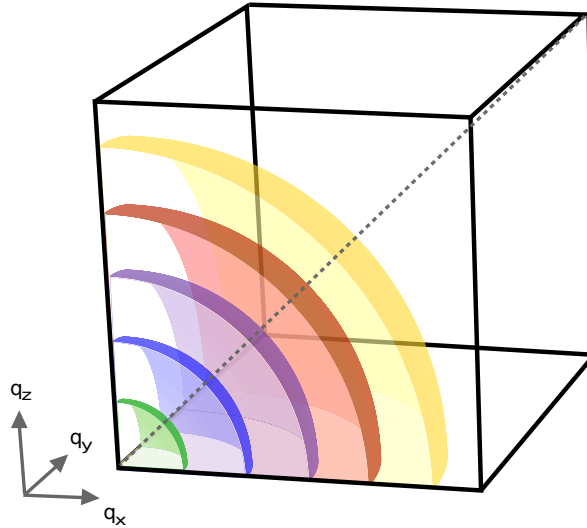


**Figure 3.1:** Schematic of shell division in  $q$  - space

As the number of calculated correlation functions and therefore the number of gained data points corresponds to the number of shells, one has to choose between a high number of data points and good statistics. The shells are chosen equidistant and therefore the statistics in the outer shells with higher  $q$ -value will be better than in the inner ones (note that the statistics in the most inner shell usually will not suffice). The  $q$ -vector given, corresponding to the calculated correlation function, has a norm which complies with the radii of the shells confining the voxel used to calculate the correlation function.

### 3.2.4 Calculating the correlation function

#### Calculating the amplitude correlation function

Once a starting period of  $t_c$  (which stands for correlation period) Monte Carlo steps plus thermalization is over, the amplitude correlation function is calculated for each following Monte Carlo step. This is done for each shell of voxels (number of voxels per shell:  $N_{\text{voxel}}$ ) in the  $q$ -space. The real and the imaginary part of the amplitude correlation function are calculated separately as:

$$G_{\text{re}}^{(1)}(i) = \sum_{dt=0}^{t_c} (A_{\text{re}}(i, t) \cdot A_{\text{re}}(i, t + dt) + A_{\text{im}}(i, t) \cdot A_{\text{im}}(i, t + dt))$$

$$G_{\text{im}}^{(1)}(i) = \sum_{dt=0}^{t_c} (A_{\text{im}}(i, t) \cdot A_{\text{re}}(i, t + dt) - A_{\text{re}}(i, t) \cdot A_{\text{im}}(i, t + dt))$$

For the normalization, which takes place after the loop, also the total intensity of all times is summed:

$$I_{\text{vox}}(i) = \sum_{t=t_c}^{t_{\text{max}}} |A(i, t)|^2$$

#### Calculating the intensity correlation function

For each shell, the amplitude correlation function is summed over all voxels:

$$G_{\text{re\_sum}}^{(1)} = \sum_{i=1}^{N_{\text{voxel}}} G_{\text{re}}^{(1)}(i)$$

$$G_{\text{im\_sum}}^{(1)} = \sum_{i=1}^{N_{\text{voxel}}} G_{\text{im}}^{(1)}(i)$$

The same is done with the overall time intensity per voxel to get the overall time intensity per shell ( $I_{\text{sum}}$ ):

$$I_{\text{sum}} = \sum_{i=1}^{N_{\text{voxel}}} I_{\text{vox}}(i)$$

This is used for normalization  $g_{\text{re/im\_sum}}^{(1)} = G_{\text{re/im\_sum}}^{(1)} / I_{\text{sum}}$  and from this the intensity correlation function can be calculated according to 1.40 as:

$$g^{(2)}(t) = 1 + \left( g_{\text{re\_sum}}^{(1)}(t) \cdot g_{\text{re\_sum}}^{(1)}(t) + g_{\text{im\_sum}}^{(1)}(t) \cdot g_{\text{im\_sum}}^{(1)}(t) \right),$$

where  $t$  runs from 0 to  $t_c$ .

## Chapter 4

# The experiment

The strongest limitation for XPCS experiments is the intensity of the coherent X-ray beam. While intensity fluctuation spectroscopy with coherent optical light sources (LASERS) can be done relatively easily and with little expenditure of time, the time it takes the detector in an X-ray experiment to collect a sufficient number of photons is usually the critical factor. This is why, with today's sources, one seeks to optimize the contrast of the sample. Contrast in this context refers to the difference in brightness of the speckles. As seen in equation (1.24) this difference in the brightness results from the difference in the atomic number ( $Z$ ). Therefore, with today's sources one has to use a component with a low and one with a high atomic number.

### 4.1 Synchrotrons

For experiments which require high intensities of nearly monochromatic X-rays one has to use synchrotron sources. The reason for this is that with laboratory X-ray sources the intensity is not high enough.

Synchrotrons store small packages of electrons, so called bunches in a storage ring. It is important to have bunches because the acceleration principle relies on an alternating magnetic field which would not work on a continuous current. The bunches from the storage ring go through a series of equidistant dipole magnets, called undulator (see figure 4.1<sup>1</sup>).

There they undergo a periodical acceleration leading to a quasi-monochromatic bremsstrahlung (with  $\Delta\lambda/\lambda$  of a few percent), called the pink beam. Note that the source size is not spherical, for the acceleration takes place in the horizontal axis, leading to a broadening of the bunch and therefore the beam gets wider in this axis as well.

---

<sup>1</sup><http://upload.wikimedia.org/wikipedia/commons/9/9f/Undulator.png> 8.6.11



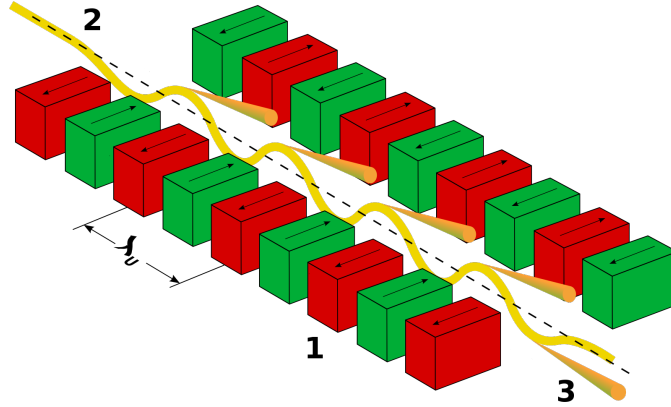


**Figure 4.1:** Schematic representations of an undulator (picture taken from WIKIPEDIA)  
1: electrons coming from the storage ring  
2: dipole magnets  
3: pink beam

The pink beam is then focused by a set of optics and the spectrum is further narrowed by monochromators (for 8 keV usually silicium). The monochromator is arranged in reflection geometry and one uses the 111-Bragg-reflex as a highly monochromatic source. As for X-rays air is the optical denser medium one can aim for total reflection on mirrors to cut out higher harmonics.

The refined beam is guided to the experimental hut where it meets our experimental setup.

## 4.2 Coherence of the beam

Contrary to a LASER, where the source produces a strictly monochromatic beam, synchrotron radiation is not monochromatic. In spite of all the monochromator technique, a strictly monochromatic X-ray beam is impossible to achieve. Sometimes one does not even exhaust monochromatization to its fullest because this would result in the intensity being too low. In order to qualify the phase relation within a package of light one defines the coherence length. The longitudinal coherence length is the length, measured along the wave front, after which the information about the phase relation is lost. It is given as  $\xi_l = \frac{\lambda^2}{2\Delta\lambda} = \frac{c}{2\Delta\nu}$ . Using the relation  $c = \lambda\nu = \lambda\frac{1}{\tau}$  one gets the coherence time as  $\tau_c = \frac{\xi_l}{c} = \frac{1}{2\Delta\nu}$  [SUTTON, 2006].

The pink beam is not a parallel light source but has the form of a light cone, leading to a number of not equally orientated wavefronts. The transversal coherence length gives information about the parallelism of the wave fronts.

It is defined as:  $\xi_t \approx \frac{\lambda D}{2a}$  where  $D$  is the distance between the sample and the light source and  $a$  is the size of the light source (see [EICHLER, (1966)]). A beam bigger than its transverse coherence length is called partially coherent.

### 4.3 Experimental setup

As the diffusivities in the sample depend on the temperature, it is important to be able to vary this parameter during the experiment. As the temperatures for measurable timescales lie well above room temperature we have to use a furnace. In the old model the sample was heated directly by conduction over the sample holder, while in the newer model we use radiation heating by a coil surrounding the sample. The setup is laid out to position the sample in the focus of the beam. In order to avoid scattering on air molecules and to prevent the sample from punctual oxidation the furnace holds a vacuum of about  $10^{-5}$  mbar.

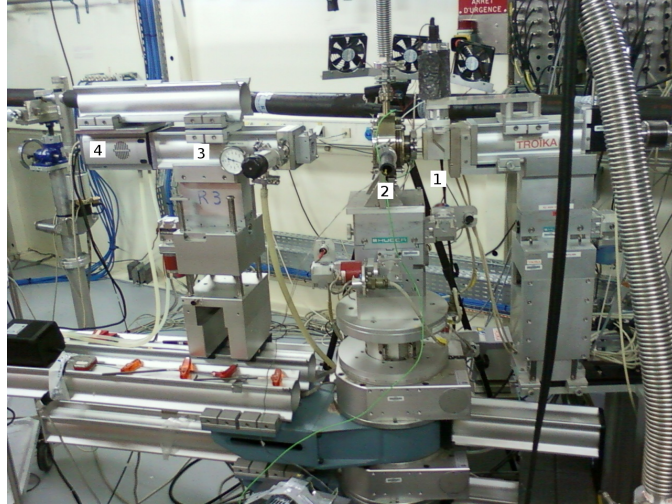


**Figure 4.2:** Picture of the experimental setup at ID10A at the ESRF

- 1: slits
- 2: furnace with sample
- 3: flight tube
- 4: CCD detector

The diameter of the beam hitting the sample should be smaller than the transversal coherence. As this is usually not the case, the smaller the beam the better. Therefore at the ESRF we use a set of slits right before the beam enters the furnace. It is important not to make the slits too small in order to keep enough intensity. Usually we choose  $10 \mu\text{m} \times 10 \mu\text{m}$ . This leads to a beam bigger than the coherence length and therefore lower contrast in the  $g^{(2)}$  function.

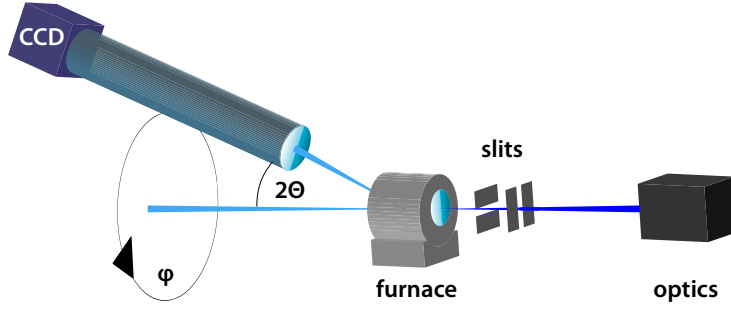


**Figure 4.3:** Schematic of experimental setup

The beam enters the furnace through a Kapton window, scatters on the sample in the center and leaves through a second Kapton window. The scattered light, after passing a short distance in the air, enters an evacuated flight tube. At the end of the flight tube there sits an X-ray sensitive CCD camera. The resolution as number of pixels per speckle is a linear function of the distance between sample and detector ( $\propto r$ ). The further away the detector is placed, the better the resolution gets. For our case the optimal ratio is met when the size of the speckles meets the size of the pixel. On the other hand intensity decays by distance squared ( $\propto r^2$ ). As we seek to optimize the product of resolution and intensity, a short setup is preferable. Therefore the flight tube should be chosen to be short. For a more precise treatment of this topic see [LEITNER, 2010].

A picture of the setup at ID10A is given in figure 4.2 and a schematic representation of the experimental setup is given in figure 4.3.

#### 4.3.1 Experimental conditions

The experiment was conducted at ID10A at the ESRF (European Synchrotron Radiation Facility) at Grenoble, France. The following information, if not cited otherwise, is taken from the ESRF homepage<sup>1</sup>.

- Energy for XPCS: 8 keV
- Energetic bandwidth :  $\frac{\Delta E}{E} = 1.4 \cdot 10^{-4}$
- Beam size after undulator:  $928 \times 23 \mu m^2 (h \times v)$  FWHM
- Beam size behind sample slits:  $10 \times 10 \mu m^2$

<sup>1</sup><http://www.esrf.eu/UsersAndScience/Experiments/SoftMatter/ID10A/>

## Chapter 5

# Data evaluation

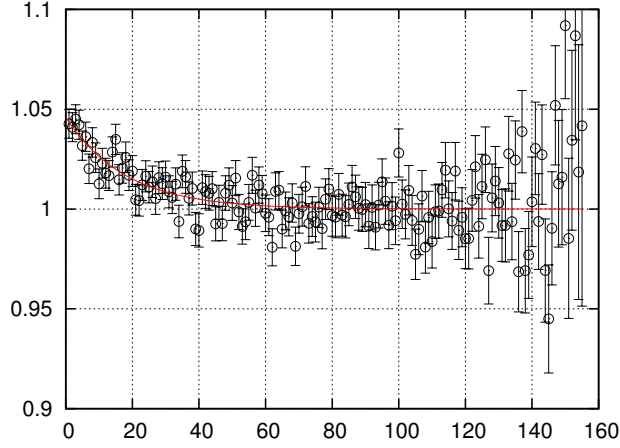
During an experiment we collect a number of pictures with the CCD camera for a certain setup. These frames provide a number of ADU's per pixel and time for certain temperatures and certain angles. Due to the high coherence of the beam the scattering pattern shows spots, so called speckles. In short if one has perfect coherence, each point in the scatterer is a source of a spherical wave which interferes with every other wave, leading to bright and dark spots in the spread pattern, the speckles. Michael Leitner (see [LEITNER, 2010]) developed a software we use to evaluate the data and find the photons in the CCD pattern.

As given by equation (1.42) the  $\mathcal{J}^{(2)}$  function can be described by an exponential decay. If jumps into different directions are detected simultaneously, as it is the case with different orientations in a polycrystal, each direction leads to its own, corresponding exponential decay. It is not possible to fit the sum of exponential decays with one exponential decay. Therefore the exponent  $\beta$  is introduced. The function the data set is fitted with is given as:

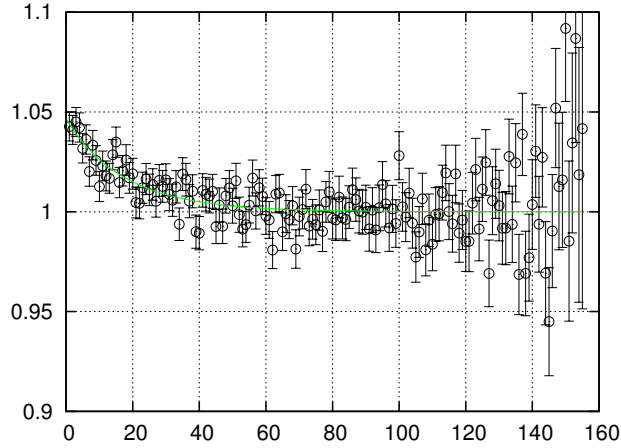
$$f(t) = c + b \cdot e^{-2(\frac{t}{\tau})^\beta} \quad (5.1)$$

As mentioned earlier, the baseline  $c$  can differ from 1 which is due to a intensity gradient in the diffuse scattering regime, appearing for example in proximity to a diffuse maximum due to short-range order. The fit parameter  $b$  is often referred to as the contrast. For a perfectly coherent beam it would be equal to one. However with a not strictly monochromatic beam it gets smaller. This can be exemplified: let us consider a static sample where no diffusion takes place. Now if the light source has a certain, monochromatic light spectrum, the pixel pattern on the screen is static. If the light is not monochromatic however the pixel pattern varies according to the wavelengths of the different photons. Also if the wave fronts are not parallel the speckle pattern varies. This variations in the pattern happen at timescales that can

not be measured by our experiment and can be interpreted as a noise in the speckle pattern which lowers the contrast of the time dependent correlation function.



(a)  $\beta = 1$



(b)  $\beta = 0.97 \pm 0.22$

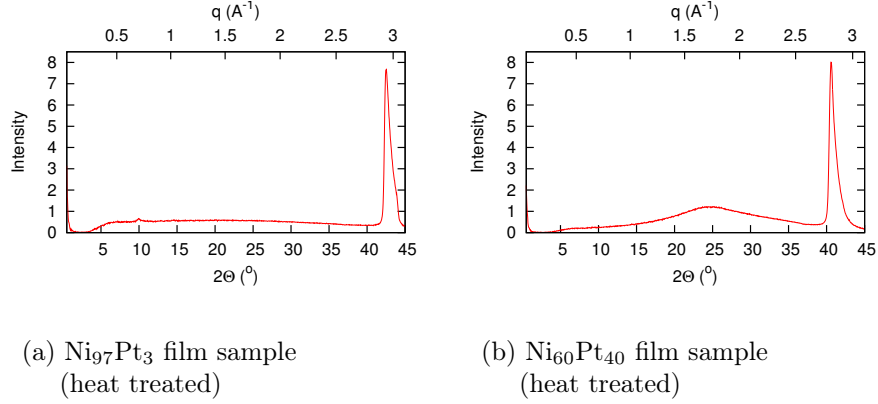
**Figure 5.1:** Fits for data collected at  $2\Theta = 20^\circ$  and  $557C^\circ$

Figure 5.1 shows a data set measured at the ESRF in beam time HS-4228 fitted with an exponent  $\beta = 1$  (5.1(a)) and a fitted exponent (5.1(b)) for  $2\Theta = 20^\circ$  at  $557^\circ C$ . The fitted parameters for (a) are given as:

$$b = 0.0460 \pm 0.0036 \text{ and } \tau = 35.9 \pm 4.1$$

and for (b) as:

$$b = 0.0466 \pm 0.0068, \tau = 35.8 \pm 4.2 \text{ and } \beta = 0.97 \pm 0.22.$$



**Figure 5.2:** Integrated intensity for different  $2\Theta$ s

The other datasets mostly show a similar behavior with  $\beta$  values slightly smaller than 1. Therefore we choose to fit all the data with  $\beta = 1$  from here on. Further justification for doing so will be given.

Collecting frames for several angles and temperatures and fitting the corresponding correlation functions gives a number of different  $\tau$  values in units of frames. At HS-4228 we had an exposure time of 10 seconds and a readout time of 0.9 seconds leading to 10.9 seconds per frame. This is used to convert  $\tau$  into seconds.

## 5.1 Estimating atomic interaction with short range order intensity

In section 1.5.1 I assumed that there is no interacting force between the particles. We will now look into the validity of this statement. If the atoms interact the alloy will be short range ordered. This would lead to an intensity variation ( $I_{\text{SRO}}(\vec{q})$ ) in the diffuse regime. In the case of the polycrystalline structure we would have variations of the intensity along the  $2\Theta$  scan. Figure 5.2 shows the  $\varphi$  integration over the image taken with the SAXS detector (see figure 2.2(a)). One can see that the diffuse intensity varies very little in the  $\text{Ni}_{97}\text{Pt}_3$  sample compared to the  $\text{Ni}_{60}\text{Pt}_{40}$  sample. Note that up to  $5^\circ$  the intensity is blocked out by the beamstop.

We can assume  $I_{\text{SRO}}$  for the sample that was not heat treated to vary even less. At the ESRF we used a point detector to measure the intensities for certain  $2\Theta$  angles (figure 5.3). In order to find the position of the sample, scans with a point detector were taken. The sample was small enough for the beam to pass it at certain positions. Therefore the intensities measured at these positions were not attenuated, giving  $I_0$  as a referenz. This data can

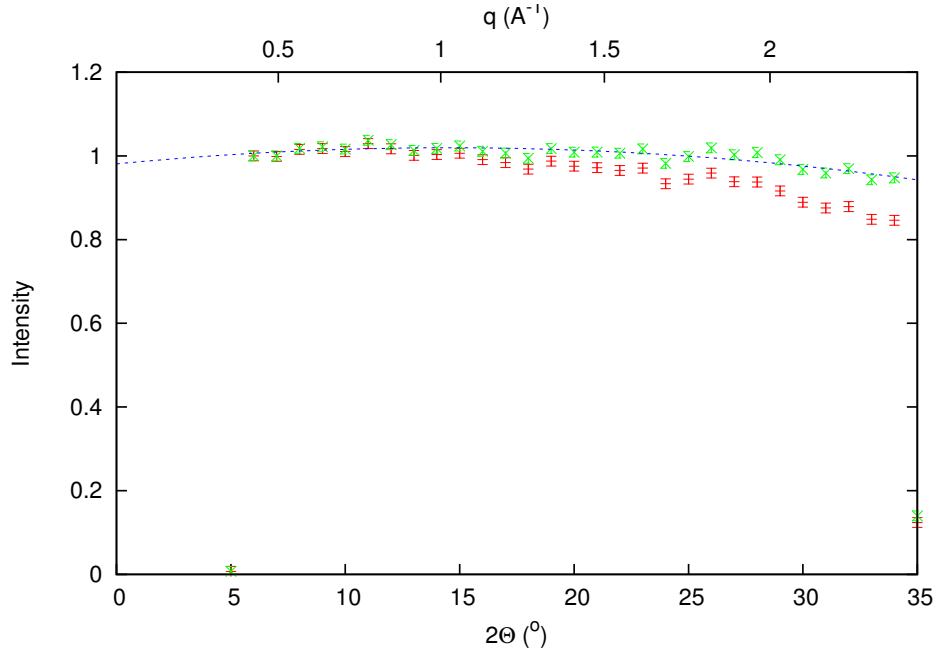


**Figure 5.3:** Diffuse intensity (normalized) corresponding to  $2\Theta$   
*red:* measured intensities  
*green:* intensities corrected according to equation (2.1)  
*blue:* fitted polynomial of second order

be used to find attenuation  $\mu d$ . Therefore we need the attenuation relation:

$$I(2\Theta) = I_0 e^{-\mu \frac{d}{\cos(2\Theta)}}$$

$2\Theta$ , which is the angle to the surface normal, is zero in our case. Therefore we get  $\mu d = 1.152 \pm 0.077$ .

This was used to correct the collected data according to 2.1. The red data points represent the normalized intensities as measured, the green ones are corrected by equation (2.1) and the blue line is a fitted polynomial of second order. The errors were taken according to Poisson noise.

Although there is a slight short range order pattern visible in the intensity profile, it is small enough to be neglected.

## 5.2 Finding the activation energy

Changing the temperature at a fixed set of angles, one can measure the temperature dependence of  $\tau$ . Using the Arrhenius theory (equation (1.18)) we can find the activation energy for the diffusion. For  $\text{Ni}_{97}\text{Pt}_3$  measured at HS-4228 the relation of  $\tau$  and the inverse temperature is given by figure 5.5 As

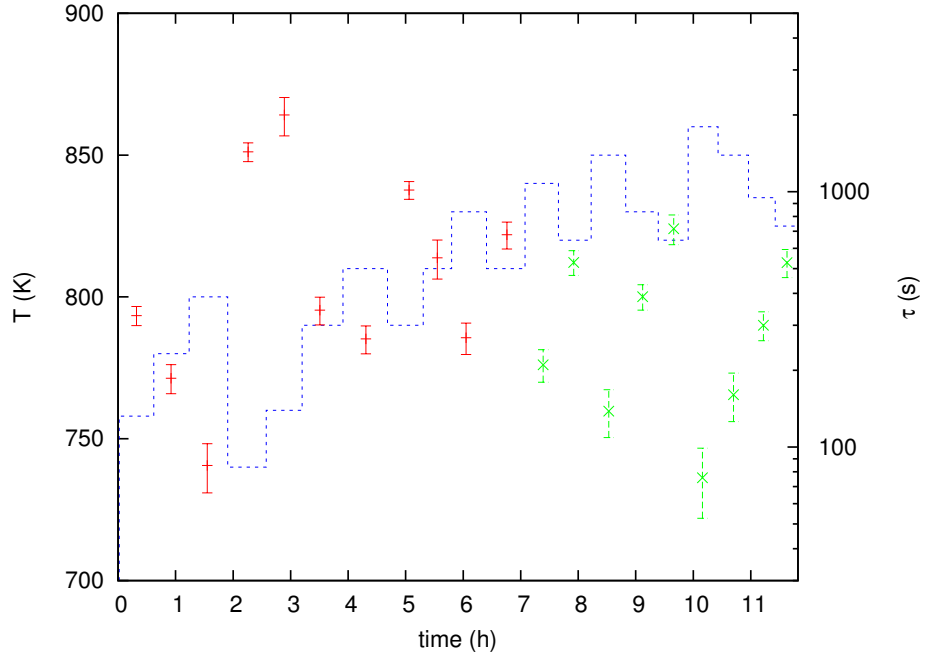


**Figure 5.4:** Measurements at  $2\Theta = 20^\circ$ ,  $\varphi = 0$  for temperatures between  $467^\circ\text{C}$  and  $587^\circ\text{C}$   
 Temperature (*blue* boxes) in comparison to measured correlation times  $\tau$  for measurements in chronological order (data points for stable system *green*, for unstable system *red*)

shown in figure 5.4 it takes a while for the diffusion rate to stabilize. Therefore it is valid to use only the data beginning with the twelfth measurement to calculate the activation energy. Figure 5.6 shows the adequate detail with the fit. Fitting was done with *gnuplot*<sup>1</sup>. The fitted parameters were given as:

$$A = (57 \pm 201)10^{-15} \text{ s}^{-1} \text{ and } \frac{E_a}{k_B} = (30.19 \pm 2.86)10^3 \text{ K.}$$

This leads to an activation energy of:

$$E_a = (2.60 \pm 0.25) \text{ eV.}$$

<sup>1</sup><http://www.gnuplot.info/>



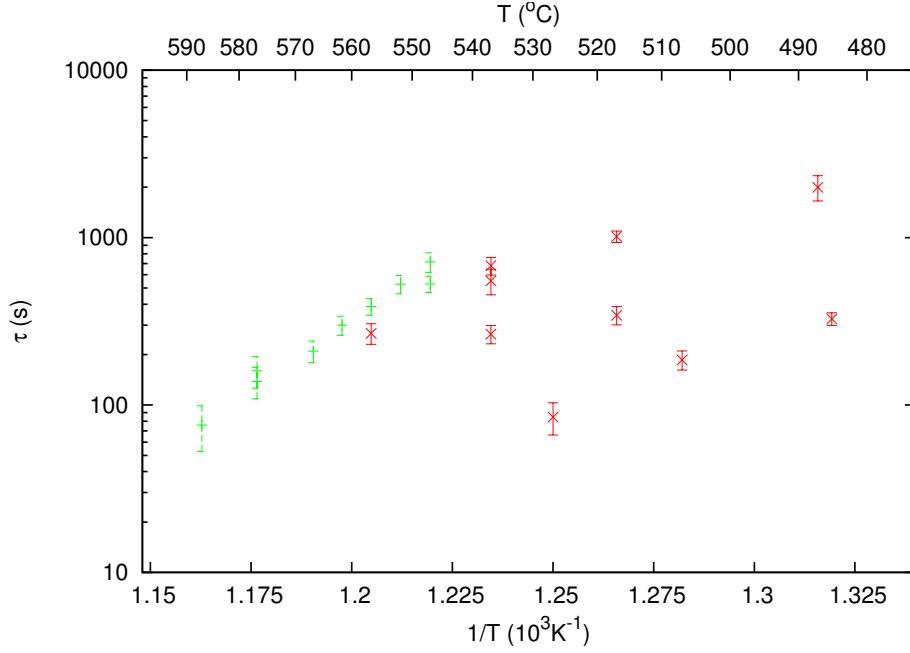


**Figure 5.5:** Measurements at  $2\Theta = 20^\circ$ ,  $\varphi = 0$  for temperatures between  $467^\circ\text{C}$  and  $587^\circ\text{C}$   
 Arrhenius plot for all measured data points  
 (data points for stable system *green*, for unstable system *red*)

The literature value for the activation energy of platinum in nickel is, according to [MILLION and KUCERA, 1973],  $286.8 \text{ kJ/mol} = 2.97 \text{ eV}$ . We can improve the fit by averaging the autocorrelation functions where we have several data points for one temperature. We do so by weighting the values for each time delay (for two values this is given as:  $p_1 = \frac{d_2^2}{d_1^2 + d_2^2}$ , where  $d_i$  is the error and  $p_i$  is the weight). As a result we get:

$$A = \tau_0 = (16 \pm 31)10^{-15} \text{ s}^{-1} \text{ and } \frac{E_a}{k_B} = (35.1 \pm 1.6)10^3 \text{ K},$$

This leads to an activation energy of:

$$E_a = (2.71 \pm 0.14) \text{ eV}.$$

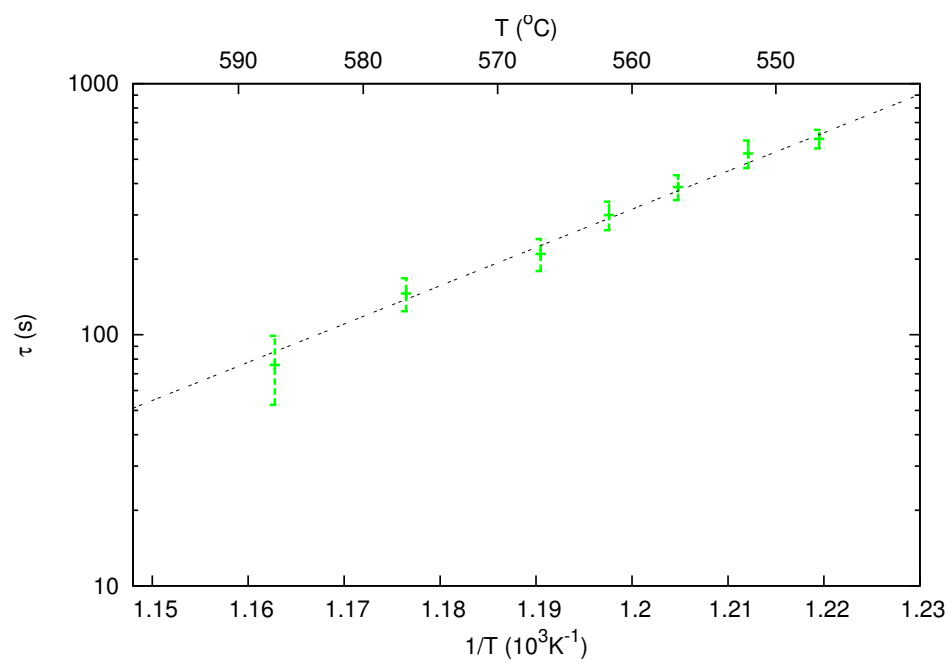


**Figure 5.6:** Arrhenius plot of valid data with fit

### 5.3 $2\Theta$ dependency

Different diffusion mechanisms lead to different jump vectors. To gain information about the mechanisms it is important to investigate the correlation time for different  $q$ -values. If we have a polycrystalline structure, we can only make statements for diffusion according to the absolute value of the  $\vec{q}$  vectors. Therefore it is sufficient to scan over  $2\Theta$ . At HS-4228 we measured the time for several  $2\Theta$  values at a temperature of  $557^\circ \text{ C}$ .

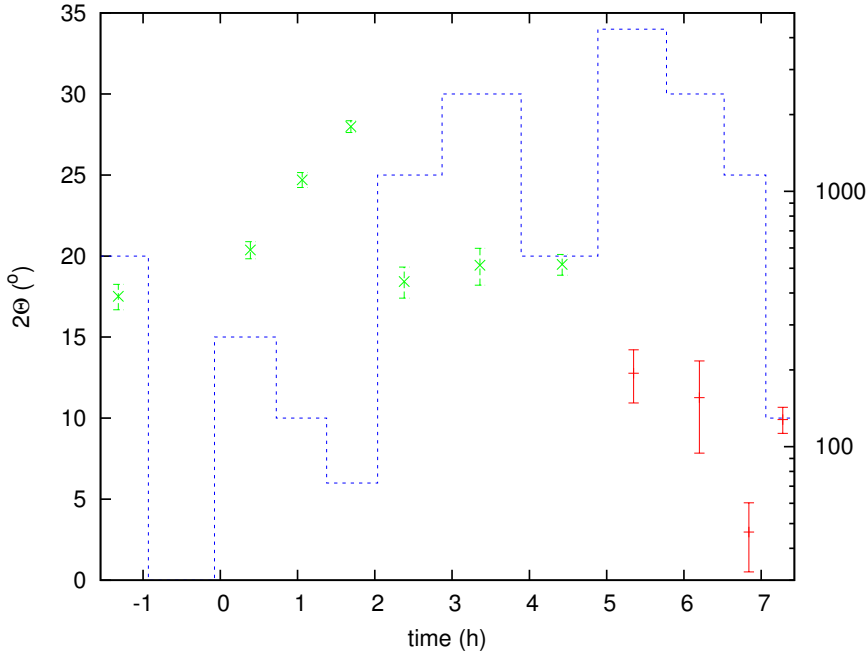


**Figure 5.7:** Measurements at a temperature of  $557^\circ$  and  $\varphi = 0$  for  $2\Theta$  between  $6^\circ$  and  $34^\circ$  (blue boxes) in comparison to measured correlation times  $\tau$  for measurements in chronological order

The relation between  $|\vec{q}|$  and  $2\Theta$  is given by  $\sin(\frac{2\Theta}{2}) = \frac{|\vec{q}|/2}{|\vec{k}|}$  where  $|\vec{k}|$  is the momentum vector corresponding to the energy of the beam ( $|\vec{k}| = \frac{E_{\text{beam}}}{\hbar c}$ ). At IDA10 we have photon energies of 8 keV, which leads to  $|\vec{k}| = 4.05 \text{ \AA}^{-1}$ . The lattice parameter  $d$  is  $3.532 \text{ \AA}$ . The measured correlation times corresponding to  $2\Theta$  are given in figure 5.8. Contrary to the Arrhenius measurement, which was taken before the  $2\Theta$  dependence, the system is stable at first but gets unstable after seven measurements (see figure 5.7). Why this is the case could not be determined with certainty. However, it can be clearly seen, that the correlation times get a lot bigger. The measurement at negative time represents the value taken from the Arrhenius measurement series and the

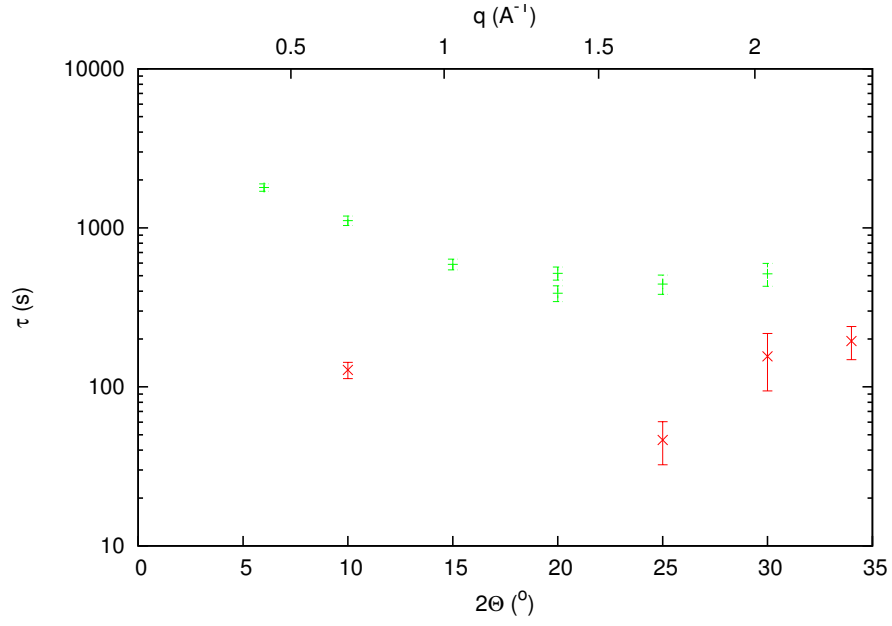


**Figure 5.8:** Measurements at a temperature of 557° and  $\varphi = 0$  for  $2\Theta$  values between 6 ° and 34 ° a stable system (*green*) and corrupt data (*red*)

gap is due to one other Arrhenius measurement taken in between. If we adjust our data set according to the time the system was stable and average over the data for  $2\Theta = 20^\circ$ , we get figure 5.9.

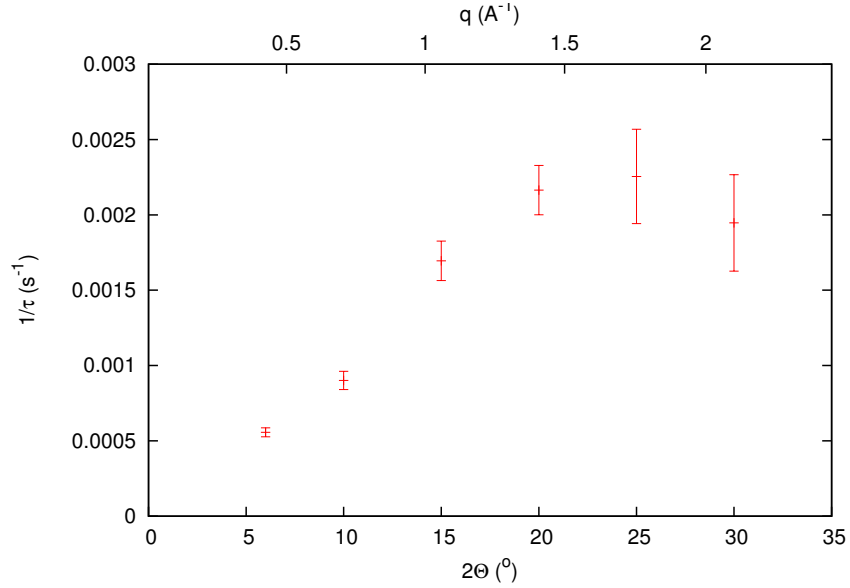


**Figure 5.9:** Measured  $q$  dependence of  $1/\tau$

### 5.3.1 Finding the diffusion mechanisms

Because of the small variations in the correlation time between fits with  $\beta = 1$  and a free exponent we assumed that fitting with  $\beta = 1$  is valid. For this case the intermediate scattering function is given by equation (1.41) which we can rewrite using  $\Gamma_{\text{inc}} = \frac{1}{\tau}$  as:

$$\mathcal{J}^{(2)}(\vec{q}) = 1 + e^{-2\Gamma_{\text{inc}}(\vec{q})t} \quad (5.2)$$

The incoherent energy broadening is given according to equation (1.32) as:

$$\Gamma_{\text{inc}}(\vec{q}) = \sum_{\Delta\vec{a}} \hat{\nu}(\Delta\vec{a}) \left(1 - \cos(\vec{q} \cdot \Delta\vec{a})\right)$$

As  $\Delta\vec{a}$  represents a particular jumping vector. This jump vector can correspond to nearest-neighbor jumps (NN), next-nearest-neighbor jumps (3N), next-next-nearest-neighbor jumps (4N) and so on. Therefore we can write the total incoherent energy broadening as a sum over energy broadenings resulting from different mechanisms:

$$\Gamma_{\text{inc}}(\vec{q}) = \Gamma_{\text{inc}_{\text{NN}}}(\vec{q}) + \Gamma_{\text{inc}_{3\text{N}}}(\vec{q}) + \Gamma_{\text{inc}_{4\text{N}}}(\vec{q}) + \Gamma_{\text{inc}_{5\text{N}}}(\vec{q}) + \dots \quad (5.3)$$

Note that the line widths are already weighted by the corresponding jump frequencies. This  $\Gamma$  values can be calculated for certain types of lattices.  $\text{Ni}_{97}\text{Pt}_3$  forms a fcc lattice. Let the lattice constant for now be  $d$ . We can then calculate the values for equation (5.3) (see appendix A.3) and get:

$$\begin{aligned} \Gamma_{\text{inc}_{\text{NN}}}(\vec{q}) &= \frac{\nu_{\text{NN}}}{Z_{\text{NN}}} \sum_{\Delta\vec{a}_{\text{NN}}} \left(1 - e^{i\vec{q}\Delta\vec{a}_{\text{NN}}}\right) \\ &= \frac{\nu_{\text{NN}}}{12} \left(12 - 4 \cdot \left(\cos(q_x \cdot \frac{d}{2}) \cos(q_y \cdot \frac{d}{2}) \right. \right. \\ &\quad \left. \left. + \cos(q_x \cdot \frac{d}{2}) \cos(q_z \cdot \frac{d}{2}) + \cos(q_y \cdot \frac{d}{2}) \cos(q_z \cdot \frac{d}{2})\right)\right) \\ \Gamma_{\text{inc}_{3\text{N}}}(\vec{q}) &= \frac{\nu_{3\text{N}}}{Z_{3\text{N}}} \sum_{\Delta\vec{a}_{3\text{N}}} \left(1 - e^{i\vec{q}\Delta\vec{a}_{3\text{N}}}\right) \\ &= \frac{\nu_{3\text{N}}}{6} \left(6 - 2 \left(\cos(q_x \cdot d) + \cos(q_y \cdot d) + \cos(q_z \cdot d)\right)\right) \end{aligned}$$

$$\begin{aligned}
\Gamma_{\text{inc}_{4\text{N}}}(\vec{q}) &= \frac{\nu_{4\text{N}}}{Z_{4\text{N}}} \sum_{\Delta \vec{a}_{4\text{N}}} \left( 1 - e^{i\vec{q}\Delta \vec{a}_{4\text{N}}} \right) \\
&= \frac{\nu_{4\text{N}}}{24} \left( 24 - 8 \cdot \left( \cos(q_x \cdot d) \cdot \cos(q_y \cdot \frac{d}{2}) \cdot \cos(q_z \cdot \frac{d}{2}) + \right. \right. \\
&\quad \left. \left. + \cos(q_y \cdot d) \cdot \cos(q_x \cdot \frac{d}{2}) \cdot \cos(q_z \cdot \frac{d}{2}) \right. \right. \\
&\quad \left. \left. + \cos(q_z \cdot d) \cdot \cos(q_x \cdot \frac{d}{2}) \cdot \cos(q_y \cdot \frac{d}{2}) \right) \right) \\
\Gamma_{\text{inc}_{5\text{N}}}(\vec{q}) &= \frac{\nu_{5\text{N}}}{Z_{5\text{N}}} \sum_{\Delta \vec{a}_{5\text{N}}} \left( 1 - e^{i\vec{q}\Delta \vec{a}_{5\text{N}}} \right) \\
&= \frac{\nu_{5\text{N}}}{12} \left( 12 - 4 \cdot \left( \cos(q_x \cdot d) \cos(q_y \cdot d) \right. \right. \\
&\quad \left. \left. + \cos(q_x \cdot d) \cos(q_z \cdot d) + \cos(q_y \cdot d) \cos(q_z \cdot d) \right) \right)
\end{aligned}$$

The jump frequencies in equation (1.32) are linked to the above as:

$$\hat{\nu}(\Delta \vec{a}_{\text{nN}}) = \frac{\nu_{\text{nN}}}{Z_{\text{nN}}}$$

nN gives the order of jump and  $Z_{\text{nN}}$  the number of neighbor sites the atom can jump to in the particular case.

Unfortunately the requested  $\vec{q}$  dependency can not be met, as with a polycrystalline sample information about the orientation of the  $q$ -vectors is lost. In order to fit our data set, we have to average the above equations over their angle dependency.  $C$  is some normalization constant and the average incoherent energy broadening is defined as:

$$\bar{\Gamma}_{\text{nN}}(q) = \int_0^{4\pi} d\Omega \tilde{C} \Gamma_{\text{nN}}(\vec{q})$$

Using this we can write:

$$\mathcal{J}^{(2)}(q) = 1 + \int_0^{4\pi} d\Omega C e^{-2\Gamma_{\text{nN}}(\vec{q})t} \approx 1 + e^{-2\bar{\Gamma}_{\text{nN}}(q)t}$$

The approximation sign is due to the fact that a sum over exponential functions can not be written as a single exponential function. Equality would only be given at time zero, because:

$$\Gamma = \frac{1}{\tau} \propto \left. \frac{d}{dt} e^{-\frac{t}{\tau}} \right|_{t=0}$$

This approach was originally introduced by C T Chudley and R J Elliott for liquids [CHUDLEY and ELLIOTT, 1961]. Now we average over the  $q$ -vectors with the same norm and choose a  $q$ -vector in a certain direction (in our case parallel to the z-axis of the system). The relative crystal vector is given in spherical coordinates:

$$\vec{q} = \begin{pmatrix} 0 \\ 0 \\ q \end{pmatrix}, \quad \Delta \vec{a} = \Delta a \begin{pmatrix} \sin(\Theta) \cos(\varphi) \\ \sin(\Theta) \sin(\varphi) \\ \cos(\Theta) \end{pmatrix}$$

Now we will integrate over all possible orientations of the crystal:

$$\begin{aligned} \int_0^{2\pi} d\varphi \int_0^\pi d\Theta \sin(\Theta) (1 - e^{i\vec{q}\Delta\vec{a}}) &= \\ \int_0^{2\pi} d\varphi \int_0^\pi d\Theta \sin(\Theta) (1 - e^{i\cdot q\Delta a \cos(\Theta)}) &= \\ 2\pi \int_{-1}^1 dx (1 - e^{iq\Delta a x}) &= \\ 2\pi \left( 2 - \frac{e^{iq\Delta a x}}{iq\Delta a} \Big|_{-1}^1 \right) &= \\ 4\pi \left( 1 - \frac{\sin(q \cdot \Delta a)}{q \cdot \Delta a} \right) & \quad (5.4) \end{aligned}$$

Using this result we can write the incoherent energy broadening as:

$$\Gamma_{\text{Ch-El}}(q) = \sum_n \frac{\nu_{\text{nN}}}{Z_{\text{nN}}} \left( 1 - \frac{\sin(q \cdot \Delta a_{\text{nN}})}{q \cdot \Delta a_{\text{nN}}} \right) \quad (5.5)$$

The jump distances for  $\text{Ni}_{97}\text{Pt}_3$  can be easily calculated. The jump distances are given as:

$$\begin{aligned} a_{\text{NN}} &= \sqrt{(d/2)^2 + (d/2)^2} &= 2.498 \text{ \AA} \\ a_{3\text{N}} &= d &= 3.532 \text{ \AA} \\ a_{4\text{N}} &= \sqrt{d^2 + (d/2)^2 + (d/2)^2} &= 4.326 \text{ \AA} \\ a_{5\text{N}} &= \sqrt{d^2 + d^2} &= 4.995 \text{ \AA} \end{aligned}$$

We can now fit the jump frequencies for the Chudley Elliott model to our data set. Figure 5.10 shows the fits for only one type of jump with the result for the corresponding jump frequency.

The next step is to try and find the weighted combination of jumps. If we try to fit all four jump frequencies to the data, we get a negative jump frequency  $\nu_{5\text{N}}$ . To avoid this, fifth nearest-neighbor jumps are neglected

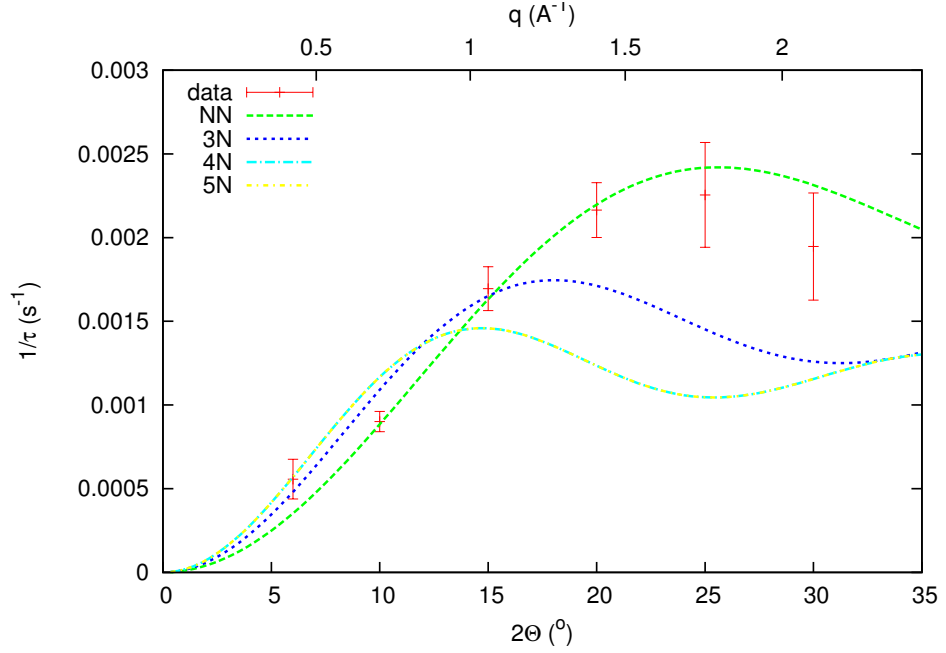


**Figure 5.10:** *Green:* nearest-neighbor jumps with a frequency of  $\nu_{\text{NN}} = (1.988 \pm 0.076)10^{-3}\text{s}^{-1}$   
*Dark blue:* next-nearest-neighbor jumps with a frequency of  $\nu_{3\text{N}} = (1.40 \pm 0.14)10^{-3}\text{s}^{-1}$   
*Light blue:* third-nearest-neighbor jumps with a frequency of  $\nu_{4\text{N}} = (1.20 \pm 0.19)10^{-3}\text{s}^{-1}$   
*Yellow:* forth-nearest-neighbor jumps with a frequency of  $\nu_{5\text{N}} = (1.07 \pm 0.21)10^{-3}\text{s}^{-1}$

( $\nu_{5\text{N}} = 0$ ). This now leads to a negative jumping frequency of next-nearest-neighbor jumps, so we also have to set third-nearest-neighbor jumps to zero ( $\nu_{4\text{N}} = 0$ ). Finally we get the fitted curve shown in figure 5.11. The calculated jump frequencies are:

$$\nu_{\text{NN}} = (1.57 \pm 0.27)10^{-3}\text{s}^{-1}$$

$$\nu_{3\text{N}} = (0.31 \pm 0.19)10^{-3}\text{s}^{-1}$$

This can be rewritten to get a temperature dependent total jump frequency and the percentaged parts:

$$\Gamma_{\text{Ch-El}}(q, T) = \nu_0(T) \sum_n p_n \left(1 - \frac{\sin(q \cdot \Delta a_{\text{nN}})}{q \cdot \Delta a_{\text{nN}}}\right)$$



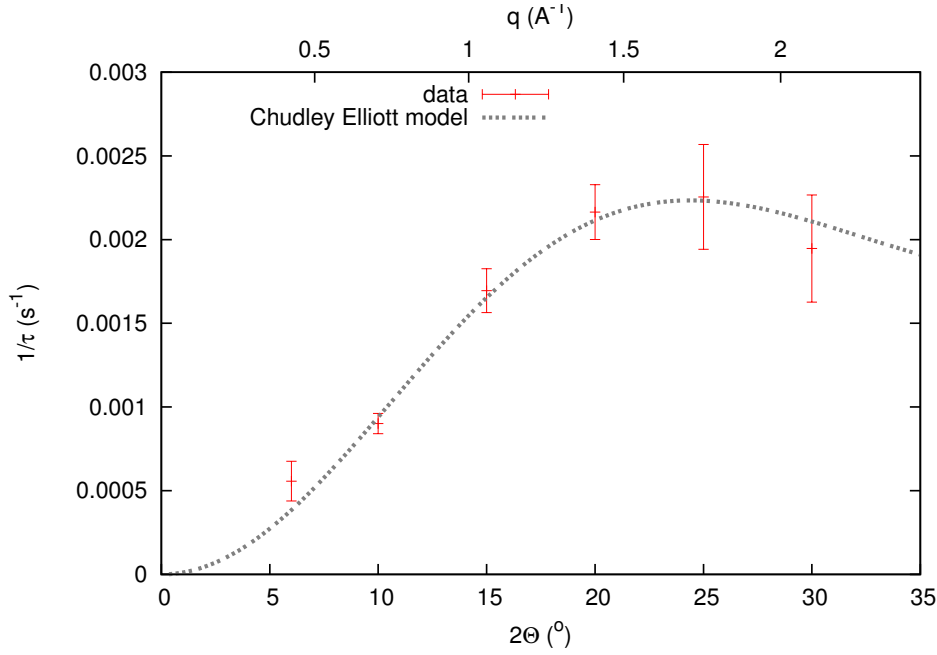


**Figure 5.11:** Fitted curve for the Chudley Elliott model

Which in the case on  $\text{Ni}_{97}\text{Pt}_3$  leads to:

$$\begin{aligned}\Gamma_{\text{Ni}_{97}\text{Pt}_3}(q, T) &= \nu_0(T) \left( p_{\text{NN}} \left( 1 - \frac{\sin(q \cdot \frac{d}{\sqrt{2}})}{q \cdot \frac{d}{\sqrt{2}}} \right) + p_{3\text{N}} \left( 1 - \frac{\sin(q \cdot d)}{q \cdot d} \right) \right) \\ &= \nu_0(T) \left( (0.84 \pm 0.14) \left( 1 - \frac{\sin(q \cdot \frac{d}{\sqrt{2}})}{q \cdot \frac{d}{\sqrt{2}}} \right) \right. \\ &\quad \left. + (0.16 \pm 0.10) \left( 1 - \frac{\sin(q \cdot d)}{q \cdot d} \right) \right)\end{aligned}$$

And at a temperature of 830K:

$$\begin{aligned}\Gamma_{\text{Ni}_{97}\text{Pt}_3}(q, 830) &= 1.88 \cdot 10^{-3} \text{s}^{-1} \left( (0.84 \pm 0.13) \left( 1 - \frac{\sin(q \cdot 2.4975)}{q \cdot 2.4975} \right) \right. \\ &\quad \left. + (0.16 \pm 0.13) \left( 1 - \frac{\sin(q \cdot 3.532)}{q \cdot 3.532} \right) \right) \quad (5.6)\end{aligned}$$

Therefore we have a probability for an atom to jump into one particular of its 12 nearest-neighbor sites of  $(0.070 \pm 0.012)\%$  and a probability for it to jump into a particular next-nearest-neighbor site, of which 6 are available, of  $(0.027 \pm 0.017)\%$ . The average residence time for an atom is 532 seconds.

### 5.3.2 Monte Carlo simulation

The first act of business is to find out how long the simulation must run in order to get a sufficient statistics. It turned out to that it was sufficient to calculate 1000 values that had to be correlated. Because of the small correlation times the correlation function is calculated every half Monte Carlo step. This means that one has to calculate 500 Monte Carlo steps. Because of random access memory limitations the number of files to be correlated is chosen to be 100. I also found dividing the  $q$ -space into 40 shells to be a good number to have enough data points but also enough voxels per shell (see section 3.2.3).

The calculated data was fitted with two functions according to equation (5.1). For the first function  $\beta$  is equal to one and for the second it is a free fit parameter. Furthermore  $c$  and  $b$  are defined to be one. This is only valid if we would not average over different orientations, which would mean a  $\beta$  value of one. However as the fitting parameters are strongly correlated fitting  $c$  and  $b$  would not give additional information. Therefore it is preferable to have divergences from the real case showing only in two parameters ( $\tau$  and  $\beta$ ) rather than in four. For the case of no interaction figure 5.12 shows the calculated data and fitted  $g^{(2)}$  functions for the innermost shell at  $q = 0.03 \text{ \AA}^{-1}$  and the outermost shell at  $q = 2.69 \text{ \AA}^{-1}$ .

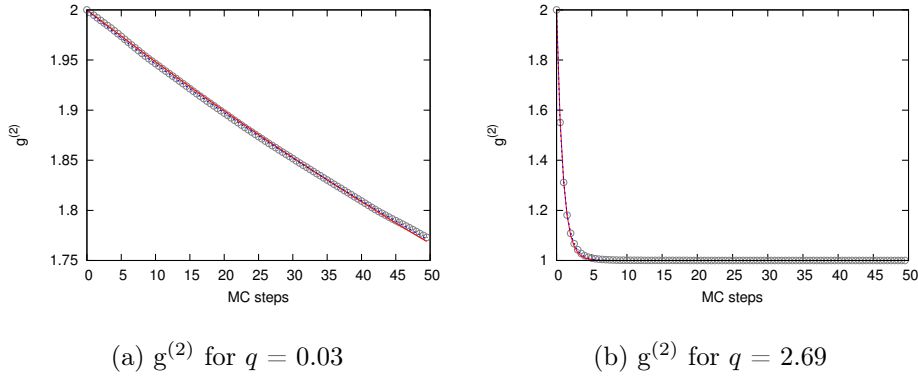


**Figure 5.12:** Fitted  $g^{(2)}$  functions (lines) and calculated data (circles) for innermost shell (a) and outermost shell (b) for no interaction potential

Three simulations were performed. The first with no interaction between the atoms. The others were performed with interaction between the platinum atoms only, namely with repelling force and an interaction potential between nearest neighbors of 0.05 eV and with attracting force and a potential of -0.05 eV. As stated above the short range order can be seen from the  $2\Theta$  dependent intensity. The calculated curves for the three cases are given in figure 5.13.

The minor deviations in the case of no interaction (figure 5.13(a)) are due to statistical noise.

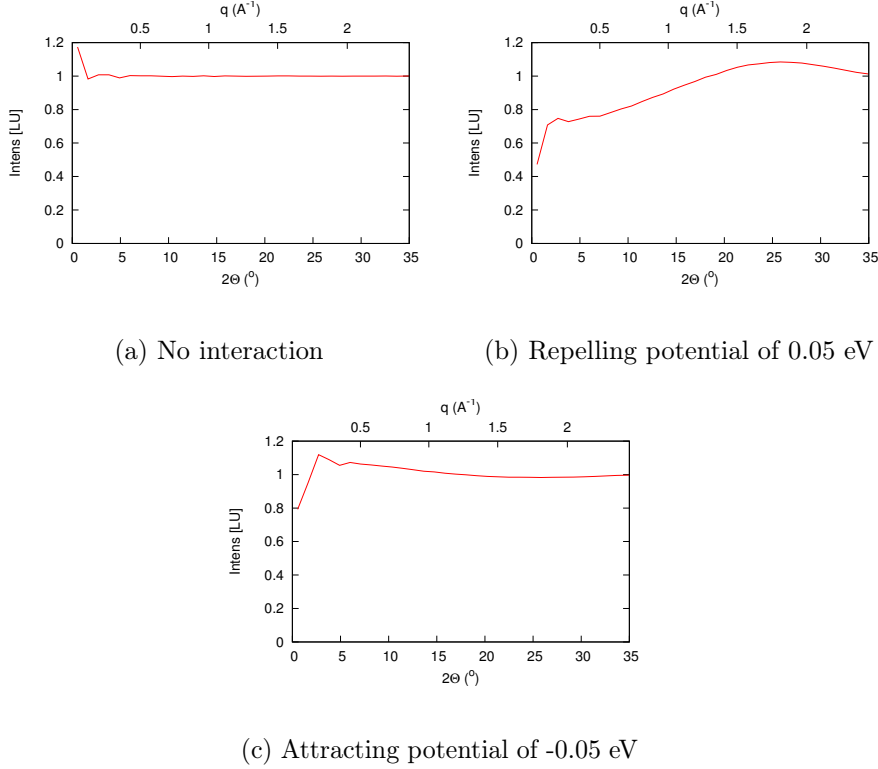


**Figure 5.13:**  $2\theta$  dependent intensities calculated with Monte Carlo simulation

Figure 5.14 shows the correlation times calculated with the program without interaction potential for fits with  $\beta = 1$  and  $\beta$  as a free parameter. The simulated correlation times are scaled to match the measured ones. From the scaling factor one sees that for a system with no interaction potential one Monte Carlo step equals 365 seconds. The difference between the correlation times is shown in figure 5.14(c). For small  $q$  values it is extremely big due to the bad statistics resulting from fewer voxels. Also subdividing one of the inner shells into sub shells would lead to a bigger gradient in the correlation times than it would be the case for an outer shell. More valuable is the information that for big  $q$  values the correlation times for the assumption of equally orientated grains with  $\beta = 1$  gets smaller than for the model with  $\beta < 1$ . Generally it can be said, however, that the correlation times vary very little. The calculated correlation times for the case of repelling and attracting interaction potentials are given in figures 5.15 and 5.16. The simulated data points again are scaled to match the experimental ones. This leads to scaling factors corresponding to 100 seconds per Monte Carlo step

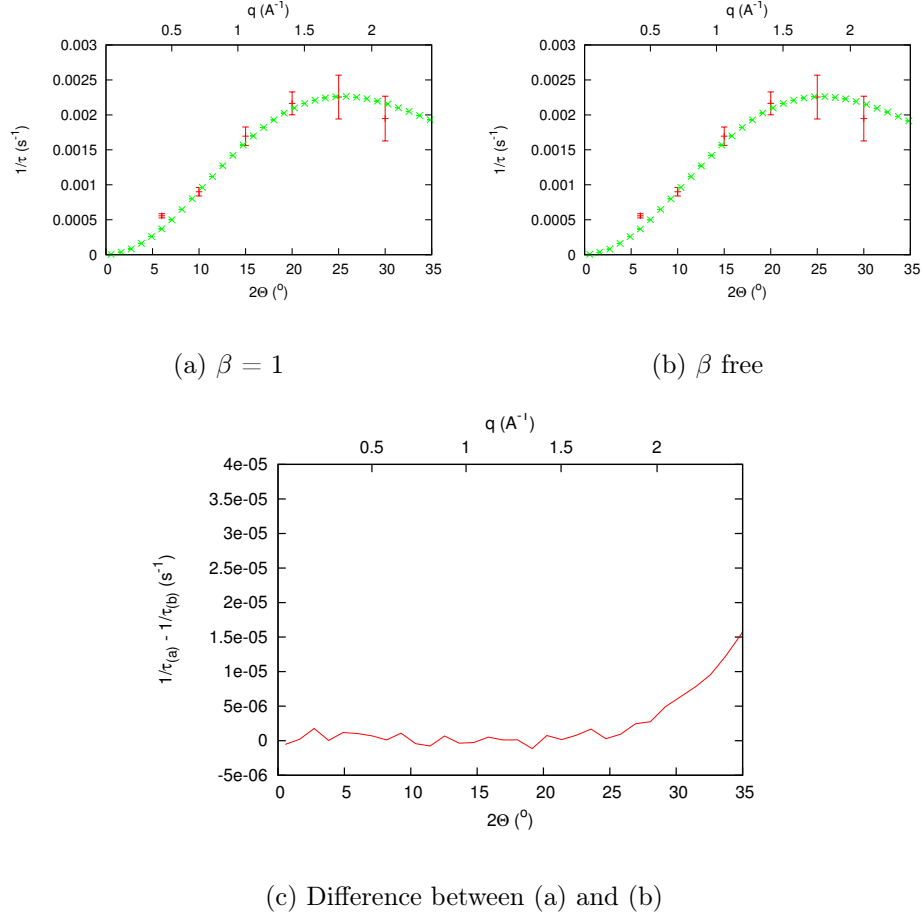
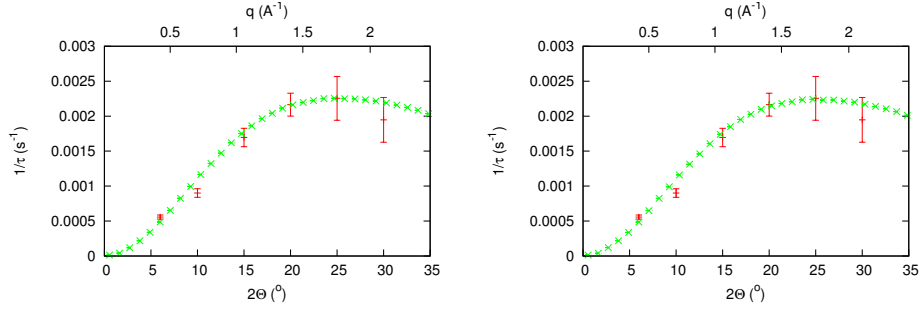


**Figure 5.14:** (a) and (b) measured correlation times in *red* and calculated in *green*; (c) difference between  $\tau$  values. All simulations completed without interaction potential.

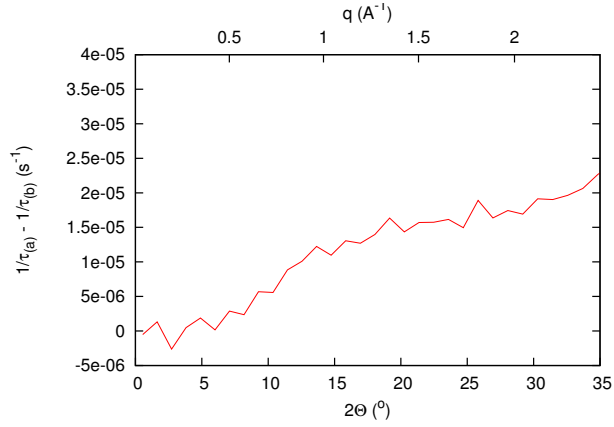
for repelling platinum atoms and again 365 seconds per Monte Carlo step for attracting ones.

Figure 5.17 shows the calculated exponents  $\beta$  for all three simulations. As already mentioned, the smaller the shell the worse the statistics plus for small  $q$ -vectors the correlation times vary more. Therefore we can expect an exponential decay with  $\beta < 1$  for small  $q$  values, as can be seen in the image. Also for angles bigger than  $2\theta = 25^\circ$ ,  $\beta$  gets significantly smaller than one. Apparently the exponents  $\beta$  get bigger for larger angles. For repelling potentials the exponents are slightly smaller and for attracting potentials bigger than for the case with no interaction potentials. Generously spoken there is no difference in the correlation time between the cases of repelling and attracting potentials.



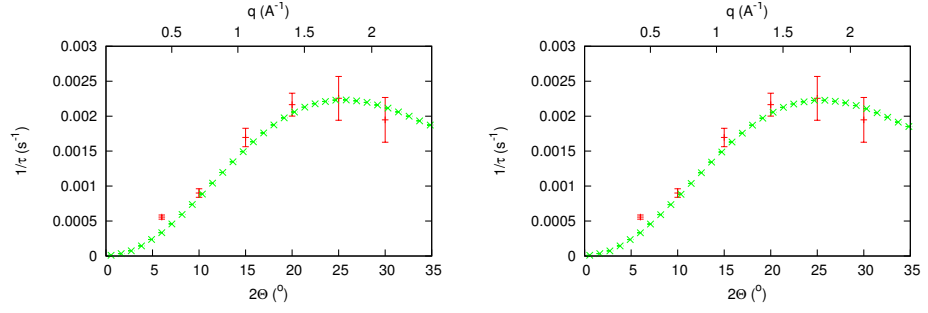
(a)  $\beta = 1$

(b)  $\beta$  free



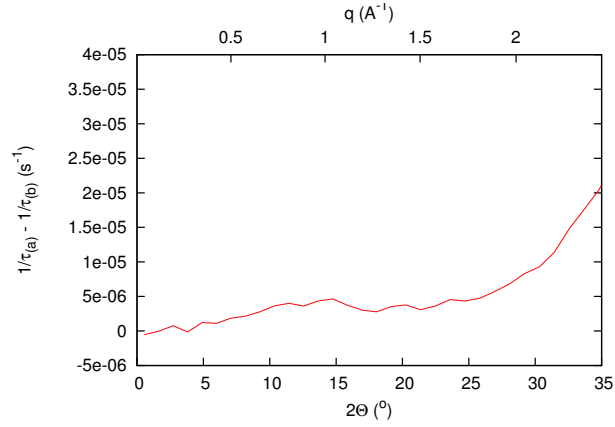
(c) Difference between (a) and (b)

**Figure 5.15:** (a) and (b) measured correlation times in *red* and calculated in *green*; (c) difference between  $\tau$  values. All simulations completed with a repelling interaction potential of 0.05 eV.



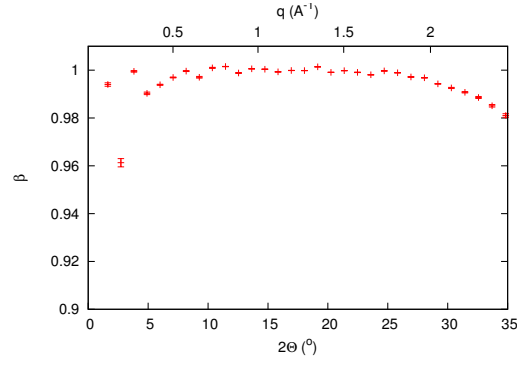
(a)  $\beta = 1$

(b)  $\beta$  free

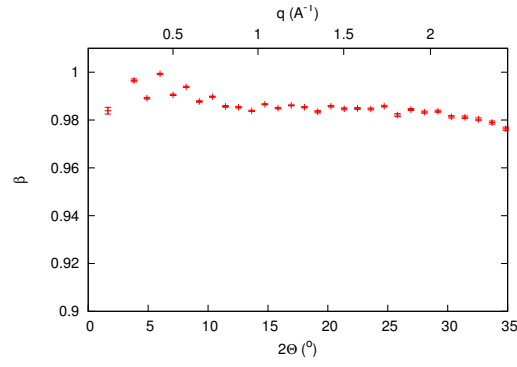


(c) Difference between (a) and (b)

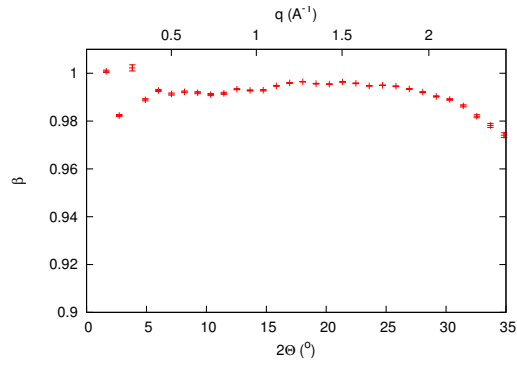
**Figure 5.16:** (a) and (b) measured correlation times in *red* and calculated in *green*; (c) difference between  $\tau$  values. All simulations completed a attracting interaction potential of -0.05 eV.



(a) No interaction



(b) Repelling potential of 0.05 eV



(c) Attracting potential of -0.05 eV

**Figure 5.17:**  $2\theta$  dependent exponents  $\beta$  calculated with Monte Carlo simulation for different interaction potentials

## 5.4 Finding the diffusion constant

There are different ways of calculating diffusion constants with the data at hand. I will introduce some of them.

### 5.4.1 Interdiffusion via self diffusion

As discussed, chemical diffusion is similar to interdiffusion. Therefore we try to find an estimate in the right order of magnitude. I will use diffusion values provided by the literature and the Darken equation (1.17), which we can rewrite as:

$$\tilde{D} = c_i \frac{a_i^3}{\bar{a}^3} D_j + c_j \frac{a_j^3}{\bar{a}^3} D_i$$

Here  $c_i$  is the contribution,  $a_i$  the lattice constant of a pure metal and  $\bar{a}$  the lattice constant of the alloy.

The literature does, as far as my research has taken me, not supply us with information about the self diffusion constants of nickel or platinum in  $\text{Ni}_{97}\text{Pt}_3$ . Therefore I will use the self diffusion constants for nickel and for platinum the impurity diffusion constant. They are given by [MADELUNG and SCHOPPER, 1988] as shown in table 5.1.

	Ni	Pt
$D_0$ ( $10^{-4}\text{m}^2 \text{s}^{-1}$ )	2.5	2.2
$Q$ ( $\text{kJ mol}^{-1}$ )	286.8	292.6
Temp. range (K)	1354 - 1481	1323 - 1477

**Table 5.1:** Self diffusion coefficient of Ni and impurity diffusion coefficient of Pt in Ni taken from Landolt Börnstein

Because of the Arrhenius relation:

$$D = D_0 \cdot e^{\frac{-Q}{RT}},$$

we get, for  $T = 830 \text{ K}$ :

$$D_{\text{Ni}} = 2.23 \cdot 10^{-22} \text{m}^2 \text{s}^{-1} = 22.3 \cdot 10^{-3} \text{\AA}^2 \text{s}^{-1}$$

$$D_{\text{Pt}} = 7.71 \cdot 10^{-23} \text{m}^2 \text{s}^{-1} = 7.71 \cdot 10^{-3} \text{\AA}^2 \text{s}^{-1}$$

The lattice constants can be found in table 2.1. Using them we can



calculate the interdiffusion constant as:

$$\begin{aligned}
\tilde{D} &= c_{\text{Pt}} \frac{a_{\text{Pt}}^3}{\bar{a}^3} \cdot D_{\text{Ni}}^I + c_{\text{Ni}} \frac{a_{\text{Ni}}^3}{\bar{a}^3} \cdot D_{\text{Pt}}^I \\
&= 0.03 \cdot \frac{3.92^3}{3.53^3} \cdot 2.23 \cdot 10^{-22} + 0.97 \cdot \frac{3.52^3}{3.53^3} \cdot 7.71 \cdot 10^{-23} \\
&= 8.33 \cdot 10^{-22} \text{m}^2 \text{s}^{-1} = 83.3 \cdot 10^{-3} \text{\AA}^2 \text{s}^{-1}
\end{aligned}$$

### 5.4.2 Small angle approximation

For small angles we can calculate the diffusion constant according to Fick's law. The second law without a driving force is given (according to equation (1.16)) as:

$$\frac{\partial c}{\partial t} = \tilde{D} \frac{\partial^2 c}{\partial x^2}$$

Performing a Fourier transform in the space regime leads to:

$$\frac{\partial \mathcal{F}(c)}{\partial t} = -\tilde{D} q^2 \mathcal{F}(c)$$

Solving this differential equation leads to:

$$\mathcal{F}(c) = e^{-\tilde{D} q^2 t}$$

According to equations (1.33) and (1.41) we can write:

$$\Gamma_{\text{inc}} = \tilde{D} q^2$$

Or, to get the diffusion coefficient:

$$\tilde{D} = \frac{1}{\tau(q) \cdot q^2} \quad (5.7)$$

We can plot  $\Gamma_{\text{inc}}$  to  $q^2$  and fit a line through the data points corresponding to equation (5.7) as shown in figure 5.18. This gives a diffusion coefficient of:

$$D = (1.95 \pm 0.42) \cdot 10^{-3} \text{\AA}^2 \text{s}^{-1} = (0.195 \pm 0.042) \cdot 10^{-22} \text{m}^2 \text{s}^{-1}$$

### 5.4.3 Einstein relation

Considering a random walk of an atom and comparing with Fick's laws leads to the Einstein-Smoluchowski relation. According to [MEHRER, 2007], it is given as 5.8.

$$D = \frac{\langle R^2 \rangle}{6\tau} \quad (5.8)$$

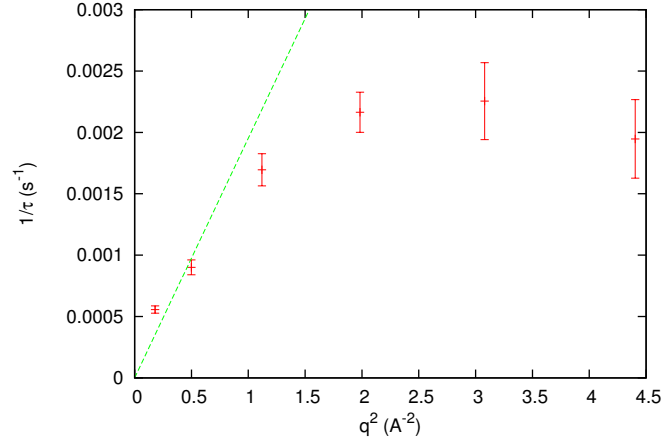


**Figure 5.18:** Energy broadening  $\Gamma_{\text{inc}}$  to  $q^2$  with fit for small angles (up to  $15^\circ$ )

For the case of nearest-neighbor jumps for example, this would lead to:

$$D = \frac{\nu_{\text{NN}} \cdot a_{\text{NN}}^2}{6}$$

Using the frequencies for jumps into nearest and next-nearest-neighbor shells we calculated above, the diffusion constant can be gained:

$$\tilde{D} = \frac{\nu_{\text{NN}} a_{\text{NN}}^2}{6} + \frac{\nu_{3\text{N}} a_{3\text{N}}^2}{6}$$

This leads, for the above calculated values (at 830K), to a chemical diffusion constant of:

$$\tilde{D} = (2.28 \pm 0.48) \cdot 10^{-3} \text{Å}^2 \text{s}^{-1} = (0.228 \pm 0.048) \cdot 10^{-22} \text{m}^2 \text{s}^{-1}$$

Obviously this result lies within the error margin of the small angle approximation.

#### 5.4.4 Interdiffusion in thin layers

Due to measurements of Alice Mikikits-Leitner on Ni-Pt multilayers<sup>2</sup>, the chemical diffusion constant at 873 K for Ni Pt - layers with three percent platinum is:

$$\tilde{D}_{\text{thin\_layer}} = 1.17 \cdot 10^{-22} \text{m}^2 \text{s}^{-1}$$

This is obviously in good agreement with the chemical diffusion constant calculated with the Chudley Elliott model.

---

<sup>2</sup>Private communication

In order to compare this with our result we use the Arrhenius theorem and the activation energy calculated in 5.2 and the relation:

$$D(T_2) = D(T_1)e^{E_a\left(\frac{1}{k_B T_1} - \frac{1}{k_B T_2}\right)}$$

which leads to:

$$\begin{aligned} D(873\text{K}) &= (0.228 \pm 0.048)e^{(2.71 \pm 0.14) \text{ eV} \left(\frac{1}{k_B 830\text{K}} - \frac{1}{k_B 873\text{K}}\right)} \cdot 10^{-22} \text{m}^2 \text{s}^{-1} \\ &= (1.47 \pm 0.15) \cdot 10^{-22} \text{m}^2 \text{s}^{-1} \end{aligned}$$

So the agreement of both experimental methods is surprisingly good.

## Chapter 6

# Conclusion

XPCS is a relatively new method for investigating diffusion. It was successfully applied to a prime example for the technique, namely a Cu-Au alloy, as shown by [LEITNER et al., 2009]. As nickel and platinum also have a big gap in their atomic numbers it seemed promising to investigate this system. The attempt to manufacture ideal samples, which would be single crystals left us facing a number of problems, which we will try to overcome in the future.

In order to test the quality of interpretations gained on a polycrystal, simulations were undertaken. Although the physical principles for the simulation were chosen as basic as possible, there was a qualitative consent with a real system. With the growing number of available potentials calculated by cluster expansion method (CE) it will be possible to simulate diffusion processes with increasing accuracy.

The key point for deducing the theory in this thesis was to neglect atomic interaction potentials. It could be shown, that for a nickel platinum system with only 3% platinum, this assumption leads to a model that gives a good representation of reality. With this model we found the activation energy for diffusion in  $\text{Ni}_{97}\text{Pt}_3$  of  $(2.71 \pm 0.14)$  eV. It was further shown that even in a polycrystal the presumption of having an exponent of  $\beta = 1$  in the fit function only leads to a venial error. Therefore it was valid to use the Chudley Elliot model to get an estimation of the jump frequencies for nearest and next nearest neighbor jumps. This led to a chemical diffusion constant of  $(0.23 \pm 0.05) \cdot 10^{-22} \text{m}^2 \text{s}^{-1}$  at 830 K. This diffusion constant is surprisingly consistent with the results found by thin layer experiments.

To get a more precise picture, however, it would be necessary to find jump frequencies matching exact  $q$  vectors. Therefore it is inevitable to have a single crystal which can be most favorably orientated. Unfortunately it was not possible to produce such a crystal until now.

## Appendix A

### Elaborate calculations

#### A.1 Solving equation 1.4

$$\begin{aligned}
G(\vec{r}, t) &= \frac{1}{\sqrt{2\pi}^3} \int d\omega \int d^3k \frac{1}{4\pi^2} \frac{1}{(|\vec{k}|^2 - \frac{\omega^2}{c^2})} e^{i\vec{k}\vec{r}} e^{i\omega t} \\
&= \frac{1}{\sqrt{2\pi}^3} \frac{1}{4\pi^2} \int_{-\infty}^{\infty} d^3k e^{i\vec{k}\vec{r}} \lim_{R \rightarrow \infty} \int_{-R}^R d\omega \frac{e^{i\omega t}}{(|\vec{k}|^2 - \frac{\omega^2}{c^2})} \\
&= \frac{1}{\sqrt{2\pi}^3} \frac{c^2}{4\pi^2} \int_{-\infty}^{\infty} d^3k e^{i\vec{k}\vec{r}} \lim_{R \rightarrow \infty} \int_{-R}^R d\omega \frac{e^{i\omega t}}{(\omega_0^2 - \omega^2)}
\end{aligned}$$

with:

$$c^2 \cdot |\vec{k}|^2 = \omega_0^2$$

$$\begin{aligned}
\text{Res}_{z \rightarrow z_0} \left( \frac{e^{izt}}{(z_0^2 - z^2)} \right) &= \lim_{z \rightarrow z_0} \left( (z - z_0) \frac{e^{izt}}{(z_0 + z)(z_0 - z)} \right) \\
&= \frac{-e^{iz_0 t}}{2z_0}
\end{aligned}$$

$$\begin{aligned}
\text{Res}_{z \rightarrow -z_0} \left( \frac{e^{izt}}{(z_0^2 - z^2)} \right) &= \lim_{z \rightarrow -z_0} \left( (z + z_0) \frac{e^{izt}}{(z_0 + z)(z_0 - z)} \right) \\
&= \frac{e^{-iz_0 t}}{2z_0}
\end{aligned}$$

$$\begin{aligned}
\oint dz \frac{e^{izt}}{(z_0^2 - z^2)} &= 2\pi i (\text{Res}_{z \rightarrow z_0} + \text{Res}_{z \rightarrow -z_0}) \\
&= 2\pi i \left( \frac{-e^{iz_0 t}}{2z_0} + \frac{e^{-iz_0 t}}{2z_0} \right)
\end{aligned}$$

$$\begin{aligned}
G(\vec{r}, t) &= \frac{1}{\sqrt{2\pi^3}} \frac{c^2}{4\pi^2} \int_{-\infty}^{\infty} d^3k e^{i\vec{k}\vec{r}} \frac{2\pi i}{2\omega_0} (e^{-i\omega_0 t} - e^{i\omega_0 t}) \\
&= \frac{c^2 i}{4\pi\sqrt{2\pi^3}} \int_{-\infty}^{\infty} d^3k \frac{e^{i\vec{k}\vec{r}}}{\omega_0} (e^{-i\omega_0 t} - e^{i\omega_0 t}) \\
&= \frac{i}{4\pi c\sqrt{2\pi^3}} \int_{-\infty}^{\infty} d^3k \frac{e^{i\vec{k}\vec{r}}}{|\vec{k}|} (e^{-i|\vec{k}|ct} - e^{i|\vec{k}|ct}) \\
&= \frac{i}{4\pi c\sqrt{2\pi^3}} \int_0^{\infty} dk k^2 \int_{-\pi}^{\pi} d\alpha \sin \alpha \frac{e^{ikr \cos(\alpha)}}{k} (e^{-ikct} - e^{ikct}) \\
&= \frac{i}{4\pi c\sqrt{2\pi^3}} \int_0^{\infty} dk k \int_{-1}^1 dx e^{ikrx} (e^{-ikct} - e^{ikct}) \\
&= \frac{i}{4\pi c\sqrt{2\pi^3}} \int_0^{\infty} dk k (e^{-ikct} - e^{ikct}) \frac{1}{ikr} e^{ikrx} \Big|_{x=-1}^1 \\
&= \frac{1}{4\pi c\sqrt{2\pi^3}} \int_0^{\infty} dk (e^{-ikct} - e^{ikct}) \frac{e^{ikr} - e^{-ikr}}{r} \\
&= \frac{1}{4\pi c\sqrt{2\pi^3}} \int_0^{\infty} dk (e^{ik(r-ct)} - e^{-ik(r+ct)} - e^{-ik(r+ct)} + e^{-ik(r-ct)}) \\
&= \frac{1}{4\pi c\sqrt{2\pi^3}} \int_{-\infty}^{\infty} dk (e^{ik(r-ct)} - e^{ik(r+ct)}) \\
&= \frac{1}{4\pi c} (\delta(r-ct) - \delta(r+ct))
\end{aligned}$$

## A.2 Calculating the angle dependent scattered radiation

The scattering intensity, as a function of the scattering angle  $2\Theta$ , is given as:

$$\begin{aligned}
I(2\Theta) &= \int_0^d dx e^{-\mu x} e^{-\mu \frac{d-x}{\cos(2\Theta)}} \\
&= e^{-\mu \frac{d}{\cos(2\Theta)}} \int_0^d dx e^{-\mu x \left(1 - \frac{1}{\cos(2\Theta)}\right)} \\
&= e^{-\mu \frac{d}{\cos(2\Theta)}} \frac{1}{-\mu \left(1 - \frac{1}{\cos(2\Theta)}\right)} \left( e^{-\mu x \left(1 - \frac{1}{\cos(2\Theta)}\right)} \right) \Big|_0^d \\
&= e^{-\mu \frac{d}{\cos(2\Theta)}} \frac{1}{\mu \left(1 - \frac{1}{\cos(2\Theta)}\right)} \left( 1 - e^{-\mu d \left(1 - \frac{1}{\cos(2\Theta)}\right)} \right) \\
&= \frac{e^{-\mu \frac{d}{\cos(2\Theta)}} - e^{-\mu d}}{\mu \left(1 - \frac{1}{\cos(2\Theta)}\right)}
\end{aligned} \tag{A.1}$$

## A.3 Calculating $\Gamma_{\text{inc}}$

$$\Gamma_{\text{inc}}(\vec{q}) = \sum_{\Delta \vec{a}} \frac{\nu_{\Delta \vec{a}}}{Z_{\Delta \vec{a}}} (1 - e^{i\vec{q}\Delta \vec{a}}) \tag{A.2}$$

$$\Gamma_{\text{inc}}(\vec{q}) = \Gamma_{\text{inc}_{\text{NN}}}(\vec{q}) + \Gamma_{\text{inc}_{\text{3N}}}(\vec{q}) + \Gamma_{\text{inc}_{\text{4N}}}(\vec{q}) + \Gamma_{\text{inc}_{\text{5N}}}(\vec{q}) \tag{A.3}$$

$$\vec{q} = \begin{pmatrix} q_x \\ q_y \\ q_z \end{pmatrix} \quad \vec{a} = \begin{pmatrix} a_x \\ a_y \\ a_z \end{pmatrix}$$

$$\begin{aligned}
\sum_{\Delta \vec{a}} e^{i\vec{q}\Delta \vec{a}} &= \sum_{\Delta \vec{a}} \cos(\vec{q} \cdot \vec{a}) \\
&= \sum_{\Delta \vec{a}} \cos(q_x a_x + q_y a_y + q_z a_z) \\
&= \sum_{\Delta \vec{a}} \cos(q_x a_x) \cos(q_y a_y + q_z a_z) - \sin(q_x a_x) \sin(q_y a_y + q_z a_z) \\
&= \sum_{\Delta \vec{a}} \cos(q_x a_x) (\cos(q_y a_y) \cos(q_z a_z) - \sin(q_y a_y) \sin(q_z a_z)) - \\
&\quad - \sin(q_x a_x) (\sin(q_y a_y) \cos(q_z a_z) + \cos(q_y a_y) \sin(q_z a_z))
\end{aligned}$$

With lattice constant:  $d$

### A.3.1 Calculating for fcc

Nearest neighbours (NN)

$$\Delta \vec{a}_{\text{NN}} = \begin{pmatrix} \frac{d}{2} \\ \frac{d}{2} \\ 0 \end{pmatrix}, \begin{pmatrix} -\frac{d}{2} \\ -\frac{d}{2} \\ 0 \end{pmatrix}, \begin{pmatrix} \frac{d}{2} \\ -\frac{d}{2} \\ 0 \end{pmatrix}, \begin{pmatrix} -\frac{d}{2} \\ \frac{d}{2} \\ 0 \end{pmatrix}, \\ \begin{pmatrix} 0 \\ \frac{d}{2} \\ \frac{d}{2} \end{pmatrix}, \begin{pmatrix} 0 \\ -\frac{d}{2} \\ -\frac{d}{2} \end{pmatrix}, \begin{pmatrix} 0 \\ \frac{d}{2} \\ -\frac{d}{2} \end{pmatrix}, \begin{pmatrix} 0 \\ -\frac{d}{2} \\ \frac{d}{2} \end{pmatrix}, \\ \begin{pmatrix} \frac{d}{2} \\ 0 \\ \frac{d}{2} \end{pmatrix}, \begin{pmatrix} -\frac{d}{2} \\ 0 \\ -\frac{d}{2} \end{pmatrix}, \begin{pmatrix} \frac{d}{2} \\ 0 \\ -\frac{d}{2} \end{pmatrix}, \begin{pmatrix} -\frac{d}{2} \\ 0 \\ \frac{d}{2} \end{pmatrix}$$

$$\begin{aligned} \sum_{\Delta \vec{a}} e^{i\vec{q} \cdot \Delta \vec{a}} &= \cos(q_x \cdot \frac{d}{2}) (\cos(q_y \cdot \frac{d}{2}) \cos(q_z \cdot 0) - \sin(q_y \cdot \frac{d}{2}) \sin(q_z \cdot 0)) \\ &\quad - \sin(q_x \cdot \frac{d}{2}) (\sin(q_y \cdot \frac{d}{2}) \cos(q_z \cdot 0) + \cos(q_y \cdot \frac{d}{2}) \sin(q_z \cdot 0)) \\ &\quad + \cos(q_x \cdot \frac{-d}{2}) (\cos(q_y \cdot \frac{-d}{2}) \cos(q_z \cdot 0) - \sin(q_y \cdot \frac{-d}{2}) \sin(q_z \cdot 0)) \\ &\quad - \sin(q_x \cdot \frac{-d}{2}) (\sin(q_y \cdot \frac{-d}{2}) \cos(q_z \cdot 0) + \cos(q_y \cdot \frac{-d}{2}) \sin(q_z \cdot 0)) \\ &\quad + \cos(q_x \cdot \frac{d}{2}) (\cos(q_y \cdot \frac{-d}{2}) \cos(q_z \cdot 0) - \sin(q_y \cdot \frac{-d}{2}) \sin(q_z \cdot 0)) \\ &\quad - \sin(q_x \cdot \frac{d}{2}) (\sin(q_y \cdot \frac{-d}{2}) \cos(q_z \cdot 0) + \cos(q_y \cdot \frac{-d}{2}) \sin(q_z \cdot 0)) \\ &\quad + \cos(q_x \cdot \frac{-d}{2}) (\cos(q_y \cdot \frac{d}{2}) \cos(q_z \cdot 0) - \sin(q_y \cdot \frac{d}{2}) \sin(q_z \cdot 0)) \\ &\quad - \sin(q_x \cdot \frac{-d}{2}) (\sin(q_y \cdot \frac{d}{2}) \cos(q_z \cdot 0) + \cos(q_y \cdot \frac{d}{2}) \sin(q_z \cdot 0)) \\ &\quad + \cos(q_x \cdot \frac{d}{2}) (\cos(q_y \cdot 0) \cos(q_z \cdot \frac{d}{2}) - \sin(q_y \cdot 0) \sin(q_z \cdot \frac{d}{2})) \\ &\quad - \sin(q_x \cdot \frac{d}{2}) (\sin(q_y \cdot 0) \cos(q_z \cdot \frac{d}{2}) + \cos(q_y \cdot 0) \sin(q_z \cdot \frac{d}{2})) \\ &\quad + \cos(q_x \cdot \frac{-d}{2}) (\cos(q_y \cdot 0) \cos(q_z \cdot \frac{-d}{2}) - \sin(q_y \cdot 0) \sin(q_z \cdot \frac{-d}{2})) \\ &\quad - \sin(q_x \cdot \frac{-d}{2}) (\sin(q_y \cdot 0) \cos(q_z \cdot \frac{-d}{2}) + \cos(q_y \cdot 0) \sin(q_z \cdot \frac{-d}{2})) \end{aligned}$$



$$\begin{aligned}
& + \cos(q_x \cdot \frac{-d}{2})(\cos(q_y \cdot 0) \cos(q_z \cdot \frac{d}{2}) - \sin(q_y \cdot 0) \sin(q_z \cdot \frac{d}{2})) \\
& - \sin(q_x \cdot \frac{-d}{2})(\sin(q_y \cdot 0) \cos(q_z \cdot \frac{d}{2}) + \cos(q_y \cdot 0) \sin(q_z \cdot \frac{d}{2})) \\
& + \cos(q_x \cdot \frac{d}{2})(\cos(q_y \cdot 0) \cos(q_z \cdot \frac{-d}{2}) - \sin(q_y \cdot 0) \sin(q_z \cdot \frac{-d}{2})) \\
& - \sin(q_x \cdot \frac{d}{2})(\sin(q_y \cdot 0) \cos(q_z \cdot \frac{-d}{2}) + \cos(q_y \cdot 0) \sin(q_z \cdot \frac{-d}{2})) \\
& + \cos(q_x \cdot 0)(\cos(q_y \cdot \frac{d}{2}) \cos(q_z \cdot \frac{d}{2}) - \sin(q_y \cdot \frac{d}{2}) \sin(q_z \cdot \frac{d}{2})) \\
& - \sin(q_x \cdot 0)(\sin(q_y \cdot \frac{d}{2}) \cos(q_z \cdot \frac{d}{2}) + \cos(q_y \cdot \frac{d}{2}) \sin(q_z \cdot \frac{d}{2})) \\
& + \cos(q_x \cdot 0)(\cos(q_y \cdot \frac{-d}{2}) \cos(q_z \cdot \frac{-d}{2}) - \sin(q_y \cdot \frac{-d}{2}) \sin(q_z \cdot \frac{-d}{2})) \\
& - \sin(q_x \cdot 0)(\sin(q_y \cdot \frac{-d}{2}) \cos(q_z \cdot \frac{-d}{2}) + \cos(q_y \cdot \frac{-d}{2}) \sin(q_z \cdot \frac{-d}{2})) \\
& + \cos(q_x \cdot 0)(\cos(q_y \cdot \frac{-d}{2}) \cos(q_z \cdot \frac{d}{2}) - \sin(q_y \cdot \frac{-d}{2}) \sin(q_z \cdot \frac{d}{2})) \\
& - \sin(q_x \cdot 0)(\sin(q_y \cdot \frac{-d}{2}) \cos(q_z \cdot \frac{d}{2}) + \cos(q_y \cdot \frac{-d}{2}) \sin(q_z \cdot \frac{d}{2})) \\
& + \cos(q_x \cdot 0)(\cos(q_y \cdot \frac{d}{2}) \cos(q_z \cdot \frac{-d}{2}) - \sin(q_y \cdot \frac{d}{2}) \sin(q_z \cdot \frac{-d}{2})) \\
& - \sin(q_x \cdot 0)(\sin(q_y \cdot \frac{d}{2}) \cos(q_z \cdot \frac{-d}{2}) + \cos(q_y \cdot \frac{d}{2}) \sin(q_z \cdot \frac{-d}{2}))
\end{aligned}$$

$$\begin{aligned}
\sum_{\Delta \vec{a}} e^{i\vec{q}\Delta\vec{a}} &= \cos(q_x \cdot \frac{d}{2})(\cos(q_y \cdot \frac{d}{2}) \cdot 1) \\
& - \sin(q_x \cdot \frac{d}{2})(\sin(q_y \cdot \frac{d}{2}) \cdot 1) + \cos(q_x \cdot \frac{-d}{2})(\cos(q_y \cdot \frac{-d}{2}) \cdot 1) \\
& - \sin(q_x \cdot \frac{-d}{2})(\sin(q_y \cdot \frac{-d}{2}) \cdot 1) + \cos(q_x \cdot \frac{d}{2})(\cos(q_y \cdot \frac{-d}{2}) \cdot 1) \\
& - \sin(q_x \cdot \frac{d}{2})(\sin(q_y \cdot \frac{-d}{2}) \cdot 1) + \cos(q_x \cdot \frac{-d}{2})(\cos(q_y \cdot \frac{d}{2}) \cdot 1) \\
& - \sin(q_x \cdot \frac{-d}{2})(\sin(q_y \cdot \frac{d}{2}) \cdot 1) + \cos(q_x \cdot \frac{d}{2})(1 \cdot \cos(q_z \cdot \frac{d}{2})) \\
& - \sin(q_x \cdot \frac{d}{2})(1 \cdot \sin(q_z \cdot \frac{d}{2})) + \cos(q_x \cdot \frac{-d}{2})(1 \cdot \cos(q_z \cdot \frac{-d}{2})) \\
& - \sin(q_x \cdot \frac{-d}{2})(1 \cdot \sin(q_z \cdot \frac{-d}{2})) + \cos(q_x \cdot \frac{-d}{2})(1 \cdot \cos(q_z \cdot \frac{d}{2})) \\
& - \sin(q_x \cdot \frac{-d}{2})(1 \cdot \sin(q_z \cdot \frac{d}{2})) + \cos(q_x \cdot \frac{d}{2})(1 \cdot \cos(q_z \cdot \frac{-d}{2})) \\
& - \sin(q_x \cdot \frac{d}{2})(1 \cdot \sin(q_z \cdot \frac{-d}{2})) + 1 \cdot (\cos(q_y \cdot \frac{d}{2}) \cos(q_z \cdot \frac{d}{2}) \\
& - \sin(q_y \cdot \frac{d}{2}) \sin(q_z \cdot \frac{d}{2})) + 1 \cdot (\cos(q_y \cdot \frac{-d}{2}) \cos(q_z \cdot \frac{-d}{2}) \\
& - \sin(q_y \cdot \frac{-d}{2}) \sin(q_z \cdot \frac{-d}{2})) + 1 \cdot (\cos(q_y \cdot \frac{-d}{2}) \cos(q_z \cdot \frac{d}{2}) \\
& - \sin(q_y \cdot \frac{-d}{2}) \sin(q_z \cdot \frac{d}{2})) + 1 \cdot (\cos(q_y \cdot \frac{d}{2}) \cos(q_z \cdot \frac{-d}{2}) \\
& - \sin(q_y \cdot \frac{d}{2}) \sin(q_z \cdot \frac{-d}{2}))
\end{aligned}$$

$$\begin{aligned}
&= \cos(q_x \cdot \frac{d}{2}) \cos(q_y \cdot \frac{d}{2}) - \sin(q_x \cdot \frac{d}{2}) \sin(q_y \cdot \frac{d}{2}) \\
&\quad + \cos(q_x \cdot \frac{d}{2}) \cos(q_y \cdot \frac{d}{2}) - \sin(q_x \cdot \frac{d}{2}) \sin(q_y \cdot \frac{d}{2}) \\
&\quad + \cos(q_x \cdot \frac{d}{2}) \cos(q_y \cdot \frac{d}{2}) + \sin(q_x \cdot \frac{d}{2}) \sin(q_y \cdot \frac{d}{2}) \\
&\quad + \cos(q_x \cdot \frac{d}{2}) \cos(q_y \cdot \frac{d}{2}) + \sin(q_x \cdot \frac{d}{2}) \sin(q_y \cdot \frac{d}{2}) \\
&\quad + \cos(q_x \cdot \frac{d}{2}) \cos(q_z \cdot \frac{d}{2}) - \sin(q_x \cdot \frac{d}{2}) \sin(q_z \cdot \frac{d}{2}) \\
&\quad + \cos(q_x \cdot \frac{d}{2}) \cos(q_z \cdot \frac{d}{2}) - \sin(q_x \cdot \frac{d}{2}) \sin(q_z \cdot \frac{d}{2}) \\
&\quad + \cos(q_x \cdot \frac{d}{2}) \cos(q_z \cdot \frac{d}{2}) + \sin(q_x \cdot \frac{d}{2}) \sin(q_z \cdot \frac{d}{2}) \\
&\quad + \cos(q_x \cdot \frac{d}{2}) \cos(q_z \cdot \frac{d}{2}) + \sin(q_x \cdot \frac{d}{2}) \sin(q_z \cdot \frac{d}{2}) \\
&\quad + 1 \cdot (\cos(q_y \cdot \frac{d}{2}) \cos(q_z \cdot \frac{d}{2}) - \sin(q_y \cdot \frac{d}{2}) \sin(q_z \cdot \frac{d}{2})) \\
&\quad + 1 \cdot (\cos(q_y \cdot \frac{d}{2}) \cos(q_z \cdot \frac{d}{2}) - \sin(q_y \cdot \frac{d}{2}) \sin(q_z \cdot \frac{d}{2})) \\
&\quad + 1 \cdot (\cos(q_y \cdot \frac{d}{2}) \cos(q_z \cdot \frac{d}{2}) + \sin(q_y \cdot \frac{d}{2}) \sin(q_z \cdot \frac{d}{2})) \\
&\quad + 1 \cdot (\cos(q_y \cdot \frac{d}{2}) \cos(q_z \cdot \frac{d}{2}) + \sin(q_y \cdot \frac{d}{2}) \sin(q_z \cdot \frac{d}{2}))
\end{aligned}$$

$$\begin{aligned}
\Gamma_{\text{incNN}}(\vec{q}) &= \frac{\nu_{\text{NN}}}{Z_{\text{NN}}} \sum_{\Delta \vec{a}_{\text{NN}}} (1 - e^{i\vec{q}\Delta \vec{a}_{\text{NN}}}) \\
&= \frac{\nu_{\text{NN}}}{12} (12 - 4 \cdot (\cos(q_x \cdot \frac{d}{2}) \cos(q_y \cdot \frac{d}{2}) + \cos(q_x \cdot \frac{d}{2}) \cos(q_z \cdot \frac{d}{2}) + \cos(q_y \cdot \frac{d}{2}) \cos(q_z \cdot \frac{d}{2})))
\end{aligned}$$

**Next nearest neighbours (3N)**

$$\Delta \vec{a}_{3\text{N}} = \begin{pmatrix} d \\ 0 \\ 0 \end{pmatrix}, \begin{pmatrix} -d \\ 0 \\ 0 \end{pmatrix}, \begin{pmatrix} 0 \\ d \\ 0 \end{pmatrix}, \begin{pmatrix} 0 \\ -d \\ 0 \end{pmatrix}, \begin{pmatrix} 0 \\ 0 \\ d \end{pmatrix}, \begin{pmatrix} 0 \\ 0 \\ -d \end{pmatrix}$$

$$\sum_{\Delta \vec{a}} e^{i\vec{q}\Delta \vec{a}} = e^{iq_x d} + e^{iq_x(-d)} + e^{iq_y d} + e^{iq_y(-d)} + e^{iq_z d} + e^{iq_z(-d)}$$

$$\begin{aligned}
\Gamma_{\text{inc3N}}(\vec{q}) &= \frac{\nu_{3\text{N}}}{Z_{3\text{N}}} \sum_{\Delta \vec{a}_{3\text{N}}} (1 - e^{i\vec{q}\Delta \vec{a}_{3\text{N}}}) \\
&= \frac{\nu_{3\text{N}}}{6} (6 - 2(\cos(q_x \cdot d) + \cos(q_y \cdot d) + \cos(q_z \cdot d)))
\end{aligned}$$

### Next next nearest neighbours (4N)

$$\Delta \vec{a}_{4N} = \begin{pmatrix} d \\ \frac{d}{2} \\ \frac{d}{2} \end{pmatrix}, \begin{pmatrix} d \\ \frac{-d}{2} \\ \frac{-d}{2} \end{pmatrix}, \begin{pmatrix} d \\ \frac{-d}{2} \\ \frac{d}{2} \end{pmatrix}, \begin{pmatrix} d \\ \frac{d}{2} \\ \frac{-d}{2} \end{pmatrix}, \\ \begin{pmatrix} -d \\ \frac{d}{2} \\ \frac{d}{2} \end{pmatrix}, \begin{pmatrix} -d \\ \frac{-d}{2} \\ \frac{-d}{2} \end{pmatrix}, \begin{pmatrix} -d \\ \frac{-d}{2} \\ \frac{d}{2} \end{pmatrix}, \begin{pmatrix} -d \\ \frac{d}{2} \\ \frac{-d}{2} \end{pmatrix}, \\ \begin{pmatrix} \frac{d}{2} \\ d \\ \frac{d}{2} \end{pmatrix}, \begin{pmatrix} \frac{-d}{2} \\ d \\ \frac{-d}{2} \end{pmatrix}, \begin{pmatrix} \frac{-d}{2} \\ d \\ \frac{d}{2} \end{pmatrix}, \begin{pmatrix} \frac{d}{2} \\ d \\ \frac{-d}{2} \end{pmatrix}, \\ \begin{pmatrix} \frac{d}{2} \\ -d \\ \frac{d}{2} \end{pmatrix}, \begin{pmatrix} \frac{-d}{2} \\ -d \\ \frac{-d}{2} \end{pmatrix}, \begin{pmatrix} \frac{-d}{2} \\ -d \\ \frac{d}{2} \end{pmatrix}, \begin{pmatrix} \frac{d}{2} \\ -d \\ \frac{-d}{2} \end{pmatrix}, \\ \begin{pmatrix} \frac{d}{2} \\ \frac{-d}{2} \\ d \end{pmatrix}, \begin{pmatrix} \frac{-d}{2} \\ \frac{-d}{2} \\ d \end{pmatrix}, \begin{pmatrix} \frac{-d}{2} \\ \frac{d}{2} \\ d \end{pmatrix}, \begin{pmatrix} \frac{d}{2} \\ \frac{d}{2} \\ d \end{pmatrix}, \\ \begin{pmatrix} \frac{d}{2} \\ \frac{-d}{2} \\ -d \end{pmatrix}, \begin{pmatrix} \frac{-d}{2} \\ \frac{-d}{2} \\ -d \end{pmatrix}, \begin{pmatrix} \frac{-d}{2} \\ \frac{d}{2} \\ -d \end{pmatrix}, \begin{pmatrix} \frac{d}{2} \\ \frac{d}{2} \\ -d \end{pmatrix}$$

$$\begin{aligned} \sum_{\Delta \vec{a}_{4N}} e^{i\vec{q}\Delta \vec{a}_{3N}} &= e^{iq_x d} e^{iq_y d/2} e^{iq_z d/2} + e^{iq_x d} e^{iq_y(-d/2)} e^{iq_z(-d/2)} + e^{iq_x d} e^{iq_y(-d/2)} e^{iq_z d/2} \\ &+ e^{iq_x d} e^{iq_y d/2} e^{iq_z(-d/2)} + e^{iq_x(-d)} e^{iq_y d/2} e^{iq_z d/2} + e^{iq_x(-d)} e^{iq_y(-d/2)} e^{iq_z(-d/2)} \\ &+ e^{iq_x(-d)} e^{iq_y(-d/2)} e^{iq_z d/2} + e^{iq_x(-d)} e^{iq_y d/2} e^{iq_z(-d/2)} + e^{iq_x d/2} e^{iq_y d} e^{iq_z d/2} \\ &+ e^{iq_x(-d/2)} e^{iq_y d} e^{iq_z(-d/2)} + e^{iq_x(-d/2)} e^{iq_y d} e^{iq_z d/2} + e^{iq_x d/2} e^{iq_y d} e^{iq_z(-d/2)} \\ &+ e^{iq_x d/2} e^{iq_y(-d)} e^{iq_z d/2} + e^{iq_x(-d/2)} e^{iq_y(-d)} e^{iq_z(-d/2)} + e^{iq_x(-d/2)} e^{iq_y(-d)} e^{iq_z d/2} \\ &+ e^{iq_x d/2} e^{iq_y(-d)} e^{iq_z(-d/2)} + e^{iq_x d/2} e^{iq_y d/2} e^{iq_z d} + e^{iq_x(-d/2)} e^{iq_y(-d/2)} e^{iq_z d} \\ &+ e^{iq_x(-d/2)} e^{iq_y d/2} e^{iq_z d} + e^{iq_x d/2} e^{iq_y(-d/2)} e^{iq_z d} + e^{iq_x d/2} e^{iq_y d/2} e^{iq_z(-d)} \\ &+ e^{iq_x(-d/2)} e^{iq_y(-d/2)} e^{iq_z(-d)} + e^{iq_x(-d/2)} e^{iq_y d/2} e^{iq_z(-d)} + e^{iq_x d/2} e^{iq_y(-d/2)} e^{iq_z(-d)} \\ &= 2 \cdot \cos(q_x \cdot d) (e^{iq_y d/2} e^{iq_z d/2} + e^{iq_y(-d/2)} e^{iq_z(-d/2)} + e^{iq_y(-d/2)} e^{iq_z d/2} + e^{iq_y d/2} e^{iq_z(-d/2)}) \\ &+ 2 \cdot \cos(q_y \cdot d) (e^{iq_x d/2} e^{iq_z d/2} + e^{iq_x(-d/2)} e^{iq_z(-d/2)} + e^{iq_x(-d/2)} e^{iq_z d/2} + e^{iq_x d/2} e^{iq_z(-d/2)}) \\ &+ 2 \cdot \cos(q_z \cdot d) (e^{iq_x d/2} e^{iq_y d/2} + e^{iq_x(-d/2)} e^{iq_y(-d/2)} + e^{iq_x(-d/2)} e^{iq_y d/2} + e^{iq_x d/2} e^{iq_y(-d/2)}) \\ &= 2 \cdot \cos(q_x \cdot d) (e^{iq_y d/2} (e^{iq_z d/2} + e^{iq_z(-d/2)}) + e^{iq_y(-d/2)} (e^{iq_z d/2} + e^{iq_z(-d/2)})) \\ &+ 2 \cdot \cos(q_y \cdot d) (e^{iq_x d/2} (e^{iq_z d/2} + e^{iq_z(-d/2)}) + e^{iq_x(-d/2)} (e^{iq_z d/2} + e^{iq_z(-d/2)})) \\ &+ 2 \cdot \cos(q_z \cdot d) (e^{iq_x d/2} (e^{iq_y d/2} + e^{iq_y(-d/2)}) + e^{iq_x(-d/2)} (e^{iq_y d/2} + e^{iq_y(-d/2)})) \\ &= 4 \cdot \cos(q_x \cdot d) \cdot \cos(q_y \cdot d/2) (e^{iq_z d/2} + e^{iq_z(-d/2)}) \\ &+ 4 \cdot \cos(q_y \cdot d) \cdot \cos(q_x \cdot d/2) (e^{iq_z d/2} + e^{iq_z(-d/2)}) \\ &+ 4 \cdot \cos(q_z \cdot d) \cdot \cos(q_x \cdot d/2) (e^{iq_y d/2} + e^{iq_y(-d/2)}) \\ &= 8 \cdot (\cos(q_x \cdot d) \cdot \cos(q_y \cdot d/2) \cdot \cos(q_z \cdot d/2) \\ &+ \cos(q_y \cdot d) \cdot \cos(q_x \cdot d/2) \cdot \cos(q_z \cdot d/2) \\ &+ \cos(q_z \cdot d) \cdot \cos(q_x \cdot d/2) \cdot \cos(q_y \cdot d/2)) \end{aligned}$$

$$\begin{aligned}
\Gamma_{\text{inc}_{4\text{N}}}(\vec{q}) &= \frac{\nu_{4\text{N}}}{Z_{4\text{N}}} \sum_{\Delta \vec{a}_{4\text{N}}} (1 - e^{i\vec{q}\Delta \vec{a}_{4\text{N}}}) \\
&= \frac{\nu_{4\text{N}}}{24} (24 - 8 \cdot (\cos(q_x \cdot d) \cdot \cos(q_y \cdot d/2) \cdot \cos(q_z \cdot d/2) + \\
&\quad + \cos(q_y \cdot d) \cdot \cos(q_x \cdot d/2) \cdot \cos(q_z \cdot d/2) + \cos(q_z \cdot d) \cdot \cos(q_x \cdot d/2) \cdot \cos(q_y \cdot d/2)))
\end{aligned}$$

### Next next next nearest neighbours (5N)

$$\begin{aligned}
\Delta \vec{a}_{5\text{N}} &= \begin{pmatrix} d \\ d \\ 0 \end{pmatrix}, \begin{pmatrix} -d \\ -d \\ 0 \end{pmatrix}, \begin{pmatrix} d \\ -d \\ 0 \end{pmatrix}, \begin{pmatrix} -d \\ d \\ 0 \end{pmatrix}, \\
&\quad \begin{pmatrix} 0 \\ d \\ d \end{pmatrix}, \begin{pmatrix} 0 \\ -d \\ -d \end{pmatrix}, \begin{pmatrix} 0 \\ d \\ -d \end{pmatrix}, \begin{pmatrix} 0 \\ -d \\ d \end{pmatrix}, \\
&\quad \begin{pmatrix} d \\ 0 \\ d \end{pmatrix}, \begin{pmatrix} -d \\ 0 \\ -d \end{pmatrix}, \begin{pmatrix} d \\ 0 \\ -d \end{pmatrix}, \begin{pmatrix} -d \\ 0 \\ d \end{pmatrix}
\end{aligned}$$

This is equal to the NN case, so we get:

$$\begin{aligned}
\Gamma_{\text{inc}_{5\text{N}}}(\vec{q}) &= \frac{\nu_{5\text{N}}}{Z_{5\text{N}}} \sum_{\Delta \vec{a}_{5\text{N}}} (1 - e^{i\vec{q}\Delta \vec{a}_{5\text{N}}}) \\
&= \frac{\nu_{5\text{N}}}{12} (12 - 4 \cdot (\cos(q_x \cdot d) \cos(q_y \cdot d) + \cos(q_x \cdot d) \cos(q_z \cdot d) + \cos(q_y \cdot d) \cos(q_z \cdot d)))
\end{aligned}$$

## A.4 Source code

### A.4.1 Building the lattice

```
int* Gitterbau( int typ, int N, double p_F, int L, int* temp_Gitter)
{
    int x, y, z, xw, yw, zw;
    int M = 0;
    int A_count, F_count, L_count;
    int F;

    if (typ == 0) // cubic
    {
        for (x = 0; x < N; x++)
        {
            for (y = 0; y < N; y++)
            {
                for (z = 0; z < N; z++)
                {
                    if (x&&0 && y&&0 && z&&0) // alle ungerade
                    {
                        temp_Gitter[(z*N+y)*N+x] = 0;
                        M = M+1;
                    }
                    else
                    {
                        temp_Gitter[(z*N+y)*N+x] = 5;
                    }
                }
            }
        }

    }

    if (typ == 1) // bcc
    {
        for (x = 0; x < N; x++)
        {
            for (y = 0; y < N; y++)
            {
                for (z = 0; z < N; z++)
                {
                    if (((x&1) && (y&1) && (z&1)) || (!(x&1) && !(y&1) && !(z&1)))
                    {
                        temp_Gitter[(z*N+y)*N+x] = 0;
                        M = M+1;
                    }
                    else
                    {
                        temp_Gitter[(z*N+y)*N+x] = 5;
                    }
                }
            }
        }

    }

    if (typ == 2) // fcc
    {
        for (x = 0; x < N; x++)
        {
            for (y = 0; y < N; y++)
            {
                for (z = 0; z < N; z++)
                {
                    if (((x&1) && (y&1) && (z&1)) || (!(x&1) && !(y&1) && (z&1)) || ((x&1) && !(y&1) && !(z&1)) || (!(x&1) && (y&1) && !(z&1)))
                    {
                        temp_Gitter[(z*N+y)*N+x] = 0;
                        M = M+1;
                    }
                    else
                    {
                        temp_Gitter[(z*N+y)*N+x] = 5;
                    }
                }
            }
        }

    }
}
```

```

    }
}
}
/* ----- Fremdatome einbauen ----- */
A_count = M;           // alle Atome sind vom Typ A
F_count = 0;

F = M * p_F / 100;

while (F_count < F)
{
    xw = rand() % N;
    yw = rand() % N;
    zw = rand() % N;

    if (temp_Gitter[(zw*N+yw)*N+xw] == 0)
    {
        temp_Gitter[(zw*N+yw)*N+xw] = 2;
        F_count++;
        A_count = A_count - 1;
    }
}
/* ----- Leerstellen einbauen ----- */
L_count = 0;

while (L_count < L)
{
    xw = rand() % N;
    yw = rand() % N;
    zw = rand() % N;

    if (temp_Gitter[(zw*N+yw)*N+xw] == 0)
    {
        temp_Gitter[(zw*N+yw)*N+xw] = 1;
        L_count++;
        A_count = A_count - 1;
    }
}

printf("Anzahl_der_vergebenen_A-atome: %i\n", A_count);
printf("Anzahl_der_vergebenen_Fremdatome: %i\n", F_count);
printf("Anzahl_der_vergebenen_Leerstellen: %i\n", L_count);
return temp_Gitter;
}

```

## A.4.2 Calculating nearest neighbors

```

void NaechstNachbar( int x, int y, int z, int N, int typ, int NN, int* N_nachbarn
)
{
    switch(typ)
    {
        case 0:           //sc
        {
            N_nachbarn[0*NN+0] = (x - 2 + N) % N;           // alle
                Nachbarnkoordinaten des Loches festlegen
            N_nachbarn[1*NN+0] = y;
            N_nachbarn[2*NN+0] = z;

            N_nachbarn[0*NN+1] = (x + 2) % N;
            N_nachbarn[1*NN+1] = y;
            N_nachbarn[2*NN+1] = z;

            N_nachbarn[0*NN+2] = x;
            N_nachbarn[1*NN+2] = (y - 2 + N) % N;
            N_nachbarn[2*NN+2] = z;

            N_nachbarn[0*NN+3] = x;
            N_nachbarn[1*NN+3] = (y + 2) % N;
            N_nachbarn[2*NN+3] = z;

            N_nachbarn[0*NN+4] = x;
            N_nachbarn[1*NN+4] = y;
            N_nachbarn[2*NN+4] = (z - 2 + N) % N;
        }
    }
}

```

```

N_nachbarn[0*NN+5] = x;
N_nachbarn[1*NN+5] = y;
N_nachbarn[2*NN+5] = (z + 2) % N;
}
break;

case 1: //bcc
{
N_nachbarn[0*NN+0] = (x - 1 + N) % N; // alle
    Nachbarkoordinaten des Loches festlegen
N_nachbarn[1*NN+0] = (y - 1 + N) % N;
N_nachbarn[2*NN+0] = (z - 1 + N) % N;

N_nachbarn[0*NN+1] = (x + 1) % N;
N_nachbarn[1*NN+1] = (y + 1) % N;
N_nachbarn[2*NN+1] = (z + 1) % N;

N_nachbarn[0*NN+2] = (x + 1) % N;
N_nachbarn[1*NN+2] = (y - 1 + N) % N;
N_nachbarn[2*NN+2] = (z - 1 + N) % N;

N_nachbarn[0*NN+3] = (x - 1 + N) % N;
N_nachbarn[1*NN+3] = (y + 1) % N;
N_nachbarn[2*NN+3] = (z + 1) % N;

N_nachbarn[0*NN+4] = (x - 1 + N) % N;
N_nachbarn[1*NN+4] = (y + 1) % N;
N_nachbarn[2*NN+4] = (z - 1 + N) % N;

N_nachbarn[0*NN+5] = (x + 1) % N;
N_nachbarn[1*NN+5] = (y - 1 + N) % N;
N_nachbarn[2*NN+5] = (z + 1) % N;

N_nachbarn[0*NN+6] = (x - 1 + N) % N;
N_nachbarn[1*NN+6] = (y - 1 + N) % N;
N_nachbarn[2*NN+6] = (z + 1) % N;

N_nachbarn[0*NN+7] = (x + 1) % N;
N_nachbarn[1*NN+7] = (y + 1) % N;
N_nachbarn[2*NN+7] = (z - 1 + N) % N;
}
break;

case 2: //fcc
{
N_nachbarn[0*NN+0] = (x - 1 + N) % N; // alle
    Nachbarkoordinaten des Loches festlegen
N_nachbarn[1*NN+0] = (y - 1 + N) % N;
N_nachbarn[2*NN+0] = z;

N_nachbarn[0*NN+1] = (x + 1) % N;
N_nachbarn[1*NN+1] = (y + 1) % N;
N_nachbarn[2*NN+1] = z;

N_nachbarn[0*NN+2] = (x + 1) % N;
N_nachbarn[1*NN+2] = (y - 1 + N) % N;
N_nachbarn[2*NN+2] = z;

N_nachbarn[0*NN+3] = (x - 1 + N) % N;
N_nachbarn[1*NN+3] = (y + 1) % N;
N_nachbarn[2*NN+3] = z;

N_nachbarn[0*NN+4] = (x + 1) % N;
N_nachbarn[1*NN+4] = y;
N_nachbarn[2*NN+4] = (z + 1) % N;

N_nachbarn[0*NN+5] = (x - 1 + N) % N;
N_nachbarn[1*NN+5] = y;
N_nachbarn[2*NN+5] = (z - 1 + N) % N;

N_nachbarn[0*NN+6] = (x + 1) % N;
N_nachbarn[1*NN+6] = y;
N_nachbarn[2*NN+6] = (z - 1 + N) % N;

N_nachbarn[0*NN+7] = (x - 1 + N) % N;
N_nachbarn[1*NN+7] = y;
N_nachbarn[2*NN+7] = (z + 1) % N;

N_nachbarn[0*NN+8] = x;
N_nachbarn[1*NN+8] = (y - 1 + N) % N;
N_nachbarn[2*NN+8] = (z - 1 + N) % N;
}

```

```

N_nachbarn[0*NN+9] = x;
N_nachbarn[1*NN+9] = (y + 1) % N;
N_nachbarn[2*NN+9] = (z + 1) % N;

N_nachbarn[0*NN+10] = x;
N_nachbarn[1*NN+10] = (y + 1) % N;
N_nachbarn[2*NN+10] = (z - 1 + N) % N;

N_nachbarn[0*NN+11] = x;
N_nachbarn[1*NN+11] = (y - 1 + N) % N;
N_nachbarn[2*NN+11] = (z + 1) % N;
    }
    break;
}

```



# Bibliography

- [BROWN, 1828] BROWN, R. (1828). *A Brief account of microscopical observations made in the months of June, July and August 1827 on the particles contained in the pollen of plants*. Ann. Phys, 14:294–313.
- [CHUDLEY and ELLIOTT, 1961] CHUDLEY, CT and R. ELLIOTT (1961). *Neutron scattering from a liquid on a jump diffusion model*. Proceedings of the Physical Society, 77:353.
- [DARKEN, 1948] DARKEN, L.S. (1948). *Diffusion, mobility and their interrelation through free energy in binary metallic systems*. Trans. AIME, 175:184–201.
- [EICHLER, (1966)] EICHLER, H.J. ((1966). *Interferenz und Beugung*, vol. 3. Walter de Gruyter.
- [FICK, 1855] FICK, A. (1855). *Ueber diffusion*. Annalen der Physik, 170(1):59–86.
- [HEITJANS and KÄRGER, 1998] HEITJANS, P. and J. KÄRGER (1998). *Diffusion in Condensed Matter*. Vieweg & Sohn.
- [HEMPELMANN, 2000] HEMPELMANN, ROLF (2000). *Quasielastic Neutron Scattering and Solid State Diffusion*. Oxford: Oxford University Press.
- [HENKE et al., 1993] HENKE, BL, E. GULLIKSON and J. DAVIS (1993). *X-ray interactions: photoabsorption, scattering, transmission, and reflection at  $E= 50\text{-}30,000$  eV,  $Z= 1\text{-}92$* . Atomic data and nuclear data tables, 54(2):181–342.
- [LEITNER, 2010] LEITNER, M. (2010). *Studying atomic dynamics with coherent X-rays*. PhD thesis, University of Vienna.
- [LEITNER et al., 2009] LEITNER, M., B. SEPIOL, L. STADLER, B. PFAU and G. VOGL (2009). *Atomic diffusion studied with coherent X-rays*. Nature Materials, 8(9):717–720.

- [LEITNER and VOGL, 2011] LEITNER, M. and G. VOGL (2011). *Quasi-elastic scattering under short-range order: the linear regime and beyond*. J. Phys.: Condens. Matter, 23:254206.
- [MADELUNG and SCHOPPER, 1988] MADELUNG, O. and H. SCHOPPER (1988). *Landolt-Börnstein: Numerical data and functional relationships in science and technology. New series. Nuclear and particle physics. Total cross-sections for reactions of high energy particles. (Including elastic, topological, inclusive and exclusive reactions)*. Springer.
- [MEHRER, 2007] MEHRER, H. (2007). *Diffusion in solids: fundamentals, methods, materials, diffusion-controlled processes*. Springer Verlag.
- [MILLION and KUCERA, 1973] MILLION, B. and J. KUCERA (1973). *Diffusion of Pt-193m in Platinum, gamma -Iron, Cobalt, and Nickel..* Kovove Materialy, 11(4):300–306.
- [NOLTING, 2007] NOLTING, W. (2007). *Grundkurs theoretische Physik: Elektrodynamik*, vol. Bd. 3. Springer.
- [SLAKHORST, 1975] SLAKHORST, J.W.H.G (1975). *The development of recrystallization textures in F.C.C. metals with a low stacking fault energy*. Acta Metallurgica, 23(3):301 – 308.
- [SUTTON, 2006] SUTTON, M. (2006). *Neutron and X-ray Spectroscopy*, pp. 297–318. Springer.
- [VAN HOVE, 1954] VAN HOVE, L. (1954). *Correlations in space and time and Born approximation scattering in systems of interacting particles*. Physical Review, 95(1):249.
- [VEGARD, 1921] VEGARD, L. (1921). *Die Konstitution der Mischkristalle und die Raumfüllung der Atome*. Zeitschrift für Physik A Hadrons and Nuclei, 5:17–26. 10.1007/BF01349680.

# Curriculum vitae

## Personal data

Name: Markus Benedikt Stana  
Date of Birth: October, 16th, 1985  
Place of Birth: Salzburg, Austria  
Nationality: Austria  
Parents: Beatrix Stana, nee Laimer  
Anton Stana

## Education

1992 - 1994: Volksschule Pfandl  
1996 - 2004: Bundesrealgymnasium Bad Ischl  
2004 - 2005: Compulsory community service  
2005 - 2006: Traveling  
2006 - Bachelor studies in astronomy at the University of Vienna  
2006 - 2011 Diploma studies in physics at the University of Vienna